THE UNIVERSITY OF HULL

The Evolution of Galaxies: Starbursts and Beyond

being a Thesis submitted for the Degree of Doctor of Philosophy

in the University of Hull

by

Charlotte Louise Wilkinson, MSc

October 2018

Acknowledgements

Firstly, I would like to acknowledge the E.A. Milne Centre. It has been a pleasure being a part of the the University of Hull's most active research group from the beginning and watching it grow and blossom. I'd like to thank the Faculty of Science and Engineering for granting me travel bursaries that have allowed me to attend conferences including EWASS and NAM where I have been able to share my science with the wider astronomy community and enrich my own learning. I gratefully acknowledge the contributions of people who provided survey data that I used in my PhD, including the SDSS, Illustris, Galaxy Zoo, FIRST and Yang Catalogue teams.

I'd like to strongly acknowledge my supervisors, Dr Kevin Pimbblet and Dr John Stott, I can't thank you enough for the help and support you have given me over the last few years. Without you both, this PhD would not have been possible and I'm so glad to have had you guys as my supervisors. I'd also like to thank my other collaborators, Gareth and Brad. Particularly to Gareth, who helped me enormously on the Illustris project, guiding me on the path to the theoretical side of astrophysics. Also, many thanks to my fellow PhD student, the now Dr Yjan Gordon, who taught me the (inefficient) ways of Python, and giving me a template for this thesis which had to be debugged in order for the bibliography to work.

Lastly, I gratefully acknowledge the support of my family and friends. Particularly my Grandparents and my fiancé for their financial and emotional support. Without you, I wouldn't have been able to pursue my passion rent and bill free. I hope I have made you all proud, regardless of whether you can understand what's in this thesis or not.

Declaration of Originality

This thesis is submitted in partial fulfilment of the degree of Doctor of Philosophy from the University of Hull. I declare that the work undertaken in this thesis is original and my own and was carried out under the supervision of Dr Kevin Pimbblet and Dr John Stott. Where work, results, or ideas have been taken from other sources, those sources are explicitly referenced.

A substantial amount of the work here has been used for peer-reviewed journal articles led by myself. The nature of modern astronomy is such that a number of co-authors is commonplace on research publications, and indeed is necessitated by the large number of observations and data reduction required. Nonetheless, the work that has been published from this thesis was the principle responsibility of myself in terms of driving the science case, analysis, and writing up. The observations used were conducted by others as part of large scale surveys, and the data products from these observations are explicitly referenced.

Chapter 2 has been published as Wilkinson et al. (2017) MNRAS 472, 1447, Chapter 3 has been published as Wilkinson et al. (2018) MNRAS 479, 758, while Chapter 4 presents work that is the basis for a paper I am leading that is in preparation.

The details of the contributions of myself and my co-authors to those works are described in the prologues of the relevant Chapters.

Candidates signature:

Date:

Abstract

Determining how galaxies evolve and what drives their evolution is one of the biggest challenges in astronomy. This thesis aims to shed light on the life-cycle of galaxies by answering the following questions: (1) How do different selection methods of post-starburst galaxies have an impact on the properties observed? (2) What are the main triggers of starburst, and hence, the post-starburst galaxies in the Illustris simulation? (3) Do starburst galaxies have a top-heavy IMF and produce heavier stars than quiescently star forming galaxies? (4) To what extent do AGN play a role in quenching star formation in starburst galaxies which lead to the post-starburst phase? For question one, we investigate the effect of different selection criteria of post-starburst galaxies, we reveal an evolutionary sequence that transitions from the blue cloud through the green valley before settling in the red sequence. We find a lack of any significant merger fractions which suggests that secular processes or minor mergers/interactions may play an important role in triggering starburst as opposed to major mergers. For question two, we investigate the triggering mechanisms of starbursts and find that over half of our starburst sample have not undergone a recent merger but have instead experienced harassment. Harassment triggered starbursts are comparable in strength to merger driven starbursts and are found in denser environments, suggesting environment plays a role in determining the processes that trigger a burst. For questions three and four, we compare optical and radio emission to determine the form of the IMF and to detect the presence of AGN in starbursts. We find that starbursts show some evidence for a top-heavy IMF, however no significant AGN fraction, suggesting other processes, such as stellar winds, quench starbursts or the overlap time between starburst and AGN phases is very small and therefore starbursts with AGN are extremely rare.

Contents

List of Figures

List of Tables

1. Introduction

1.1 Cosmology

Cosmology is the study of the Universe as a whole, how it began and how it will evolve. From this, we can determine how structures like galaxies form and evolve. In this section we will discuss the 'standard model' of cosmology adopted in this thesis.

1.1.1 Evidence for the Big Bang

It is a well established theory in astronomy that the Universe began with a Big Bang, in which a cosmic singularity containing all of the Universe's energy exploded and expanded to form the Universe we see today. In the beginning, the Universe was hot and dense, but as it expanded it cooled such that quarks bound together to form hadrons. As cooling continued, hadrons clumped together forming large primordial clouds. These clouds fragmented and collapsed under gravity to form the first stars. The first stars are thought to be predominantly massive with masses around 100 $M_{\odot}$ (Bromm et al. 1999, 2002; Nakamura & Umemura 2001; Abel et al. 2000, 2002; Bromm & Larson 2004). With the formation of stars, galaxies formed which led to the large-scale structure of the Universe we observe today. In this section we discuss the four key pieces of evidence that support the idea of a Big Bang Universe.

Hubble's Law

The first evidence supporting the Big Bang theory is Hubble's Law. The initial Copernican principles state that the Universe is homogeneous, isotropic and temporally infinite. However, a priest and mathematician named George Lemaître disagreed with the idea that the Universe does not have a beginning. After studying Einstein's theory of relativity, Lemaître began to test the hypothesis that the Universe is static. Using the Doppler shift, Lemaître (1927) finds that galaxies are redshifted, i.e. their spectral lines are shifted to longer wavelengths compared to laboratory values. This means they are receding from us (Hubble 1929).

Edwin Hubble later expanded this work and determined the linear relationship between recession velocity and distance measured using Cepheid variable stars (Fig. 1.1), now known as Hubble's Law, see Eq. 1.1 below.

$$v = H_0 \, r \, , \tag{1.1}$$

where v is recession velocity, H_0 is Hubble's constant and r is distance from the Earth (Hubble 1929). Hubble's law states that galaxies at greater distances are receding at higher velocities than those at lesser distances. For example, if galaxy B is distance x away from A moving at velocity v and galaxy C is the same distance and velocity from B then C is $2x$ away from A moving away at velocity $2v$. This idea is clearly shown in Fig. 1.2. The current measure of Hubble's constant is 73.45 $\text{kms}^{-1}\text{Mpc}^{-1}$ (Riess et al. 2018), however, different values arise from different methods of calculation. One method to calculate H_0 is by measuring the gradient in Fig. 1.1 which uses distances derived from Cepheid variable stars or supernova. Another method is to use temperature fluctuations in the cosmic microwave background (discussed in the next section) and compare them to theoretical models that predict the expansion and evolution of the Universe to find H_0. By inverting the Hubble constant we can approximate the age of the Universe which is 13.8 billion years, this is a good approximation as we do not see stars older than 13.8 billion years old.

Cosmic Microwave Background

The next piece of evidence supporting the Big Bang theory is the existence of the cosmic microwave background (CMB). The theory predicts that electromagnetic radiation left over from the Big Bang from the moment matter decoupled from photons should be visible everywhere. We consider photons in the Universe to have a blackbody spectrum, when the Universe expanded the wavelengths of higher energy photons redshifted into the microwave range. At the time of decoupling, the Universe is estimated to have been 3000 K, the expansion of the Universe would have expanded the blackbody spectrum 1000 times giving a present day temperature of 3 K. The actual temperature of the Universe is calculated to be ~2.7 K. With modern technology, such as the telescope developed by the Planck Collaboration, we

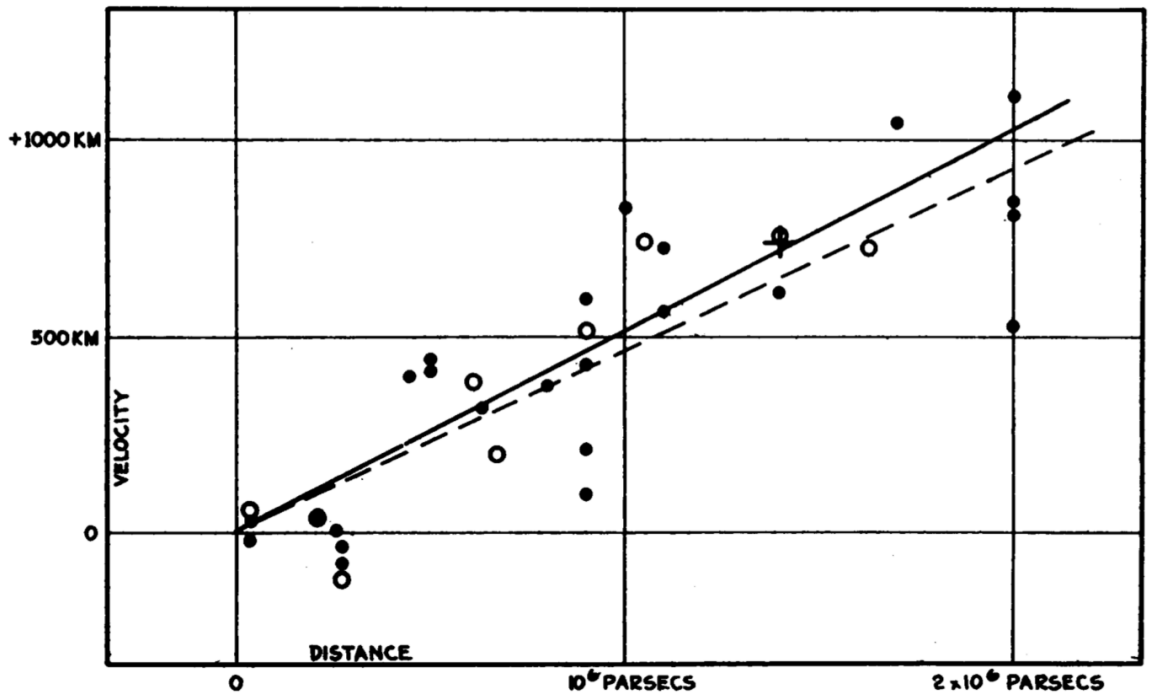

Figure 1.1: The linear relationship between distance and recession velocity of galaxies from Hubble (1929). Hubble used Cepheid variable stars because the period of their pulsations correlated strongly with their luminosities, which allows for a accurate measure of their distance. Their velocities are calculated using their spectra and were plotted against distance. Hubble found a positive correlation in which the gradient of the line, Hubble's constant (H_0), can be inverted to determine the age of the Universe. This implies that galaxies further away from us are moving at a quicker velocity than those closer, suggesting the Universe is expanding. This trend is only found when using distant galaxies because in nearby galaxies, the velocity of galaxies is dominated by their peculiar velocity rather than their velocity due to expansion.

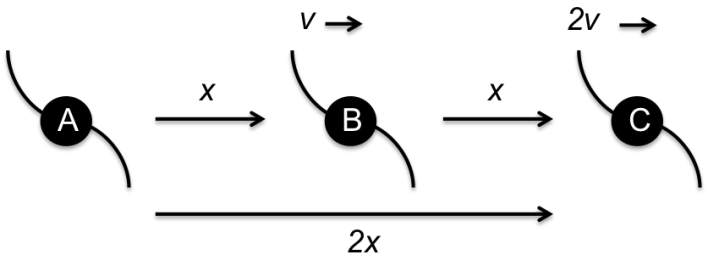

Figure 1.2: Illustration showing Hubble's Law. Galaxy B is a distance x away from A travelling a velocity v, galaxy C is distance x away from B hence $2x$ from A therefore it is travelling at twice the velocity of B away from A.

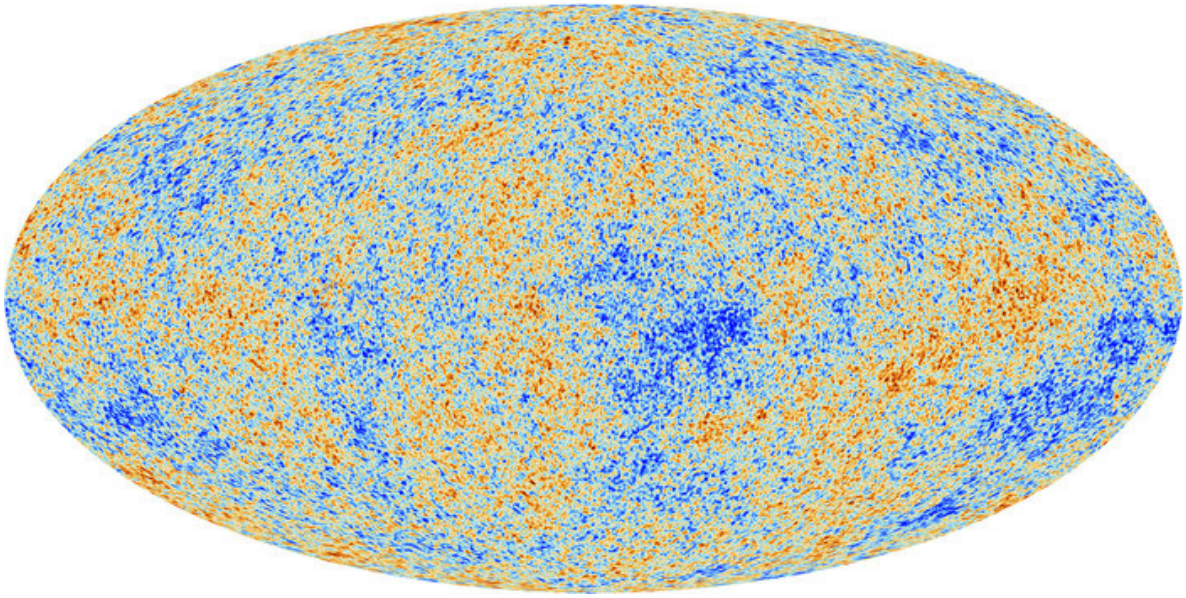

Figure 1.3: The cosmic microwave background (CMB) as observed by the Planck mission (Collaboration et al. 2014). This image shows the oldest light in our Universe. The variations in colour represent slight variations in density of the Universe which has led to the large scale galactic structures we see today. Image credit: http://www.esa.int/spaceinimages/Images/2013/03/Planck_CMB

can see these microwaves in great detail everywhere in the Universe, this is known as the cosmic microwave background. Fig. 1.3 shows the CMB as observed by the Planck mission (Collaboration et al. 2014). This detailed image of the CMB shows slight variations (difference of 0.0002 K between red and blue regions) in density in the early Universe. It is within the regions of higher densities that galaxies form, the variations in the CMB are the seeds for the variations we witness in the positions of galaxies. This is known as the large-scale structure of the Universe or the cosmic web. The cosmic web is clearly shown in the 2dF Galaxy Redshift Survey, shown in Fig. 1.4, in which galaxies are positioned in a web like structure, at higher redshifts, the web appears to fade in Fig. 1.4 as we become more biased to only observing bright massive galaxies.

Abundance of Light Elements

The next piece of evidence for the Big Bang is the observed abundances of light elements such as hydrogen, helium, deuterium, lithium and beryllium. The presence of these elements and the lack of elements with proton numbers greater than 4, suggests that the Universe

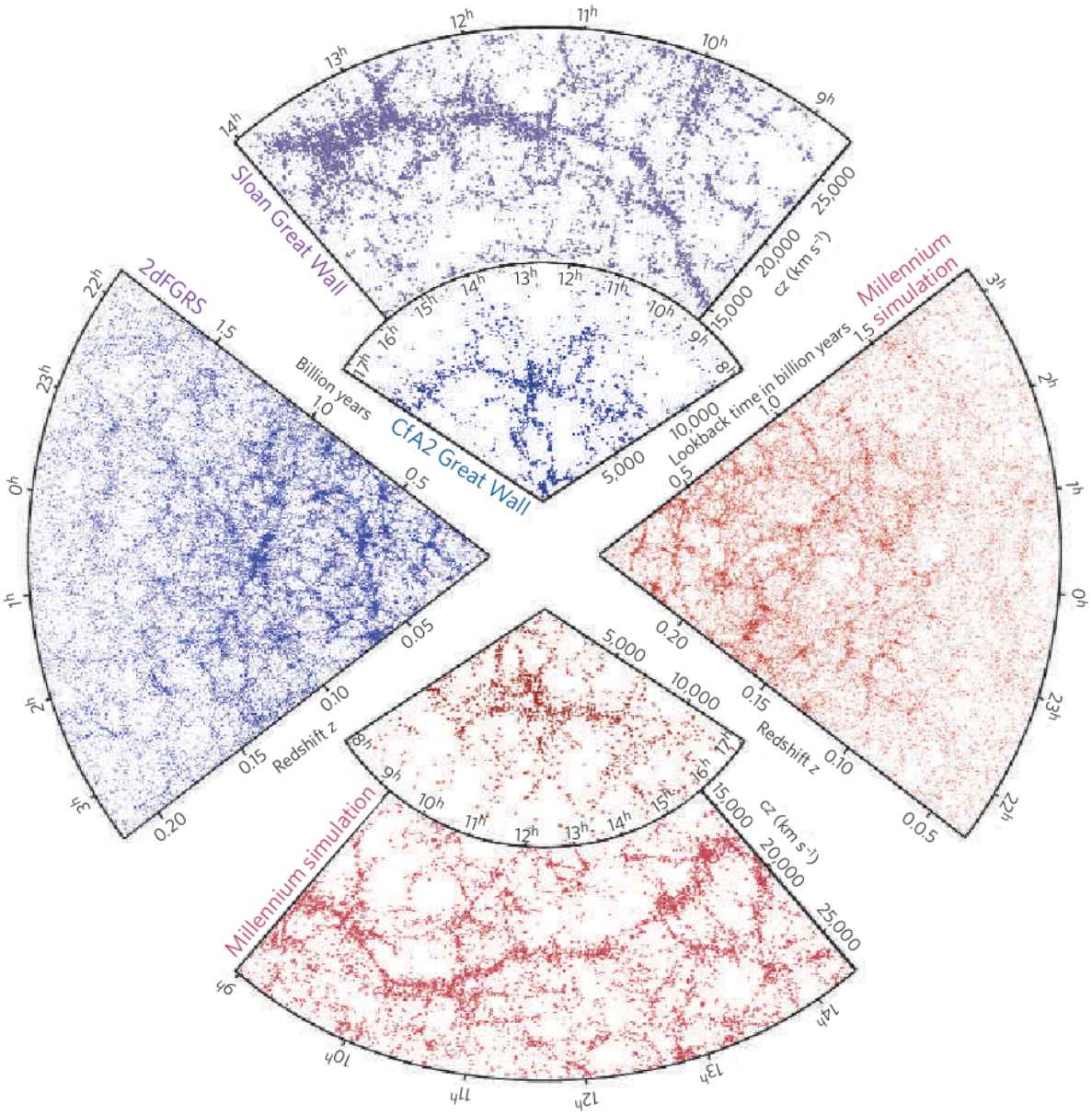

Figure 1.4: Figure 1 from Springel et al. (2006) showing the large scale distribution of galaxies obtained from spectroscopic redshift surveys and cosmological simulations. The top slice shows the 'Great Wall' from SDSS (large slice) and CfA2 (small slice), in which the Coma cluster is at the centre. The Great Wall contains over 10,000 galaxies and is considered one of the largest structures in the Universe. The blue slice on the left is data from the 2dFGRS survey containing 220,000 galaxies. At local redshifts the structure of the cosmic web can be clearly seen although at higher redshifts, brighter galaxies dominate and the large scale structure is harder to determine. The red slices on the bottom and to the right show data from the Millennium simulation. The simulation produces similar distributions to those seen in observational surveys (blue) such that the 'Great Wall' is witnessed.

began extremely hot and expanded rapidly such that fusion could not occur past beryllium. The Big Bang theory predicts the abundances of hydrogen and helium well (~75% and ~25% respectively; Lépine-Szily & Descouvemont 2012). Hydrogen is not produced in stars, so must have been formed when photons decoupled from matter and protons and electron recombined to form neutral hydrogen. However, the Big Bang theory predicts three times more lithium than is actually observed, this is known as the lithium problem. The generalised velocity distribution of nuclei, characterised by a parameter, q, is typically in the form of a Maxwell-Boltzmann distribution, where $q = 1$. However, Hou et al. (2017) find that by using a Tsallis distribution instead, where $1.069 \leq q \leq 1.082$, the predicted lithium abundance becomes closer to the observed value. Whilst stars can produce deuterium, lithium and beryllium these elements are easily broken down by stars so their abundance in the Universe cannot have come from a stellar origin but nucleosynthesised in the Big Bang.

1.1.2 ΛCDM Cosmology

In this thesis, we assume a ΛCDM cosmology. The ΛCDM model of cosmology, also known as the 'standard model', explains how the Universe was created in a Big Bang which has been expanding ever since and the evolution of the Universe is driven by gravitation (Alam et al. 2016). It assumes the Universe is flat and dominated by the cosmological constant, Λ, which is associated with dark energy, and cold dark matter (CDM). The model assumes Einstein's theory of general relativity is correct in describing gravity and that the Universe is both homogeneous and isotropic on the cosmic scale (Condon & Matthews 2018).

Dark Matter

The ΛCDM model describes the presence of dark matter which makes up approximately 85% of the mass of the Universe. The existence of dark matter was first suggested by Lord Kelvin in 1884. He used the velocity dispersions of stars in the Milky Way to calculate its mass. The mass he calculated is much higher than the mass calculated using the mass-light ratio of stars, this led to the conclusion that there must be dark bodies within the galaxy (de Swart et al. 2017). It wasn't until 1933 that Fritz Zwicky found major evidence suggesting dark matter

was more common than luminous matter (Zwicky 1933). Cold dark matter is non-baryonic, does not emit photons and is collisionless, but can only interact with itself and other matter via gravity, acting as a cosmic glue which prevents galaxies from flying apart (cold because its velocity is much less than the speed of light). Further research into dark matter shows galaxies form and reside within spheroidal dark matter halos (Fellhauer et al. 2006) which are regions of overdensity in the underlying dark matter distribution (Quinn et al. 1986; Frenk et al. 1990). The fluctuations in the dark matter distribution stem from primordial density fluctuations which are still visible in the CMB (Guth 1981). These fluctuations are enhanced by gravitational interactions which lead to an inhomogeneous distribution of matter (Abel et al. 2001), without them there would be no cosmic web today as it would take a much longer time to form.

Inflation

The modern cosmological model includes cosmic inflation, a period of time shortly after the Big Bang in which the Universe exponentially expanded. There are four pieces of evidence for inflation; the horizon problem, the flatness problem, the smoothness problem and the lack of magnetic monopoles. The horizon problem suggests something has broken causality to form fragments visible in the CMB, Guth (1981) suggests that regions within the CMB were once causally connected but rapid expansion broke this connection. The flatness problem arises from the cosmological density parameter, Ω, to equal precisely one. Inflation solved this problem because any curvature would be smoothed out during expansion. The smoothness problem finds that variations in the CMB are relatively small (or smooth) in comparison to the predicted quantum fluctuations. Inflation theory solves this problem as these fluctuations would be smoothed our during rapid expansion. Lastly, is the lack of magnetic monopoles; monopoles were hypothesised by Paul Dirac in 1931 to explain the quantization of electric charge. Magnetic monopoles cannot be created inside a particle collider, this means that the energy needed to create them is so vast that only extreme processes in the cosmos can form them. As there have been no sign of monopoles in the Universe, it is thought that inflation have spread these particle far enough apart that they are extremely rare and possible to the

extent that they do not exist inside the observable Universe (Bendtz et al. 2013).

The Universe is still expanding, albeit not at the rate it was during inflation, and with that the density of the Universe is decreasing. This decrease in density has a significant effect on the evolution of galaxies. Bell et al. (2006) use close galaxy pairs as a proxy for calculating merger rates, a significant driver in galaxy evolution. They find the fraction of pairs, therefore mergers, increase with redshift. This change in galactic evolution is observed in the Madau plot, Fig. 1.5, which shows star formation rate density has been decreasing since $z = 2$ (Madau & Dickinson 2014). The rate at which galaxies evolve through external processes will continue to decline and secular evolution will begin to dominate how galaxies evolve (Kormendy & Kennicutt 2004). This may lead to an almost exclusive fraction of spirals locally that passively evolve onto the red sequence, like the passive spirals found in Ishigaki et al. (2007).

1.2 Classifying Galaxies

Throughout the Universe, galaxies come in all different morphologies (Hubble 1936) and colours (Taylor et al. 2014) to name but a few parameters. Determining what drives this variation is one of the biggest questions in astronomy. Whilst categorising galaxies allows us to determine their current activity, past interactions and at what point in their evolution they are in, sometimes our classifications can hold us back. For example, classifying a galaxy only by its colour or morphology does not give us the full story about a galaxy's evolution; spiral galaxies do not always have to be blue in colour (Masters et al. 2010a) nor do ellipticals have to be red (Dressler & Gunn 1983). Only by looking at the overall picture of a galaxy including morphology, colour, star formation activity and AGN activity can we really understand a galaxy's evolutionary history.

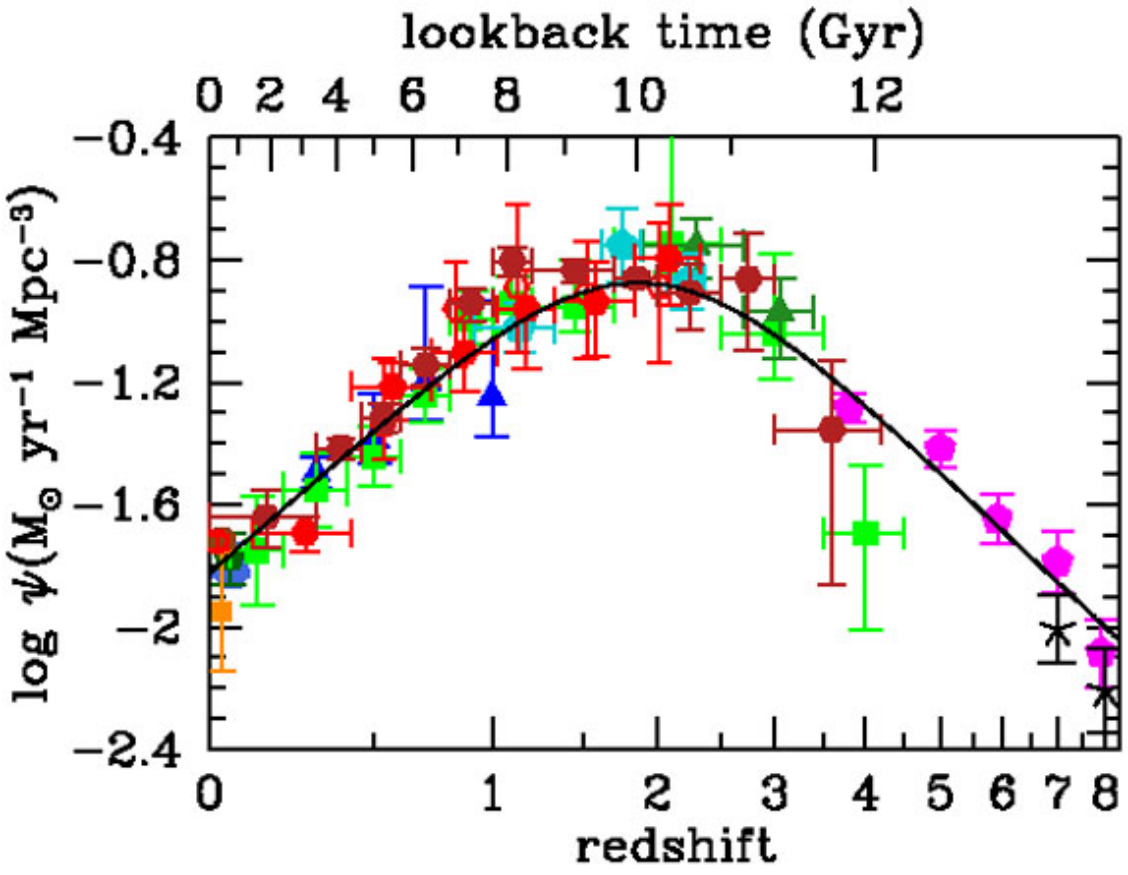

Figure 1.5: The Madau plot from Madau & Dickinson (2014) showing the decline in star formation rate density since $z = 2$. The red and orange points are star formation histories derived from IR luminosities and pink, green and blue points are derived from UV data. This plot shows that star formation in the Universe peaks at $z \simeq 2$ and declines toward $z = 0$. This could suggest that as the Universe has been expanding the processes that drive star formation, for example mergers and interactions are becoming fewer as galaxy density decreases.

1.2.1 Morphological Classifications

There are multiple ways in which galaxies can be classified. The most famous morphological classification scheme is that by Edwin Hubble (Hubble 1936), shown in Fig. 1.6, where Hubble grouped similar galaxies together according to their structure. Known as Hubble's tuning fork, the scheme includes spiral and elliptical morphologies with the S0 morphology linking the two ends of the 'fork'.

Further research and simulations into galaxy formation and structure has revealed galaxies begin as spirals (Mo et al. 1998; Kormendy & Kennicutt 2004) and lose their delicate disk structures as they transition into elliptical galaxies (Cole et al. 2000). Hubble noted the presence of a bar feature within spiral classifications (Combes & Sanders 1981; Bournaud & Combes 2002) and includes the S0 morphology that lies between the elliptical and spiral morphologies (Larson et al. 1980; Quilis et al. 2000). The range of morphologies observed between spirals and ellipticals suggests an evolutionary sequence that galaxies transition through. This is why it is important to classify galaxy morphology (Bland-Hawthorn & Gerhard 2016) to understand at what stage in their evolution they are. However, there are still unanswered questions as to what processes are responsible for driving the evolution of spirals to ellipticals and what other effects these processes have. In subsequent sections, we discuss the possible processes described throughout the literature that could create morphological changes to a galaxy.

By classifying galaxies we are able to determine at what point in their evolutionary life they are and what processes they have undergone, such as mergers. Up until the end of the 20th century, galaxy studies usually contained relatively small sample sizes, so classifying galaxies by eye was not too time consuming. However, with the rise of large astronomical surveys, such as CfA redshift survey (Huchra et al. 1983), 2dF galaxy redshift survey (Colless 1999) and the Sloan digital sky survey, the process of classifying large quantities of galaxies became very time consuming and inefficient. In this thesis we make significant use of the Sloan digital sky survey that has spectroscopic data for over 900,000 galaxies (Abazajian et al. 2009). If, for example, an astronomer takes one minute to classify one galaxy and works continuously, then it would take them approximately two years to classify each one. And for many galaxies,

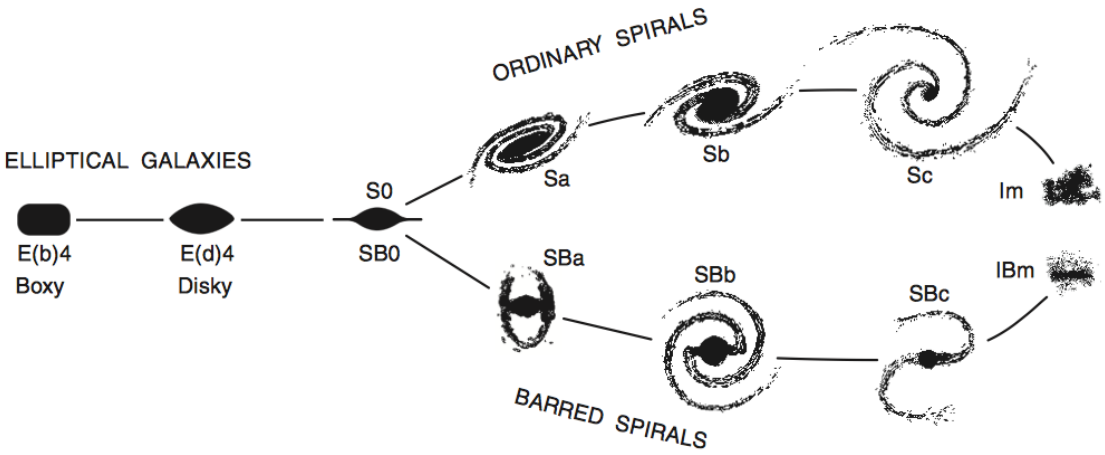

Figure 1.6: A revision of Hubble's tuning fork diagram by Kormendy & Bender (1996). Hubble grouped similar galaxies together based on their morphology. The tuning fork includes different types of spiral galaxies based on whether there is a bar or not and the tightness of the spiral. On the other end of the tuning fork is the elliptical morphology and the S0 morphology that forms a link between spirals and ellipticals.

their morphology might not be so clear cut, such that one astronomer will disagree with the classifications made by another. Whilst machine learning technology, like those used by Lahav et al. (1995), is becoming ever more advanced, it is still not as capable as the human brain in recognising the patterns that divide ellipticals from spirals. In order to tackle this classification problem, thousands of people are needed to inspect galaxy morphology in the form of citizen science. Below, we discuss one citizen science project, Galaxy Zoo (Lintott et al. 2008, 2011), that has revolutionised the way we classify large survey galaxies.

Galaxy Zoo

The Galaxy Zoo project (Lintott et al. 2008, 2011) uses citizen science to classify galaxies on a large scale. More than half a million members of the general public have visually inspected galaxies with spectroscopic data from the entire Sloan Digital Sky Survey (SDSS, Abazajian et al. 2009). The galaxies within Galaxy Zoo have on average 40 classifications each and have an associated uncertainty, due to the scale of the project classifications from Galaxy Zoo are comparable in quality to expert astronomers (Lintott et al. 2008).

Figure 1.7 shows the questions that users are presented with and how classifications are determined (Willett et al. 2013). Questions include 'Is the galaxy simply smooth and rounded

with no sign of a disk?', 'How rounded is it?', 'Is the disk viewed edge-on?' and 'How tightly wound do the spiral arms appear?' to name a few. The questions probe the overall shape of the galaxy to determine it's morphology, orientation, compactness and number of arms if a spiral. The answers to these questions shed light on unusual features such as tidal tails, mergers, gravitational lensing or distorted shapes. The results from galaxy zoo provide a well rounded view of the the true morphology of the galaxy under study. Studies such as Masters et al. (2010a) and Tojeiro et al. (2013) use the morphological classifications within Galaxy Zoo to identify the presence of red spirals which are important in understanding secular evolution of galaxies. Whilst studies by Cheung et al. (2015), Galloway et al. (2015) and Kruk et al. (2017, 2018) use Galaxy Zoo data to select barred spirals to investigate whether the bar fuels AGN (discussed later in section 1.2.4).

Since the first iteration that used primarily SDSS images, the latest version uses galaxy images from the Dark Energy Camera Legacy Survey (DECaLS, Schlegel et al. 2015). The telescope used in this survey is larger and 10 times more sensitive to light than that used in the SDSS survey. This means that we can see more details in the galaxies and features previously not picked up by SDSS due to their dimness, which are now visible in the DECaLS Survey.

1.2.2 Colour Classifications

Colour is strongly correlated with star formation rate and therefore can tell us a great deal about the activity going on within a galaxy within the last 5 Gyr (Bamford et al. 2009) such that colour is just the superposition of the stars within a galaxy. Star forming galaxies produce OB-class stars which are very hot and because of their high masses are short-lived . The maximum flux of these stars peaks in the blue end of the spectrum giving galaxies a bluer appearance. Quiescent galaxies however, are heavily populated with cooler M-class stars that are lower in mass and therefore have long lifetimes. The maximum flux of these stars peaks at the red end of the optical spectrum giving quiescent galaxies a redder colour. Massive OB-class stars can out-shine M-class stars by many orders of magnitude so a relatively small population of OB-class stars can dominate a galaxy's light output.

The distribution of colour is bimodal, representative of the two main phases of galaxy

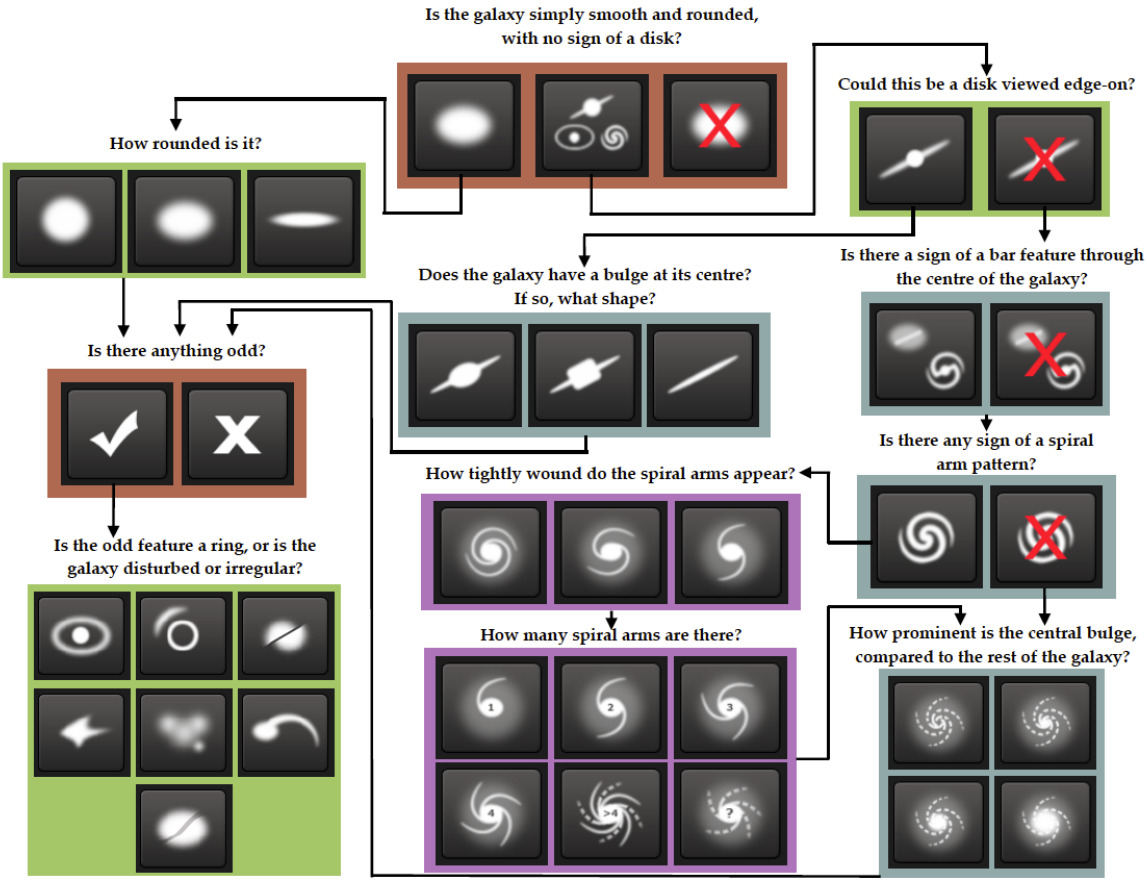

Figure 1.7: Galaxy Zoo flowchart from Willett et al. (2013), showing the questions and multiple choice answers users are presented with when classifying galaxies. There are questions included that can reveal any unusual features such as gravitational lensing, tidal tails and irregular morphologies.

evolution (Strateva et al. 2001; Hogg et al. 2003; Baldry et al. 2004; Balogh et al. 2004; Faber et al. 2007; Taylor et al. 2014); star forming and quiescent. Fig. 1.8 shows the colour magnitude diagram by Schawinski et al. (2014) and highlights the bimodal nature of galactic colour. Fig. 1.8 highlights the locations of the 'blue cloud', which contains star forming galaxies, the 'red sequence' which contains quiescent galaxies, and the 'green valley' sandwiched between the red and blue regions. The green valley is less populated than the blue cloud and red sequence indicating galaxies transition quickly between the two regions of the colour magnitude diagram (Bell et al. 2004b; Wyder et al. 2007; Mendez et al. 2011; Schawinski et al. 2014). Bremer et al. (2018) conclude that it takes between 1 and 2 Gyr for galaxies to migrate across the green valley, similar to the quenching time scale Smethurst et al. (2015) find, and whilst environment may play a role in triggering this migration, it has negligible effect on the migration time-scale. This leads to the question as to whether environment drives galaxy evolution.

Colour links very strongly with morphology; the blue cloud is almost entirely made up of star forming spiral galaxies, whilst the red sequence is mainly composed of older, elliptical galaxies which are less likely to be forming stars (Strateva et al. 2001; Blanton et al. 2003; Shen et al. 2003; Bell et al. 2004a; Ellis et al. 2005; Driver et al. 2006; Papovich et al. 2012; Taylor et al. 2014). Skibba et al. (2009) find that when a galaxy's morphology changes from spiral to elliptical a colour change usually follows. Across the green valley, Bremer et al. (2018) find that galaxies have significant bulge and disk components and evolve through secular fading of the disk whilst the bulge is present before star formation declines. The link between colour and morphology indicates whatever process is responsible for driving changes in morphology also drives changes to the star formation history (Blanton et al. 2003; Kauffmann et al. 2003).

However, not all galaxies follow this simple bimodality. Studies such as van den Bergh (1976), Goto et al. (2003b), Masters et al. (2010a) and Fraser-McKelvie et al. (2016, 2018) have observed and confirmed the presence of optically red spiral galaxies. Whilst red galaxies are characteristic of quiescence, some studies, like those mentioned above, find red spirals are likely to be heavily encased in dust due to signatures of low-level star formation such as the presence of Hα and UV emission. However, spirals could be allowed to turn quiescent through

secular evolution in which they haven't undergone processes like major mergers that destroy the disk. On the other end of the colour magnitude diagram, blue ellipticals have been found in studies such as Schawinski et al. (2007, 2009) and Tojeiro et al. (2013). Blue ellipticals are important in galaxy evolution because they are transitionary species which allow us to probe the processes and mechanisms that allow galaxies to transform from star forming spirals to quiescent ellipticals (Dressler & Gunn 1983; Tran et al. 2003; Yang et al. 2004).

1.2.3 Star-Gas-Star Cycle

The interstellar medium (ISM) and star formation are linked by the star-gas-star cycle (also known as the cosmic baryon cycle), shown in Fig. 1.9. Clouds of cold atomic hydrogen (visible at λ = 21 cm) condense to form molecular clouds (also visible in the radio regime) that later collapse under gravity to form stars. As stars age, heavier elements are formed which are expelled into the surrounding ISM, when the star goes supernova (Nomoto et al. 2013). Stellar winds and supernovae push gas outwards to form hot bubbles that emit radiation at X-ray wavelengths. Some of this gas escapes the gravitational potential of the galaxy and is unable to be recycled (Chevalier & Clegg 1985; Heckman et al. 1990, 2000; Veilleux et al. 2005). This hot gas is incapable of forming stars as fusion cannot occur in highly thermal conditions. As the bubbles cool, gas falls back onto the disk like a galactic fountain (Shapiro & Field 1976) and condenses to make atomic hydrogen clouds, starting the cycle again (Anglés-Alcázar et al. 2017). However, this recycling of gas is not 100% efficient, as some gas becomes trapped within low-mass stars, white dwarfs, neutron stars and black holes (Lilly et al. 2013). This gradual loss of gas from the gas-star-gas cycle contributes to the secular evolution of galaxies, eventually halting the production of stars (Chisholm & Matsushita 2016). Observing the regions of atomic hydrogen, molecular clouds and stars comes with challenges for astronomers, for example, the visible wavelengths emitted by stars are prone to dust obscuration, whilst radio wavelengths are less affected by dust, are limited by spatial resolution, making detailed images hard to achieve.

As well as stellar and supernova feedback, AGN also contribute to the regulation of star formation within galaxies. AGN can inhibit star formation by consuming/heating up the

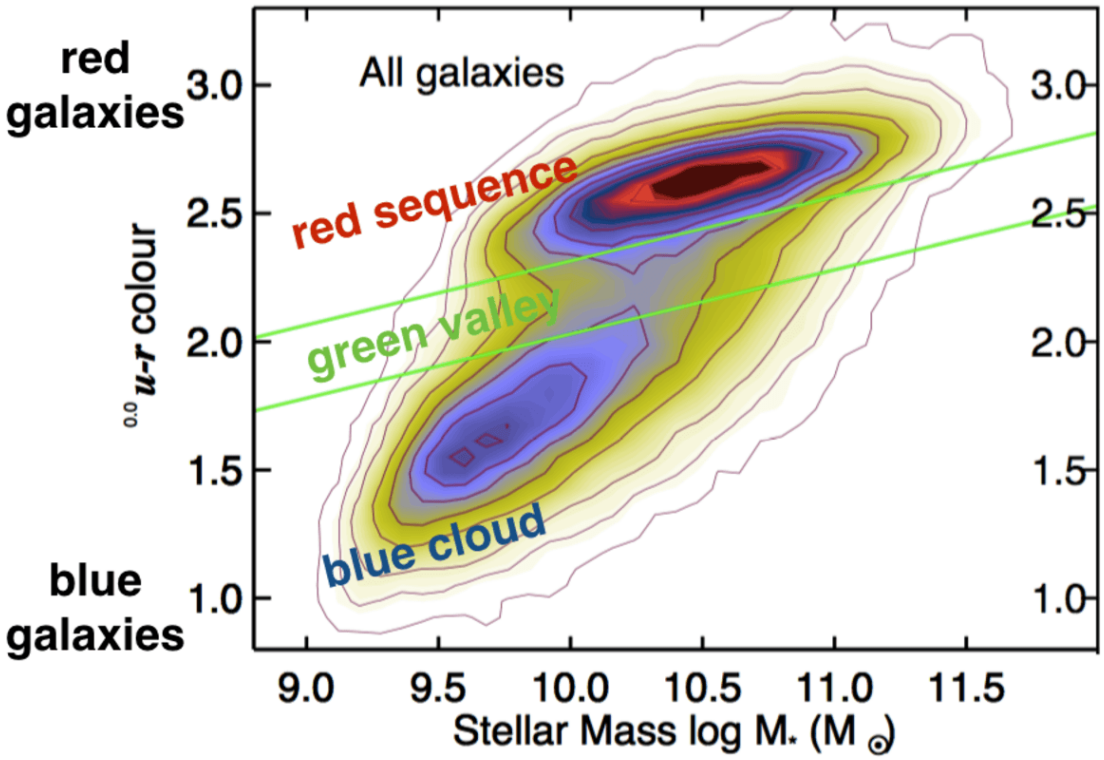

Figure 1.8: Colour magnitude diagram from Schawinski et al. (2014). The diagram highlights the two main populations of galaxies; blue cloud galaxies and red sequence galaxies. Galaxies situated in the blue cloud are typically late-type galaxies with on-going star formation whilst red sequence galaxies are typically quiescent early-types. In between these regions is the green valley which is less densely populated, this suggests that the time it takes for galaxies to migrate from the blue cloud to the red sequence is relatively short and therefore the green valley represents a transitionary phase in galaxy evolution.

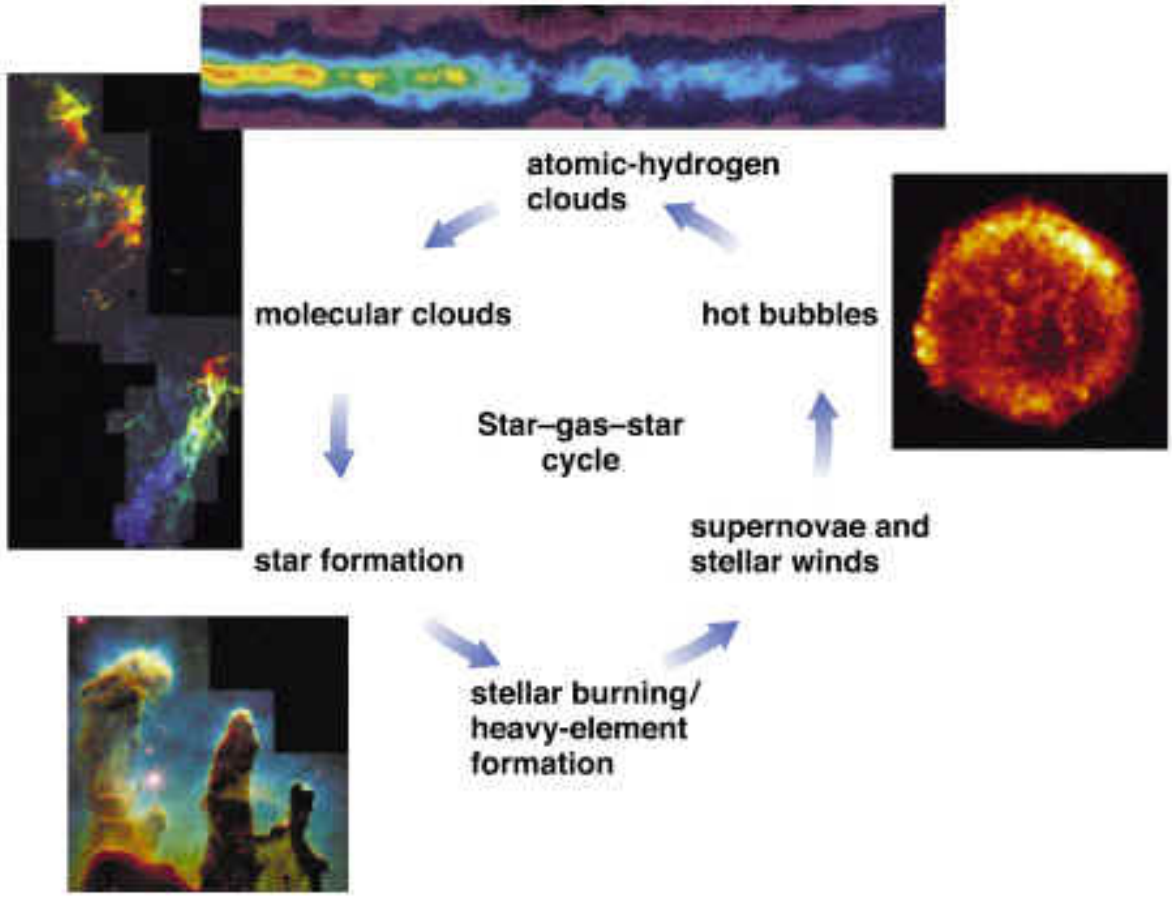

Figure 1.9: The star-gas-star cycle from www.unf.edu. The diagram shows the star formation cycle within galaxies. Cold clouds of atomic hydrogen condensed to form molecular clouds. These molecular clouds are used to form stars which initiate stellar burning and the formation of heavy elements. Stellar winds and supernovae push surrounding gas outwards to create hot bubbles of gas which is unusable for star formation. As the gas cools, it falls back to disk to form atomic hydrogen and the cycle starts again.

surrounding gas within the ISM (Lambourne 2010), but may also trigger star formation by ejecting material from its poles through jets, as seen in Centaurus A. As the jet gas cools, clumps of molecular gas form which fuel the production of stars (Salomé et al. 2017). A more detailed description of AGN and star formation tracers are given in 1.2.4.

1.2.4 Spectroscopic Classifications

By measuring the star formation rate we can evaluate galaxy evolution over a long redshift range (see Fig. 1.5). There are many star formation indicators in emission for star formation when examining the spectra of galaxies such as: [OII], [OIII], Hα, Hβ, Hγ and Hδ at optical

wavelengths (Kewley et al. 2002; Goto 2007b; Mahajan 2013). The Balmer absorption lines in particular are useful in inferring the ages of stellar populations (Kauffmann et al. 2003), we discuss Hδ absorption later in chapter 2. In this thesis, we primarily utilise optical spectra to infer star formation. However, in chapter 4, we make use to radio luminosities to infer star formation and discuss our method of calculation in that chapter.

During star formation, hot young stars ionise the surrounding gas in the galactic nebula (Calzetti et al. 2004; Hong et al. 2011; Calzetti 2013) which produces emission line spectra synonymous with young stellar populations. The [OII]λ3726/λ3729 forbidden line, which is a doublet, is formed in this way, particularly around the shell of gas around new born stars (Rosa et al. 1984) and although it suffers from greater dust contamination than Hα λ6563, [OII] is used extensively in the literature when inferring star formation over large redshift ranges (Zabludoff et al. 1996; Kewley et al. 2002; Poggianti et al. 2009; Vergani et al. 2010; Rodríguez Del Pino et al. 2014). Hα, whilst the strongest of the Balmer lines, becomes redshifted out of the optical range at high redshifts so cannot be measured in optical spectroscopic surveys (Lamareille 2010). The [OIII]λ emission line however, suffers from strong contamination from AGN such that star formation contributes relatively little to [OIII] emission (Tanaka 2012).

There are some problems inferring star formation from certain spectral lines as some are more prone to contamination from AGN and dust than others as previously mentioned. Dust makes galaxies appear redder by absorbing the optical and ultraviolet light emitted from star forming regions, heats up and re-emits light at infrared wavelengths (Calzetti 2001), this is why bluer spectral lines like [OII] are more affected by dust than redder spectral lines like Hα. Corrections for dust extinction can be made by approximating the amount of dust in the galaxy. This is done by measuring the ratio of Hβ to Hα, known as the Balmer decrement. When calculating SFR, we correct for dust by using the Calzetti dust law, described in Calzetti (2001), in which we apply an extinction correction from Treyer et al. (2007), we assume A_v 0.5. We also make use of previously derived star formation rates from Brinchmann et al. (2004) that use the Balmer decrement to estimate the dust attenuation of Hα in order to correct for dust.

Not all Hα emission however, comes from star formation, AGN can also emit Hα. This adds complexity when trying to calculate the contribution to Hα from star formation. Diagrams such as the BPT diagram (Baldwin et al. 1981), and the WHAN diagram (Cid Fernandes et al. 2010, 2011), aim to split star forming galaxies from those with AGN.

In this thesis, we use spectral data from the Sloan Digital Sky Survey (SDSS hereafter). The SDSS covers over 7,500 square degrees of the northern galactic cap and provides public spectral data for more than 800,000 galaxies making it one of the largest large scale surveys in the world (Abazajian et al. 2009). SDSS benefits from value-added catalogues, in which usable parameters are given, like mass, star formation rates and velocity dispersions. We choose to use SDSS data due to the large amount of data available, its ease of access and quality of data. We note however, that for a significant proportion of data, some parameters have been unable to be calculated due the simulations and code used, in some cases certain parameters can only be calculated up to a given redshift. When using SDSS data we keep these limitations in mind and minimise the effects by using appropriate selection criteria.

The Star Formation Main Sequence

By measuring star formation rates and masses of galaxies we can determine their evolutionary phase over multiple wavelengths. Large statistical studies of galaxies have revealed the existence of a well defined relationship between star formation rate and mass, this is known as the star formation main sequence (Speagle et al. 2014) which holds true over high (Daddi et al. 2007) and low redshifts (Salim et al. 2007). The star formation main sequence is used extensively in the literature (Brinchmann et al. 2004; Noeske et al. 2007; Elbaz et al. 2007; Peng et al. 2010; Santini et al. 2017). Fig. 1.10 shows the correlation between mass and star formation rate. The majority of star forming galaxies group together to form the main sequence, shown in blue on Fig. 1.10. Main sequence galaxies are typically blue, and reside in the blue cloud region of the colour magnitude diagram (Fig. 1.8). However, there are outliers to this trend which allow us to understand the different phases in galaxy evolution. A significant population of outliers are red sequence galaxies, also known as 'red and dead' galaxies. These galaxies are quiescent and gas deficient. Above the main sequence are galaxies that have star

formation rates higher than expected for a given mass, these are starburst galaxies and make up between 5 and 10% of the galaxy population (Rodighiero et al. 2011). Starburst galaxies are a significant phase in galaxy evolution as they may represent a transitionary phase between star forming spirals and quiescent ellipticals. Sandwiched between the main sequence and the red sequence are sparsely populated green valley galaxies, that are considered to be a transitionary phase (Bremer et al. 2018), however later in their evolution compared with starbursts which have recently been enhanced. Santini et al. (2017) find that scatter along the main sequence decreases with increasing stellar mass suggesting that in low mass galaxies there is a greater variety of star formation histories.

AGN

At the centre of almost every massive galaxy lies a supermassive black hole (SMBH; Magorrian et al. 1998; Kormendy & Richstone 1995). Although there remains uncertainty about how these black holes form but what the observations do show is that the masses of supermassive black holes strongly correlate with the velocity dispersion of the galactic bulge they are in, this is known as the $M - \sigma$ relation, (Gebhardt et al. 2000). This indicates that the evolution of black holes is strongly connected to the evolution of galaxies.

In most galaxies, supermassive black holes lay dormant at low redshifts, but a few per cent of these black holes actively accrete matter, these are known as active galactic nuclei or AGN for short (Huchra & Burg 1992). Black holes have large gravitational potential wells and for those that are active matter infalls onto the SMBH from the accretion disk. The accretion disk forms as a result of the conservation of angular momentum which is a balance between the kinetic forces pulling outwards and the gravitational forces pulling inwards. Matter within the accretion disk feels the effects from the tidal and frictional forces, this heats up the gas to the extent it emits vast amounts of radiative energy at X-ray wavelengths, hence appearing luminous (approaching the Eddington luminosity limit) and this in turn reduces the momentum of the matter enabling it to fall into the SMBH (Lambourne 2010).

AGN studies date back to work by Seyfert (1943) who identified optical emission lines in spiral nebula. This led galaxies containing AGN to be initially called Seyfert galaxies.

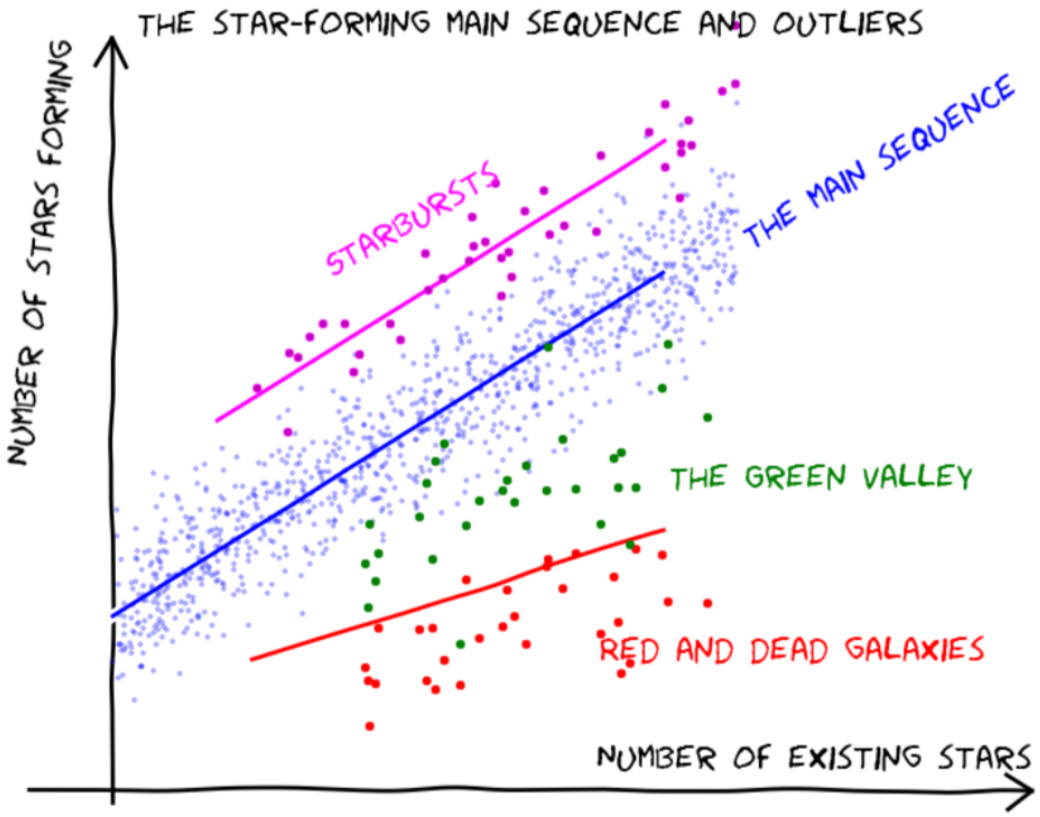

Figure 1.10: Informal diagram of the star formation main sequence. Regular star forming galaxies group together to form the main sequence shown in blue. Above the main sequence are starburst galaxies (pink) that have higher than expected star formation rates for their given mass. Red galaxies that are no longer forming stars reside below the main sequence with green valley galaxies in between. The star formation main sequence shows the different phases in galaxy evolution and is another way of representing the colour-magnitude diagram. Image credit: http://candels-collaboration.blogspot.com.au/2013/02/ star-formation-in-mountains.html

Further work by Khachikian & Weedman (1974) show that Seyferts can be split into two categories; Seyfert Is, showing broad line emission and Seyfert IIs that show narrow line emission. These two types of Seyferts are not driven by intrinsic difference in the galaxies but rather the orientation at which they are viewed. This is known as the unified model which is shown in Fig. 1.11. The 'unified model' (Antonucci 1993) includes a dusty torus that enshrouds the accretion disk, so if viewing edge on (Seyfert IIs) the broad line region near the accretion disk is obscured with only the narrow line region visible. When observing face on (Seyfert Is) the core is unobstructed so both the broad line and narrow line regions can be viewed.

Emission from the broad line region stems from the high velocity of the gas in and around the accretion disk. The cumulative effect of Doppler shifting (caused by the distribution of velocities of the gas) leads to what is called Doppler broadening in which the width of the emission line increases (Ferland & Persson 1989; Ferland et al. 1992). The narrow line region however, stems from a much larger region around the poles of the AGN, whilst larger than the broad line region, the gas within is much sparser (Koski 1978). The low density of the gas means emissivity is high and when viewed can dominate the AGN spectrum. It gives rise to forbidden lines such as [OIII] doublet at λ = 5459 Å and 5007 Å (Kaiser et al. 1999; Baskin & Laor 2005).

Other types of AGN include quasi-stellar objects (QSOs or quasars) and low ionising nuclear emission regions (LINERs). The main distinction between these types of AGN are in their luminosities; QSOs have much higher luminosities than Seyferts (Scheuer & Readhead 1979; Boroson & Green 1992) whilst LINERs have much lower luminosities than Seyferts. QSOs have powerful jets caused by the AGN spewing out materials from its poles (displayed in Fig. 1.11), the gas particles within these jets have velocities comparable with the speed of light and are therefore considered relativistic, and because of this they emit strongly at radio wavelengths due to synchrotron radiation. Bahcall et al. (1997) and McLure et al. (1999) find QSOs reside predominantly within old early-type galaxies and only 15% in spiral hosts, similarly Kauffmann et al. (2003) find 30% of QSOs have spiral hosts. However these results are heavily disputed by further studies such as Schmitt et al. (1999), González Delgado et al.

(2001) and Cid Fernandes et al. (2001) who find young stellar populations in over half of the QSO host galaxies in their samples suggesting they play a role in galaxy evolution. Kauffmann et al. (2003) find that a large proportion of their AGN sample have experienced a starburst in the last 1-2 Gyr, which supports the link to galaxy evolution as any process that causes gas accretion on to an AGN could also trigger a starburst such that their duty cycles are connected (Di Matteo et al. 2005; Hopkins et al. 2006; Melnick et al. 2015). We further discuss the connection between AGN and starbursts/post-starbursts in section 1.4.3.

1.2.5 The IMF

The initial mass function (IMF hereafter) describes the distribution of mass for a population of newly formed stars. It is responsible for many properties we observe in galaxies from their luminosity functions to their distribution of chemical elements. There has been a great effort in trying to understand the general form of the IMF as shown in Fig. 1.12 (Offner et al. 2014). Fig. 1.12 displays the models of Salpeter (1955), Kroupa (2001), Chabrier (2005), Thies & Kroupa (2007) and de Marchi & Paresce (2001).

The initial form of the IMF determined by Salpeter (1955) adopts a power-law distribution in the form of $dN \propto M^{-\alpha} dM$, where $\alpha = 2.35$. For stars over 1 $M_\odot$, this model fits well and has been considered the standard ever since. However, for stars below 1 $M_\odot$, the function begins to diverge indicating a break in the IMF. Miller & Scalo (1979) find that the IMF is best represented as a log-normal distribution between 0.1 and 30 $M_\odot$ with a flattening below 1 $M_\odot$. More modern studies such as Chabrier (2003) and Chabrier (2005) combine these distributions opting for a log-normal distribution at low masses and a power-law distribution at higher masses.

As seen in Fig. 1.12, there is an agreement in fit towards the high mass regime. However, at low masses there are still uncertainties regarding what is the best fit of the IMF. This uncertainty stems from what assumptions are used; whether the study assumes the star formation process is continuous or whether different processes dominate around the stellar/sub-stellar boundary (Thies & Kroupa 2007, 2008; Kroupa et al. 2013).

Within the local Universe, telescopes such as the Hubble Space Telescope (HST), are

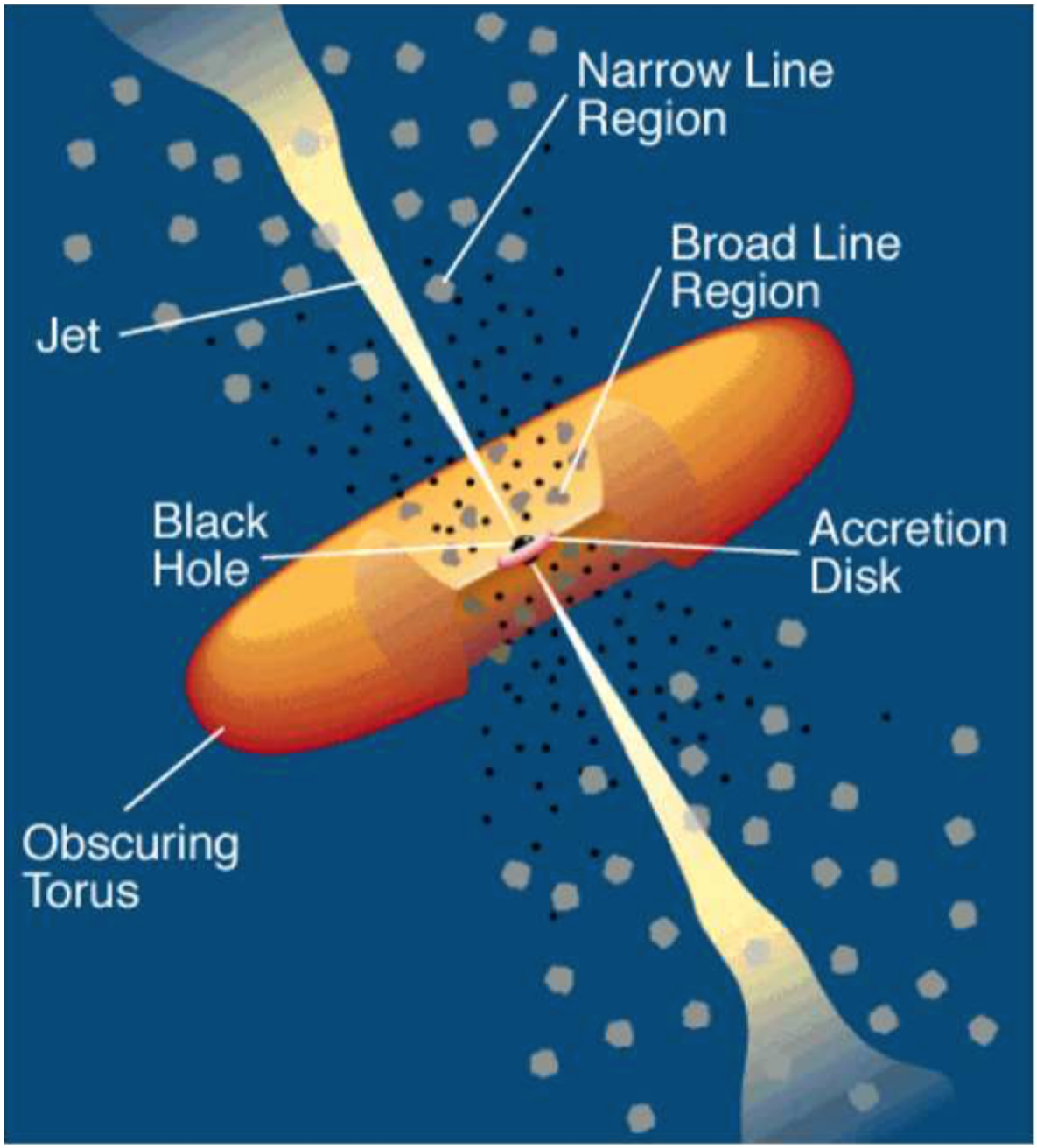

Figure 1.11: Unified AGN model by Urry & Padovani (1995) updated by Costa et al. (2010). Surrounding the supermassive black hole in the galactic centre, is an accretion disk which feeds the black hole. Beyond the accretion disk is a dusty torus which obscured the black hole such that when facing edge on the only sign of an active galactic nuclei is the powerful jets, if any that are emitted from the poles. In this orientation the AGN is classed as a seyfert II as the central broad line region is obscured However, if viewing from a face-on angle the AGN is referred to as a seyfert I as both the broad and narrow line regions are visible.

powerful enough to resolve individual stars which allow astronomers to probe star formation histories and determine the IMF directly. However, in extragalactic environments more indirect approaches must be taken to infer the IMF. There are two main methods to determine the IMF (Offner et al. 2014); the first, and most popular method compares the mass-to-light ratios against the predictions of stellar population synthesis (SPS) models, such as those done by Bruzual & Charlot (2003) and Cappellari et al. (2012). The second method determines the relative numbers of low-mass stars ($M < 0.5$ M$_\odot$) by using gravity-sensitive integrated spectral features (van Dokkum & Conroy 2010).

There are many studies throughout the literature that debate the nature of the IMF within extragalactic environments. Many studies such as Bell & de Jong (2001), Cappellari et al. (2006) and Hunter et al. (2010) suggest the IMF is 'universal' and shows very little variation. Others however, show evidence of variations within the IMF. Amongst the variations, the IMF is described as either 'bottom-heavy' or 'top-heavy'. A galaxy with a 'bottom-heavy' IMF has an over-abundance of lower mass stars whilst a 'top-heavy' IMF contains an over-abundance of higher mass stars.

1.3 Galaxy Evolution

Galaxies are not static objects randomly dispersed around the Universe. Galaxies can and do change their morphology, colour, activity and position, but what processes are responsibly for this. In this section, we discuss the various processes capable of causing change to a galaxy and what observational effects these cause.

1.3.1 Environmental Trends

When looking at the large scale structure of the Universe, we find that galaxies form a structure known as the cosmic web, seen in Fig. 1.13. The majority of galaxies reside along the dense filament regions of the web within the dark matter halos (Bond et al. 1996; Codis et al. 2012; Cautun et al. 2014; Libeskind et al. 2018), however galaxies can exist within the less dense voids (Gregory & Thompson 1978; Kirshner et al. 1981; Pan et al. 2012). There are differences observed in morphologies, spectral properties and chemical abundances

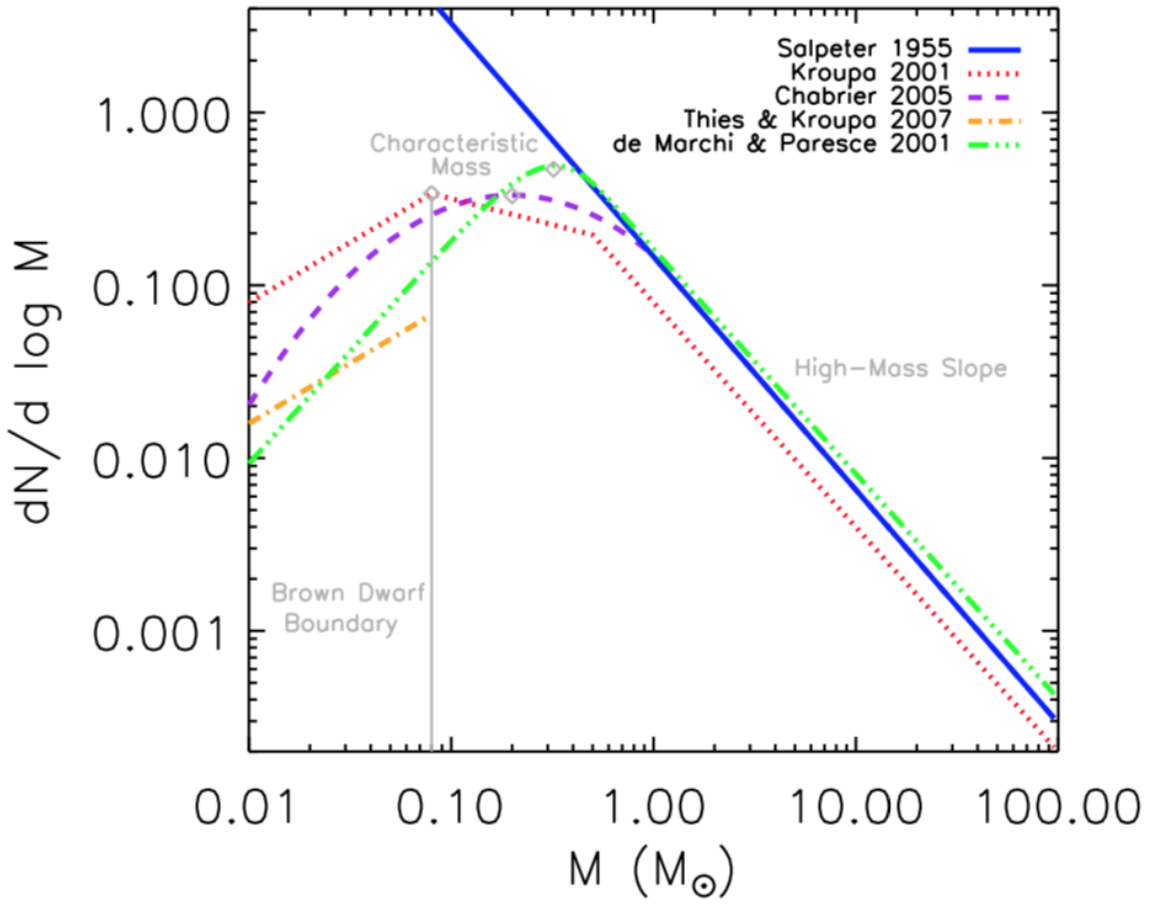

Figure 1.12: Figure 1 from Offner et al. (2014). This plot shows the various forms of the IMF as described by Salpeter (1955), Kroupa (2001), Chabrier (2005), Thies & Kroupa (2007) and de Marchi & Paresce (2001). The Salpeter slope (blue) represent a simple power-law distribution in which the fraction of low-mass stars is over predicted. The Kroupa and Chabrier IMFs adopt a log-normal distribution and better represent the low mass regime, however, there is more discrepancy amongst the predicted fraction of low mass stars. In the high mass regime, most of the IMF models agree on incorporating a power-law distribution.

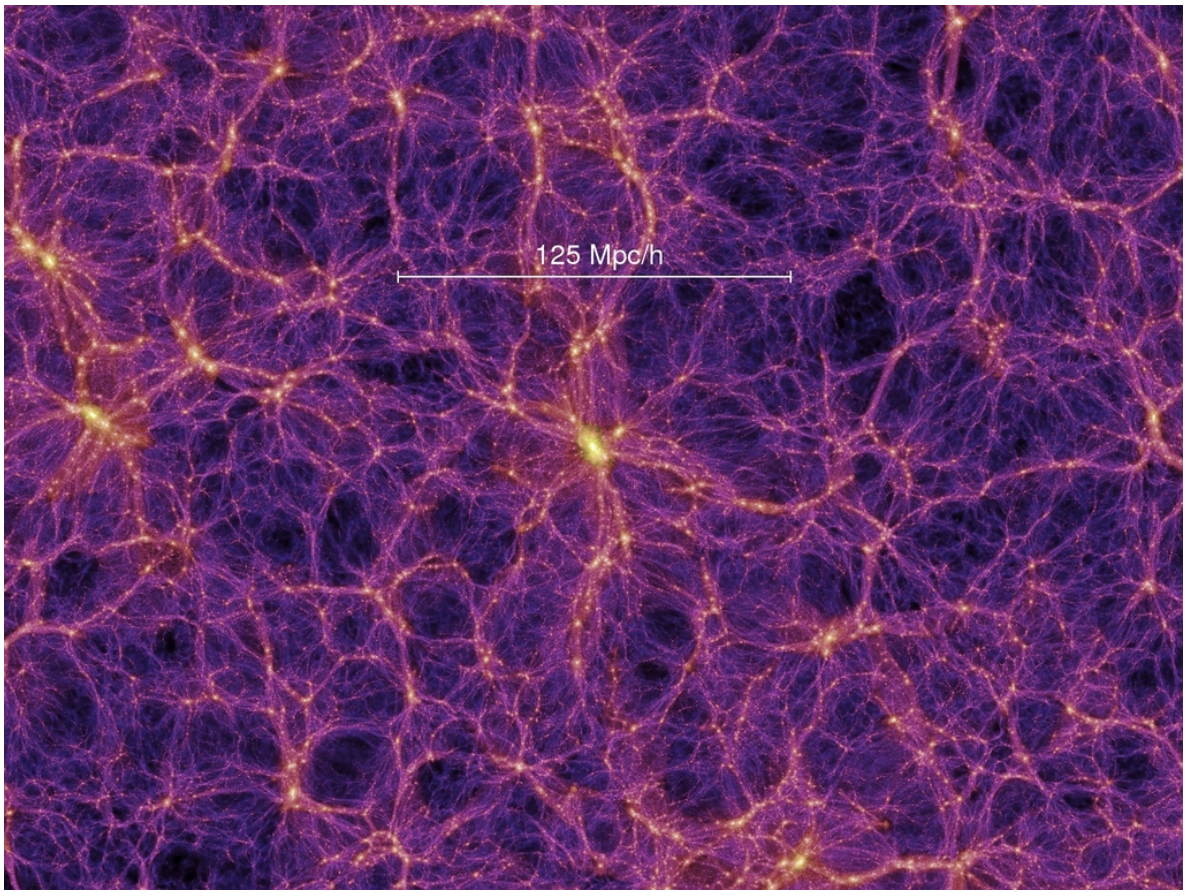

Figure 1.13: Snapshot of the Millennium simulation by Springel et al. (2005). The image shows how the large scale structure of the Universe resembles a cosmic web, where the bright denser regions contain the the highest amount of galaxies and dark matter. Image credit: https://wwwmpa.mpa-garching.mpg.de/galform/virgo/millennium/seqD_063a_half.jpg

when comparing cluster environments to the field (Balogh et al. 1999; Gómez et al. 2003; Baldry et al. 2006; Poggianti et al. 2006). These differences in galactic properties suggest environment plays a significant role in how galaxies evolve. One of these trends is known as the morphology-density relation, explained below. This suggests certain galaxy morphologies and colours take up preferential positions in the galactic environment. Could environment be driving galaxy evolution?

The Morphology-Density Relation

In the denser regions of the Universe, such as groups and clusters, galaxies are more likely to take up elliptical morphologies (Dressler 1980; Bamford et al. 2009; Bait et al. 2017).

Whitmore et al. (1993) find that in nearly all cluster centres galaxies are predominantly elliptical, and spirals are absent from nearly all cluster cores. For S0 morphologies, that are between spirals and ellipticals (Larson et al. 1980; Quilis et al. 2000) in Hubble's tuning fork (Fig. 1.6), Dressler (1980) find that these galaxies follow a similar trends to elliptical galaxies, shown in Fig. 1.14. The figure shows the fractions of ellipticals and S0 galaxies increase with density, whilst the fraction of spirals decreases with increasing density. By assuming that galaxies evolve from spirals to ellipticals we can infer that they evolve from sparse environments to dense environments. Could environment be driving morphological evolution, such that the migration of spirals onto groups/clusters disturbs the disk turning spirals into S0 morphologies as found by Gregg & West (2017)?

As colour strongly correlates with morphology (Shen et al. 2003; Skibba et al. 2009; Taylor et al. 2014) it is not surprising to find correlations between colour and environment (Bait et al. 2017). Red passive galaxies take up denser regions in the Universe, whilst blue star forming galaxies favour less dense 'field' environments. Bamford et al. (2009) find that colour dependence on environment is stronger than that of morphology. They suggest that the time-scale for the colour transformation must be shorter than the morphological transition.

The morphology-density relation is thought to indicate that environment affects galaxy evolution (Vollmer 2013). As galaxies accrete onto a group or cluster, evidence suggests this suppresses star formation (Taranu et al. 2014). These processes could include ram pressure stripping, galaxy strangulation and galaxy harassment, explained later in section 1.3.2.

Butcher-Oemler Effect

Cluster galaxies are typically members of the red sequence due to quenching effects of the cluster environment. However, a blue excess in the cores of distant clusters was found by Harvey Butcher and Augustus Oemler Jr. in 1978, which sparked debate as to why blue galaxies exist in clusters cores. Butcher & Oemler (1978) examined galaxies within two clusters at $z = 0.39$ and $z = 0.46$ and found that the cores of intermediate-redshift clusters contain a higher fraction of blue galaxies compared to low-redshift clusters (Butcher & Oemler 1978). Further work examining 33 rich galaxy clusters out to $z \sim 0.5$ revealed the same trend

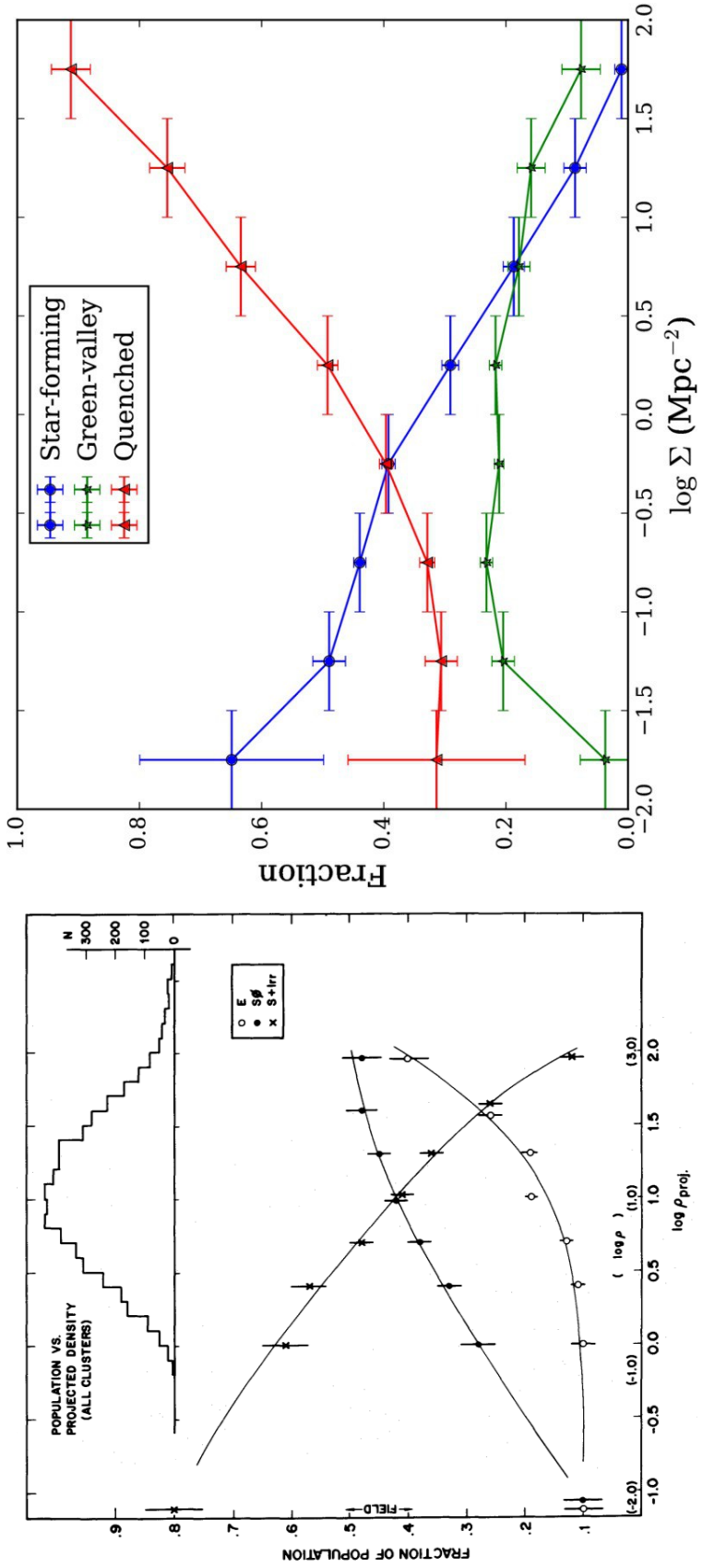

Figure 1.14: Left - Morphology-density relation from Dressler (1980). Elliptical and S0 fractions increase with density inferring that bulge dominated galaxies prefer denser environment such as groups and clusters. Meanwhile the fraction of spiral galaxies decreases with a rising density meaning spiral galaxies have a preference for sparser environments like the field. By assuming that galaxies evolve from spirals to ellipticals, the morphology density relation suggests that galaxies evolve from sparse environments to dense environments. The evolution in morphology could be driven by migration onto groups and clusters. Right - Colour-density relation from Bait et al. (2017). The star-forming (blue) and quenched (red) galaxies follow the same trends and spiral and elliptical galaxies respectively. However, there is some variation between S0 and green valley galaxies, such that the green valley fraction peaks at density in which the star forming and quenched galaxies cross. This supports the idea that green valley galaxies are a transitionary phase between star forming and quenched galaxies.

(Butcher & Oemler 1984). This became known as the Butcher-Oemler effect. Later work by Rakos & Schombert (1995) finds that the fraction of blue galaxies rises from 20% at z=0.4 to 80% at z=0.9 indicating strong evolution of galaxy clusters. As well as colour varying with redshift, Goto et al. (2003a) find that morphology also varies with redshift such that the fraction of late-type galaxies increasing with redshift. Goto et al. (2003a) find that richer clusters have lower fractions of late-type galaxies, this indicates that ram pressure stripping is a significant contributor in the evolution of star forming late-type galaxies to quiescent early-types.

Studies such as Dressler & Gunn (1992) that look into what these blue galaxies are, suggest that the blue excess is probably the result of either starburst galaxies, with extreme rates of star formation (hence appearing blue and showing spectral signs of Hδ absorption), post-starburst galaxies, which have similar colours and Hδ absorption as starbursts, or AGN, which have high excitation spectra. Loh et al. (2008) find that less than 5% of the blue excess is made up of starburst galaxies, indicating that the Butcher-Oemler effect is not caused by starbursts. A more likely cause of the Butcher-Oemler effect is the presence of E+A galaxies, which we discuss later in section 1.4. However, various other studies highlight issues with the Butcher-Oemler effect. Andreon & Ettori (1999) suggest that the Butcher-Oemler effect is a consequence of varying X-ray luminosity as a function of redshift, whilst Loh et al. (2008) find limitations in creating large samples with uniform photometry. Whilst Margoniner et al. (2001) find that the Butcher-Oemler effect also depends on the richness of the cluster.

1.3.2 Evolution Through Environmental Processes

In this section we discuss various environmental mechanisms that have the capability to alter a galaxy's appearance or quench its star formation.

Ram Pressure Stripping and Strangulation

In section 1.1.2 we discussed how galaxies reside in dark matter halos (Fellhauer et al. 2006). These halos and their residing galaxies clump together to form a giant halo that contains multiple galaxies, known as clusters. Surrounding cluster galaxies is a very hot diffuse gas,

primarily primordial gas, known as the intracluster medium (ICM). As galaxies fall onto a cluster they are hit by a drag force, similar to wind resistance (Gunn & Gott 1972). If this force is greater than the binding force of the galaxy's interstellar medium (ISM) then gas is stripped away truncating star formation particularly from the disk as the binding energy decreases with radius from the core (van Gorkom 2004). As well as stripping gas and quenching star formation, studies such as Dressler & Gunn (1983) and Gavazzi et al. (1995) find that the gas in the galaxy core remains intact and shocks from the outer regions can trigger a burst of star formation.

Ram pressure stripping can be directly observed through the identification of 'Jellyfish' galaxies (Smith et al. 2010; Ebeling et al. 2014; McPartland et al. 2016; Poggianti et al. 2016; Bellhouse et al. 2017) and is a significant example of violent galactic evolution. The disks of infalling galaxies are most affected by ram pressure stripping, such that the disk gets stripped away forming tails in shape of tentacles which gives rise to the name 'Jellyfish' galaxies. As well as this significant morphological change, Ebeling et al. (2014) find that a vigorous starburst is triggered due to a shock compression of gas at the galaxy-gas interface and within the tails. This triggering of rapid star formation, makes 'Jellyfish' galaxies some of the brightest galaxies within a cluster, this enhancement however declines as infalling galaxies become more established in their new cluster environment.

A slower (quenching timescale ≈ 4 Gyr) and more gentle way of quenching star formation is through strangulation (Peng et al. 2015). This process occurs when a galaxy infalls onto a cluster and becomes encased in the hot ICM. Cold gas from the halo that would have fed star formation is halted, star formation continues until the cold gas reservoir in the disk is depleted (Balogh et al. 2000; Balogh & Morris 2000). Studies such as Larson et al. (1980) and Balogh et al. (2000) believe the differences in field and cluster galaxies stem from the strangulation process. Studies such as van den Bosch et al. (2008), Prescott et al. (2011) and Peng et al. (2015) find that for satellite galaxies the main method of quenching is via strangulation and this process is responsible for the build-up of red sequence galaxies. This suggests that the quenching mechanism of an infalling galaxy is dependant on how that galaxy falls onto a group/cluster; galaxies that infall head on into a cluster undergo ram pressure stripping whilst

galaxies that orbit a cluster and gradually infall undergo strangulation. Unlike ram pressure stripping, the disk remains intact which could explain the presence of passive red spirals (Masters et al. 2010a) which may eventually lead to an S0 morphology (Larson et al. 1980; Kawata & Mulchaey 2008). Strangulation has been found to take place in group environments, Kawata & Mulchaey (2008) find that even within low-mass groups strangulation suppressed star formation which would explain why star formation rate of group galaxies is lower than in field galaxies. These findings suggest that the migration of galaxies into denser environments has a significant impact on their evolution and could be driving the evolution of star forming spirals into quiescent ellipticals.

Mergers

When two galaxies come together to form one, this is known as a merger (White & Rees 1978). Mergers are very important in galaxy evolution and have the potential to change a galaxy's morphology, black hole activity and stellar populations. Evidence of past mergers can be seen as tidal tails (Zabludoff et al. 1996), ripples, multiple motions of gas and unusual morphologies (Schweizer 1982). Merger rate is found to vary with cosmological time (Darg et al. 2010; Rodriguez-Gomez et al. 2015. Rodriguez-Gomez et al. (2015) find a strong redshift dependence in the Illustris simulation where merger rate is proportional to $(1+z)^{2.4-2.8}$. This trend is likely due to the expansion of the universe, as the universe becomes less dense with time there is more distance between galaxies such that the rate of collision will decrease. This suggests that galaxy evolution driven by mergers will decrease with time. Whilst density increases the probability of interactions, in the densest environments such as clusters, the high velocity dispersion of galaxies mean that they move too quickly for gravity to take hold and coalescence to occur. Because of this, mergers are less likely to take place in cluster environments and are more likely to occur in 'intermediate' environments, as described by Darg et al. (2010).

Depending on the properties of the two colliding galaxies, mergers can be labelled as either major, intermediate or minor when considering the mass ratio of the two progenitors. If considering the gas content, mergers can be labelled as wet, moist or dry (Sánchez-Blázquez

et al. 2009). Major merger is termed when two galaxies with a mass ratio of 1:4 or smaller collide. Major mergers can drastically distort a galaxy's morphology and are thought to be responsible for producing elliptical galaxies (Cox et al. 2006). Wild et al. (2009) and Snyder et al. (2011) find that particularly gas-rich major mergers are responsible for triggering the starburst phase. Starbursts occur when the tidal torques, triggered in a merger, funnel gas into the galactic core. This increase in gas density provides fuel for a rapid burst of star formation. It is important to note that not all mergers produce an enhancement in star formation (Di Matteo et al. 2008). These types of merger are found to be more common in low-density environments like the 'field' (Bekki et al. 2001; Lin et al. 2010; Sánchez-Blázquez et al. 2009).

Minor mergers occur when the mass ratio is greater than 1:4 but typically greater than 1:10. Studies such as Bournaud et al. (2005) introduce the intermediate merger category for mass ratios between 1:4 and 1:10. Minor mergers are much more common than major mergers due to the distribution function of galaxy mass. Because of this it is thought that minor mergers lead to more efficient growth and contribute more to the late evolution of early-type galaxies (Naab & Burkert 2003).

Mergers can be classified as wet, dry or moist according to the degree of gas involved between the two interacting galaxies. When two elliptical galaxies collide this can be referred to as a dry merger, this is because elliptical galaxies are typically gas deficient. Dry mergers are thought to be the driving force for the late time growth of massive ellipticals found in the Universe. Depending on the type of elliptical progenitor this can have an effect on any tidal features that can be observed post-merger. Dry mergers (as well as moist mergers) reside in environments much denser than wet mergers, this is mainly due to the colour-density relation (Lin et al. 2010).

When two spiral galaxies collide this is known as a wet merger due to the high gas abundance within the galaxies. When two spirals collide (assuming a major merger has occurred) the settled result usually ends in an elliptical galaxy being produced. A collision in this manner can end in two ways, star formation being quenched or a starburst can be triggered. Star formation can be quenched by the removal of the building blocks of stars;

gas and dust. A starburst could be triggered by the unbalanced gravitational potential that cause some regions to become more dense and have an increase in pressure which are key for star-formation (Sánchez-Blázquez et al. 2009).

A moist merger (sometimes referred to as a damp or mixed merger) is when an elliptical and spiral merge. The elliptical may disturb the spiral galaxy's gas however, it will not be as extreme as a wet merger.

Harassment

When two galaxies fly past each other, their gravitational potentials interact which can cause changes to their internal properties and morphologies, this is known as a harassment. Moore et al. (1996) find that whilst direct mergers are rare, most galaxies undergo close encounters with other galaxies frequently and could solve the problem of what mechanism triggers star-bursts in cluster environments. Through hydrodynamical simulations they find that these close encounters have the ability to drive and quench star formation as well as cause morphological changes. Further research by Moore et al. (1996, 1998); Lake et al. (1998); Cales et al. (2013); Sparre & Springel (2017) find similar results and suggest harassment events heat and strip the gas which leads to the suppression of star formation (Mo et al. 2010).

Velocity dispersions in clusters are higher than in field or group environments (Mulchaey & Zabludoff 1998), therefore galaxies are more likely to fly-by each other than coalesce in a merger. The close proximity however, is enough to add turbulence to the gas resulting in the triggering of star formation or the stripping of gas and stars (Tonnesen et al. 2007). Tonnesen et al. (2007) find that for galaxies in the outer regions of the cluster, harassment events are the most likely mechanisms that drive the evolution of cluster galaxies. Moore et al. (1998) find that harassment events are only capable of transforming purely disk galaxies into spheroids whilst giant ellipticals and spiral bulges are not affected. Tonnesen et al. (2007) find that whilst ram pressure stripping is the dominant mechanism of evolution in cluster galaxies, harassments also play a significant role in the evolution of galaxies.

1.3.3 Evolution Through Internal Secular Processes

Galaxies do not necessarily need external processes to determine how they evolve. Internal mechanisms, such as stellar feedback from both supernova, AGN and stars, can contribute to the distribution and density of the gas within, therefore regulating its own star formation. These internal processes make up what is known as secular evolution which act slowly over a galaxy's lifetime and do not necessarily disturb galaxy morphology. Below, we discuss the two main internal secular process that contribute to the evolution of galaxies.

Disc and Bar Instabilities

The most common secular process that contributes to galaxy evolution stems from instabilities in the disk, particularly in the bar of spiral galaxies (Combes & Sanders 1981; Masters et al. 2010b). Kormendy & Kennicutt (2004) find that gas funnels along the bars from the outer disk to the galactic centre, this promotes growth of the bulge. The enhancement in gas fraction around the core could trigger a nuclear starburst whilst at the same time emptying the gas reservoir in the outer disk, quenching star formation in the outer regions (Masters et al. 2010b). This suggests that the disks in galaxies form first and bulges develop later as galaxies evolve (Courteau et al. 1996). Debattista et al. (2006) use simulations to investigate the secular evolution of disk structures, they find that bars within disk galaxies are robust such that they are difficult to destroy and are more resistant to mechanisms that would otherwise disrupt a disk. Discs are present in approximately 30% of spirals at both low (Sellwood & Wilkinson 1993) and high redshift (Jogee et al. 2004) so are likely to play an important and significant role in secular evolution of disk galaxies.

The disks in spiral galaxies are not perfect and in almost every case their symmetry is broken resulting in branching arms and fragmented regions (Sellwood & Carlberg 1984). A disk becomes unstable when its surface density is high enough, and the velocity dispersion and circular velocity are low enough (Toomre 1964). As the disk begins to fragment and clumps grow, these clumps eventually begin to collapse so that their surface density becomes higher than the general molecular cloud populations (Ceverino et al. 2010). These now dense gas rich regions are the perfect environment for star formation to occur and possibly migrate to

the core of the galaxy triggering a starburst (Dekel et al. 2009; Ceverino et al. 2010; Cacciato et al. 2012; Sparre et al. 2015).

Stellar Feedback

When stars come to the end of their life, they explode and their luminosity becomes as bright as their host galaxy, this is known as a supernova Prialnik (2009). These events are rare as the enhancement of their luminosity only lasts between several months and a few years. Supernova are powerful enough to effect star formation through both kinetic (Dalla Vecchia & Schaye 2008) and thermal feedback (Dalla Vecchia & Schaye 2012). Supernova explosions produce bubbles of enriched hot gas that inject kinetic energy into their surroundings, creating turbulence in the interstellar medium (ISM). The walls of these bubbles however, are composed of cold dense gas that has built up during the formation and expansion of the bubble (Fierlinger et al. 2016). The bubble walls provide ideal conditions for star formation (Deharveng et al. 2010; Koenig et al. 2011; Yasui et al. 2016). As well as promote star formation, supernova explosions quench star formation. A shock wave is produced in a supernova explosion, this shock wave can disrupt surrounding molecular clouds halting star formation within. Within the outer envelope of the bubble, mixing occurs between the hot gas in the bubbles and the cold gas built up in the wall. Mixing heats up the ISM making it unusable for star formation. Newton & Kay (2013) find that in isolated galaxies, supernova feedback dominates quenching, whilst in mergers strong feedback from AGN dominates. Hopkins et al. (2012) find that only the combination of stellar and supernova winds are capable of driving galaxy-scale winds. Single mechanisms are not enough to generate observed galactic winds.

Modelling Star Formation and Feedback in Simulations

Later in this thesis, we use the Illustris simulation to investigate the triggering and quenching mechanisms of starburst galaxies. Simulations, like Illustris, model a volume of the Universe (Crain et al. 2015; Vogelsberger et al. 2013). The simulated Universe is split into a grid, in the case of Illustris, the grid is adaptive such that higher density regions become more resolved (Vogelsberger et al. 2013). Due to size and mass resolution, a sub-grid analytical prescription

is required that dictates how and when star formation is triggered. When conditions satisfy a pre-defined equation, star formation occurs and a distribution of stars are formed based on the initial mass function used in the simulation. Stellar and AGN feedback is modelled by injecting energy into the surrounding grid in the form or kinetic or thermal energy, or a combination of the two defined within the code. This feedback affects the conditions of the gas within the grid and either halts or promotes star formation. Due to the size and mass limitations, individual stars or molecular clouds cannot be resolved, so instead cells of gas, dark matter and stars are used to represent populations of particles. Some of the issues found by using a sub-grid model are disks of spirals that are less extended than observed (Crain et al. 2015),

1.4 E+A Galaxies

The Butcher-Oemler effect describes how the cores of intermediate redshift clusters contain a higher fraction of bluer galaxies than those at low redshifts (Butcher & Oemler 1978) however, why these galaxies are bluer was not fully understood. Whilst studying the blue excess (the difference between the observed colour index and the mean colour index) in high redshift clusters, Dressler & Gunn (1982, 1983) discovered E+A galaxies. In their sample, they find that 26 galaxies display spectra showing no [OII] or Hα emission but have deep Balmer absorption lines. [OII] is typically seen when there is on-going star formation because of its absence this means star formation has ceased, from this you'd expect to see old K-class stars. The presence of a Hδ absorption line however, is a typical sign of A-class stars which are young and recently formed. This mix suggests a recent starburst, approximately 1-5 Gyr ago, which is a relatively short time-scale, meaning these galaxies are rare (Dressler & Gunn 1983). Another study investigating the Butcher-Oemler effect, via a spectroscopic study of three rich galaxy clusters is Couch & Sharples (1987). They find that the blue excess in these clusters display signs of a starburst that occurred 0.1 to 1.5 Gyr ago (these are now known to be E+As due to their elliptical morphology and significant fraction of A-class stars). E+A galaxies, also known as 'k+a' galaxies due to the mixture of K- and A-class stars, are a type of post-starburst galaxy. They are rare and by identifying them we are essentially catching them

in the act of transitioning from spirals to ellipticals. Rodighiero et al. (2011) find that whilst starbursts play only a minor role in star formation they play a critical role in quenching star formation and transforming morphologies of galaxies. It is estimated that 30% of elliptical galaxies have passed through this phase at some point in their lifetime making the E+A phase an important part of galaxy evolution (Tran et al. 2003; Goto 2005). In this section, we discuss their discovery, properties and why they are vital at gaining a better understanding of how galaxies evolve.

1.4.1 Morphology and Colour

E+As are primarily blue, however, studies by Tran et al. (2004) and Vergani et al. (2010) find that E+As are positioned towards the redder end of the blue cloud and reaching out into the green valley. However other studies by Quintero et al. (2004) and Hogg et al. (2006) find opposite results, they find E+As are positioned towards the bluer end of the red sequence and into the green valley. Whilst different, these studies both state E+As are found in the green valley, reinforcing the idea that these galaxies are in a transitionary phase between blue star forming spirals and red and 'dead' ellipticals. But why are different colours being observed? Could it be that the selection methods used have an effect on observed colour or could dust obscuration be the reason?

Further studies, such as Yang et al. (2004), find that most of these blue galaxies are either elliptical or S0 type galaxies and some studies find E+As can contain a prominent disk (Tran et al. (2003); Yang et al. (2004)). The S0 morphology found by Yang et al. (2004) supports the hypothesis that E+A galaxies are a link between spirals and ellipticals. Yang et al. (2004) find that E+As are generally bulge dominated but can have an underlying disk. Could the different colours observed in E+As correlate with the presence of disks? Their surface brightness profiles have been found to resemble a power-law, like those found in early-type galaxies. Tran et al. (2003) finds that for cluster E+As, their underlying disk is more prominent than those in the field environments which could indicate that environmental effects play a role in galaxy evolution. Varying results of the colour and morphologies of E+As have been found which means there are still open questions regarding the status of E+As. This thesis aims to

shed light on what processes cause these variations.

1.4.2 Environment

E+As are found in both cluster (Dressler & Gunn 1983) and 'field' environments (Zabludoff et al. 1996). Tran et al. (2003) finds that between 7% and 13% of clusters at $z > 0.33$ contain E+As. They find that only low-mass E+As appear in nearby cluster. Similar results are found by Poggianti et al. (2009) who find that E+As are predominantly found in clusters at high redshifts ($z > 0.4$). Other results suggest that E+As prefer weak group environments with between 4 and 10 group members. When examining local X-ray bright clusters, Mahajan (2013) finds the presence of substructure amongst 86% of the clusters. Substructure is when clusters are clumpy, and are almost made up of multiple smaller groups. Within 91% of these groups, E+A galaxies were found leading to the conclusion that E+A are pre-processed before entering the cluster environment. Pre-processing occurs when a galaxy enters a group environment before that group is accreted onto a cluster.

Whist many studies have primarily focused on the cluster environment at intermediate redshifts, there are a vast number of articles that suggest E+As prefer a weaker and less dense field environment. The main study focusing on the environment of E+As is Zabludoff et al. (1996). They find that out of a sample of 21 local E+As, 75% are located within the field. Their work was inspired by the work of Oegerle et al. (1991) who find at least one E+A that is not in a rich-cluster. The fraction of E+As are found to correlate with redshift. Studies such as Dressler & Gunn (1983), Fabricant et al. (1991) and Caldwell et al. (1993) find that E+As are scarcer towards low redshifts, accounting for less than 1% at $z = 0$ from approximately 10% at $z = 0.3$. Whilst still rare, Caldwell et al. (1993) find there are sufficient numbers locally to examine their properties and environments. Blake et al. (2004) find that E+As tend to follow the general galaxy population which are field dominated at low redshifts and cluster dominated at higher redshifts.

1.4.3 Triggers and Quenching

During earlier studies, which focus on cluster E+As, their triggers and quenching mechanisms were speculated to be such process as ram pressure stripping (Dressler & Gunn 1983) or

interactions with the cluster potential (Byrd & Valtonen 1990). However, in the majority of studies, mergers have been attributed to triggering starbursts. Articles such as Carter et al. (1988), Oegerle et al. (1991) and Zabludoff et al. (1996) find some of the E+As in their samples display tidal features, such as tails, which are linked to previous mergers. Liu & Kennicutt (1995) find evidence of mergers within the field having spectra analogous to E+A galaxies, this indicates merger remnants could evolve into E+A galaxies.

But what quenches a starburst? RAM pressure stripping is thought to play a role in quenching, if assuming the post-starburst galaxy is accreted onto a cluster (Dressler & Gunn (1983); Byrd & Valtonen (1990)). But, for the majority of studies focusing on the quenching mechanisms within starbursts, AGN feedback has been extensively discussed (Caldwell & Rose 1997; Kaviraj et al. 2007; Melnick et al. 2015; Baron et al. 2017). Yet to what extent AGN play a role in quenching is still undetermined. Studies such as Cicone et al. (2014) and Yesuf et al. (2014) suggest that AGN do not play a role in the initial quenching of star formation in the burst but complement mechanisms in the burst that quench star formation. Cicone et al. (2014) find that AGN enhance the outflows of the starburst, pushing gas away from the central star forming region whilst Yesuf et al. (2014) find that AGN only suppress low-level star formation after the initial quenching has taken place. However, other studies such as Coil et al. (2011) find that galactic winds driven by supernova, not AGN as suggested by Debuhr et al. (2012), are strong enough to quench star formation.

1.5 Summary

In this section, we summarise the main findings within the literature regarding starburst and post-starburst galaxies. Studies by Zabludoff et al. (1996) and Blake et al. (2004) show that E+As at low redshifts predominantly reside in low density environments however, some clusters and groups can contain E+As (Dressler & Gunn 1983; Poggianti et al. 2009). However, little is known as to whether triggering and quenching mechanisms differ between these two density regimes or if pre-processing allows E+As to move from low to high-density environments.

By examining colour and morphology of E+As, we find conflicting results. Poggianti

et al. (1999) and Poggianti et al. (2009) state that E+As display a bi-modal colour distribution, whilst work by Tran et al. (2004) and Vergani et al. (2010) describe E+As as being 'green valley' galaxies, this disagrees with earlier work by Dressler & Gunn (1983) and Yang et al. (2004) who find E+As to be primarily blue in colour. Similar difference are found in morphologies of E+As. Initial studies by Dressler & Gunn (1983) describe E+As to be blue ellipticals, however, recent studies by Tran et al. (2003) and Yang et al. (2004) find they resemble an S0 morphology in which there is the presence of a central bulge with and underlying disk. Work by Zabludoff et al. (1996) also find tidal tails in some E+As suggesting mergers to be the primary trigger for starbursts and findings by Melnick et al. (2015) and Baron et al. (2017) suggest AGN are responsible for quenching. However, there are little comparative studies into triggering and quenching mechanisms to draw conclusive results as to the principle mechanisms. The selection criteria used in these studies are not coherent which leads us to believe this is the cause for variations in results. If selection criteria don't have a significant impact on the observed properties of post-starburst galaxies then what is driving these variations?

1.6 Thesis Aims

Whilst there has been extensive study on starburst and post-starburst galaxies, there are still conflicting results found in the literature, such as differing colours, morphologies and environments of E+A galaxies. The extent at which mergers play a role in triggering starbursts and the processes that quench them are still heavily debated. This thesis aims to investigate the nature of starburst and post-starburst galaxies, both a significant phase in galactic evolution. In this thesis, we aim to answer the following science questions:

- How do different selection methods of post-starburst galaxies have an impact on the properties observed?
- What are the main triggers of starburst, and hence, the post-starburst galaxies in the Illustris simulation?
- Do starburst galaxies have a top-heavy IMF and produce heavier stars than quiescently

star forming galaxies?

- To what extent do AGN play a role in quenching star formation in starburst galaxies which lead to the post-starburst phase?

In Chapter 2, we test three selection methods of E+A galaxies to determine what differences arise in their observational properties. In Chapter 3, we use the Illustris simulation to track starburst galaxies over a 4 Gyr period to determine what are their triggers and how this affects their properties. In Chapter 4, we use radio data from the FIRST survey to determine whether the IMF in starburst galaxies are top-heavy and if any radio AGN are present. In Chapter 5, we summarise and conclude our findings from this thesis.

2. The Evolutionary Sequence of Post-Starburst Galaxies

Declaration

This Chapter consists of the published work 'The Evolutionary Sequence of Post-Starburst Galaxies' (Wilkinson et al. 2017) in Sections 2.1-2.8. This work selects post-starburst galaxies using different selection methods found in the literature and examines how these different methods affect observational properties. In Section 2.9, we build on this published work and include analysis which did not make it into the published article.

Abstract

There are multiple ways in which to select post-starburst galaxies in the literature. In this work, we present a study into how two well-used selection techniques have consequences on observable post-starburst galaxy parameters, such as colour, morphology and environment and how this affects interpretations of their role in the galaxy duty cycle. We identify a master sample of Hδ strong (EW$_{H\delta}$ > 3Å) post-starburst galaxies from the value-added catalogue in the 7th data release of the Sloan Digital Sky Survey (SDSS DR7) over a redshift range 0.01 < z < 0.1. From this sample we select two E+A subsets, both having a very little [OII] emission (EW$_{[OII]} > -2.5$Å) but one having an additional cut on EW$_{H\alpha}$ (> -3Å). We examine the differences in observables and AGN fractions to see what effect the Hα cut has on the properties of post-starburst galaxies and what these differing samples can tell us about the duty cycle of post-starburst galaxies. We find that Hδ strong galaxies peak in the 'blue cloud', E+As in the 'green valley' and pure E+As in the 'red sequence'. We also find that pure E+As have a more early-type morphology and a higher fraction in denser environments compared with the Hδ strong and E+A galaxies. These results suggest that there is an evolutionary sequence in the post-starburst phase from blue disky galaxies with residual star formation to passive red early-types.

2.1 Introduction

Post-starburst galaxies are a vital link between star-forming spirals and quiescent E/S0 galaxies. E+A galaxies, also known as k+a galaxies, are a specific type of post-starburst galaxy that were identified by Dressler & Gunn (1983) as having an elliptical morphology but rich in A-class stars. Dressler & Gunn (1983) find that 26 E/S0 galaxies display spectra showing no [OII]$_{\lambda 3727}$ or Hα emission but have deep Balmer absorption lines. The absence of [OII] indicates that there is no ongoing star formation whilst the presence of Hδ absorption is a typical sign of young and recently formed A-class stars. This mix of spectral lines and morphology suggests a recent starburst approximately 1-3 Gyr ago, that has been quenched by an 'unknown' process (Dressler & Gunn 1982; Couch & Sharples 1987).

E+A galaxies are thought to be a transitionary phase between star-forming disks and quiescent early-type galaxies. Since their discovery, there have been many studies on E+As, but there is a large variance on how they are defined. Most observational work adopts a lack of [OII] emission and strong absorption in the Hδ Balmer line to classify E+As (Poggianti et al. 2009; Vergani et al. 2010; Rodríguez Del Pino et al. 2014). Some have combined the Balmer absorption lines such as Hδ with Hγ and/or Hβ (Zabludoff et al. 1996; Norton et al. 2001; Chang et al. 2001; Blake et al. 2004; Tran et al. 2004; Yang et al. 2004) in order to maximise their E+A samples.

However, there are a number of studies that use a lack of Hα emission (an indicator of star-formation) in their selection, such as Quintero et al. (2004), Hogg et al. (2006), Goto (2007a) and Goto (2007b). While this method eliminates dusty star-formers it simultaneously excludes those E+As that contain Hα caused by an active galactic nucleus. With different lines being used to select post-starburst galaxies, we ask if this has an impact on their characteristics and what can this tell us about their star formation duty cycle?

In earlier works E+A galaxies have been observed to be blue (Dressler & Gunn 1983; Couch & Sharples 1987). This disagrees with the original belief that galaxies turn red immediately after a starburst (Larson et al. 1980). Poggianti et al. (1999, 2009) select E+As on the basis of having EW$_{[OII]}$ emission < 5Å and EW$_{H\delta}$ absorption > 3Å and find that there are two populations of E+As; blue and red, although without a discussion of their origin.

Further works by Tran et al. (2004) and Vergani et al. (2010), who select E+A primarily on [OII] emission and Balmer absorption lines, find that their location on a colour magnitude diagram is towards the redder end of the blue cloud and into the green valley. However, Quintero et al. (2004) and Hogg et al. (2006), who select E+As without Hα emission, find that E+As are located towards the bluer end of the red sequence and into the green valley on the colour-magnitude diagram. This suggests that the lack of Hα emission could be the cause of the red E+A galaxies found in Poggianti et al. (1999).

Work on the morphology of E+A galaxies reveals them to be generally bulge dominated and in some cases having an underlying disk component (Tran et al. 2004, Quintero et al. 2004). This combination of bulge and disk components replicates the S0 type morphology and reinforces the link between late- and early-type galaxies. This may suggest that the starburst triggering the E+A phase is centrally located, and not in the disk. The latter study opts for different selection methods yet their results on morphology are unanimous: Hα has no effect on the morphology of post-starburst galaxies. Poggianti et al. (1999) find that the majority of E+A galaxies contain signs of spiral morphology; this indicates that the time-scale or process responsible for quenching star-formation is different from the process responsible for a morphological transformation. In turn, this could indicate multiple processes involved in triggering the E+A phase. Some have been shown to have a disturbed morphology, which is an indicator of a recent merger (Yang et al. 2004). By identifying E+A galaxies we are essentially catching them in the act of transition. Not all starbursts are strong enough to trigger the E+A phase (McIntosh et al. 2014), but it is estimated that 30% of elliptical galaxies have passed through the E+A phase at some point during their evolutionary duty cycle (Tran et al. 2003; Goto 2005) making the E+A phase an important and significant part of galaxy evolution.

The properties of E+A galaxies are found to vary with different environments. For example, cluster E+A galaxies contain a more prominent disk component than those outside a cluster (Tran et al. 2003) and are found to be 1.5σ bluer than those in the field at $z \sim 0.1$. This finding goes against the typical colour-density relation that suggests galaxies in clusters should be redder, not bluer (Hogg et al. 2003). This difference in colour is attributed to

differing galaxy masses in both field and cluster E+A galaxies. Clusters have been found to contain much smaller E+As than in the field (Tran et al. 2003).

E+A galaxies are found both in a cluster environment as well as a field environment, however, different studies show different environmental preferences. From a sample of 21 nearby E+A galaxies (selected by [OII] and Balmer lines) from the Las Campanas Redshift Survey, Zabludoff et al. (1996) finds 75% of the E+As are in the field. They find 5 E+A galaxies within their sample display tidal features, a typical sign of galaxy-galaxy interactions and mergers. This suggests that mergers and galaxy-galaxy interactions could be the trigger for the E+A phase. The type of mergers found to dominate in low density environments are gas-rich (Bekki et al. 2001; Lin et al. 2010; Sánchez-Blázquez et al. 2009) which are most likely to trigger a starburst strong enough of producing an E+A signature.

When Hα is included into the selection criteria different results are found; Mahajan (2013) find that E+A galaxies prefer a weak-group environment ranging from 4 to 10 galaxies. For local X-ray bright galaxy clusters at $0.02< z <0.06$, they find 86% of local clusters contained some form of substructure on a weak group-scale (4-10 members) and 91.4% of these weak-groups contained E+A galaxies. This result suggests that star-formation is quenched due to a galaxy being pre-processed in a weak-group environment before being accreted into a cluster environment.

Opposite results are found by Poggianti et al. (2009): at higher redshifts ($0.4 < z < 0.8$) E+A galaxies are predominantly in clusters where the star-formation has been quenched on a short time scale of $\ll 1$ Gyr. Poggianti et al. (2009) find only a few E+A galaxies are located in other environments such as the field and in weak-groups and that the variation in E+A fraction is found to be dependant on environment (Mahajan 2013). Regardless of whether Hα has been used in the selection criteria of E+As there is a discrepancy in what different works report with regards to environmental preference. Lemaux et al. (2016) suggests that 'true' E+As (those with no Hα) have a higher fraction in a cluster environment compared to those selected by 'traditional' methods (using only Balmer absorption lines and the absence of [OII]). Could environment be driving changes in Hα emission or are we seeing two different stages of the E+A duty cycle?

A typical sign that star-formation has ceased is a lack of Hα emission and as E+As galaxies are no longer producing stars, one would expect to see no significant Hα emission. Although not commonly used as a criteria for E+A selection, this work aims to test whether including a cut in Hα could explain some of the differences found in other studies and connect up these potentially different phases of post-starburst evolution. Here we present a study of the properties of low redshift post-starburst galaxies using different selection criteria from the Sloan Digital Sky Survey Data Release 7 (SDSS DR7; Abazajian et al. 2009) with the broad aim of testing the star formation duty cycle of post-starburst galaxies.

In section 2.2, we describe the data used in this study and the different selection cuts we impose. In sections 2.3, 2.4, 2.5 and 2.6, we analyse and discuss the results. Our discussion and conclusions are presented in sections 2.7 and 2.8. We assume the following cosmological parameters for a flat Universe: $H_0 = 69.3\,\mathrm{kms}^{-1}\mathrm{Mpc}^{-1}$, $\Omega_\mathrm{M} = 0.238$ and $\Omega_\Lambda = 0.762$ (Spergel et al. 2007).

2.2 Sample Selection

Using the MPA/JHU value-added catalogue from SDSS DR7 (Abazajian et al. 2009), we create a master sample of 234 Hδ strong ($\mathrm{EW}_{H\delta} > 3$Å; note that positive/negative values for equivalent widths refer to absorption/emission respectively) post-starburst galaxies with $0.01 < z < 0.10$. This limit on Hδ is comparable to studies such as Poggianti et al. (1999), Bekki et al. (2001), Vergani et al. (2010) and Rodríguez Del Pino et al. (2014). The lower limit on the redshift range ensures we exclude any stars from our sample. Although the SDSS spectroscopy aims to be 100% complete at r = 17.77 (Strauss et al. 2002), we find that our sample is ~80% complete at this level, as shown in Fig.2.1. In this study and throughout this thesis, we use the 'model' magnitudes from SDSS in the r-band as it provides the best SDSS colours. SDSS calculates magnitudes based on an exponential and de Vaucouleurs light profile, the model magnitude uses the best of these two fits. We note here, that at these low redshifts, k correction is negligible and therefore we do not apply k corrections to our magnitudes. Most studies of post-starbursts use a typical S/N of 3-5 in the continuum, as evidenced by Pracy et al. (2005) (S/N > 5); Couch & Sharples (1987) (S/N > 3) and Brown

Sub-Sample	N	Hδ	O[II]	Hα
Hδ Strong	192	> 3 Å	-	-
E+A	67	> 3 Å	> -2.5 Å	-
Pure E+A	25	> 3 Å	> -2.5 Å	> 3 Å

Table 2.1: This table shows the selection criteria for each of our three sub-samples; Hδ Strong, E+A and pure E+A galaxies. We have also listed the number of galaxies in each of the sub-samples.

et al. (2009) (S/N > 4), hence we adopt a minimum S/N of 5.

Our complete S/N > 5 Hδ strong sample contains 192 galaxies. In the appendix, we list these galaxies in a data table (A.1), listing their positions and spectral lines used in our selection method. Using this sample we apply additional cuts to create a further two sub-samples; E+As and 'pure' E+As (E+As with low Hα emission) in order to test whether different criteria for post-starburst galaxies can explain the differences found in literature and to gain a better insight into the post-starburst duty cycle.

Our first sub-sample is based on the Poggianti et al. (1999) definition of E+A galaxies. With the primary selection of $EW_{H\delta}$ > 3Å, we apply an additional cut of > −2.5Å in the equivalent width of $[OII]_{\lambda 3727}$ (Zabludoff et al. (1996); Yang et al. 2004). This sample of E+As contains 67 galaxies.

To account for this, our second sub-sample ensures there is no ongoing (potentially dusty) star-formation in the E+A sample by applying a further cut in Hα emission ($EW_{H\alpha}$ > -3Å) (Goto 2007b). Doing this we obtain 25 pure E+A galaxies. We list the selection criteria for our three post-starburst sub-samples in table 2.1.

We test whether or not we would expect to see Hα given the limit on [OII] emission stated above. We use a simple approach by plotting $EW_{[OII]}$ against $EW_{H\alpha}$ as shown in Fig. 2.3. In this plot we witness a significant amount of scatter (regression analysis gives R^2 to be 0.3), however, there is an underlying trend present and we are able to fit a regression line using a robust linear model (Huber 1981). From this we see at the $EW_{[OII]}$ limit we would expect $EW_{H\alpha}$ to be -2.1Å in emission. On average the [OII] cut should remove any significant star formation indicated by Hα. However, the large scatter means that there is a population of

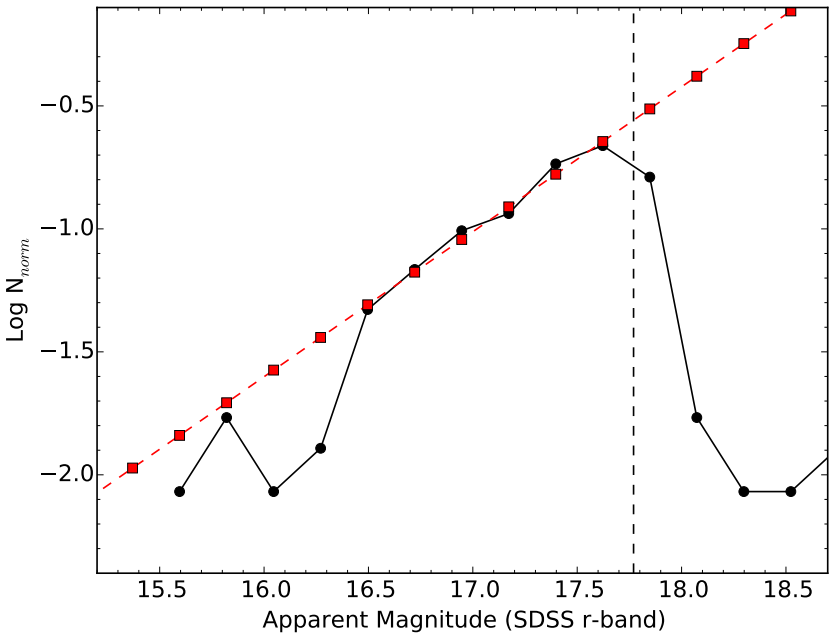

(a)

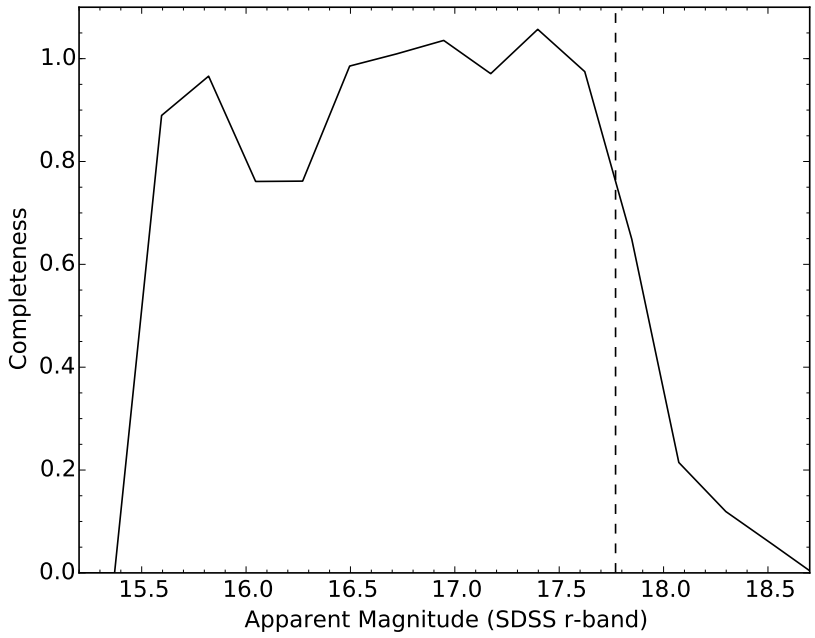

(b)

Figure 2.1: Plot (a) shows the normalised distribution of apparent (model) magnitude in the SDSS r-band of our Hδ strong galaxy sample. The red dashed line shows the line of best fit which is plotted to the linearly increasing region(16.5<r<17.5). From this line we obtain plot (b) that shows a completeness diagnostic plot, here we find that we are ~80% complete to a magnitude limit of r=17.77. The dip observed around magnitude 16 could be an effect of having low number statistics towards higher masses.

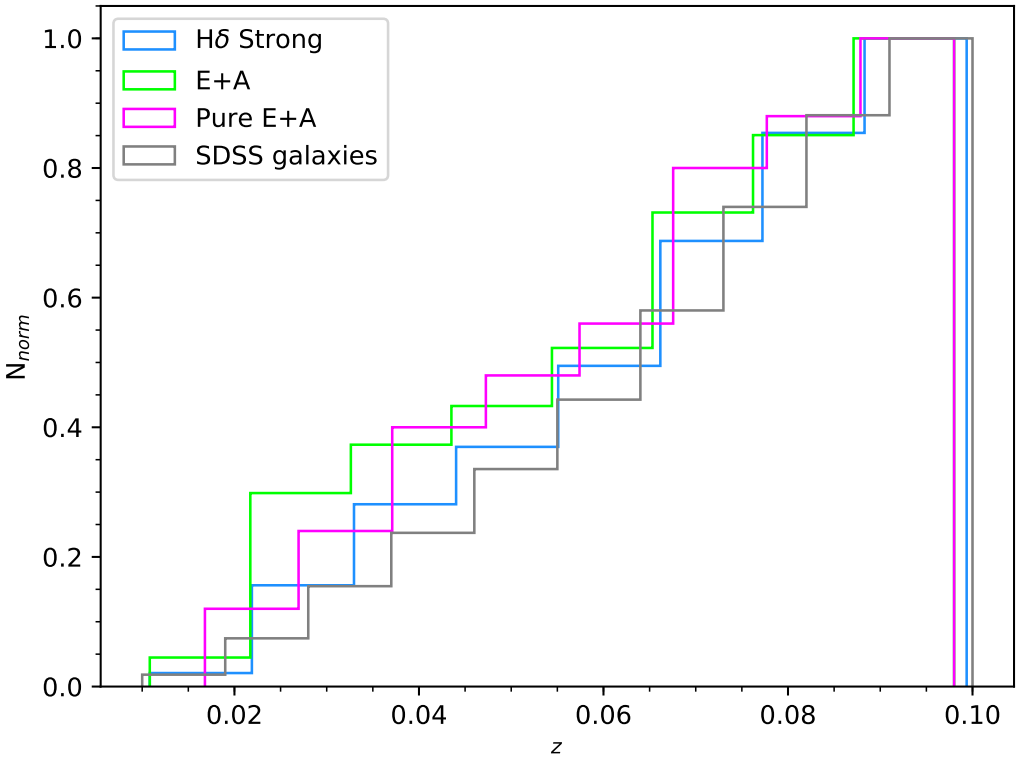

Figure 2.2: This plot shows a cumulative histogram of the redshift distributions of our three sub-samples; Hδ strong, E+A and 'pure' E+A galaxies. We see that within our selected redshift range, E+A galaxies take a preference for a more local redshift.

galaxies with up to EW=-15Å of Hα emission at the [OII] limit (See fig. 2.3). We also calculate the star formation rate derived from the Hα flux, SFR$_{H\alpha}$ from Kennicutt (1998) and apply an extinction correction ($10^{A/-2.5}$) from Treyer et al. (2007). Assuming Av = 0.5 we find the average SFR$_{H\alpha}$ for Hδ strong galaxies that didn't make the E+A cut to be 0.07M$_{\odot}$/yr^{-1}. For the E+A that are not classed as pure we find SFR$_{H\alpha}$ to be 0.06M$_{\odot}$/yr^{-1} and pure E+A have an average SFR$_{H\alpha}$ of 0.01M$_{\odot}$/yr^{-1}. Stacked spectra for our three sub-samples can be found in Fig. 2.4. We note here that emission-filling could potentially affect our Hδ measurements. We believe this would be a small effect (Goto et al. 2003c; Blake et al. 2004). However, the usual method of measuring this in conjunction with, e.g., Hα to determine the strength of its effect is unable to be achieved due to our sample selection approach. We note here that we do not apply a correction for extinction in the magnitudes used for selection.

2.3 Colour

In this section we investigate whether the differences in selection criteria, based on spectral lines, has an impact on the colours of the post-starburst population. This will allow us to determine why Poggianti et al. (1999, 2009) finds two populations of E+A galaxies that peak in the red sequence and blue cloud.

To study the differences in colour between our samples we first plot a colour magnitude diagram, shown in Fig. 2.5. Using the galaxies from the SDSS DR7 catalogue, we are able to locate the red sequence and blue cloud regions and over plot our samples to see which regions they reside (Fig.2.5).

We include a colour histogram (Fig. 2.6) that shows the bimodality of the colour distribution. Using Fig. 2.5 and Fig. 2.6 we find that the Hδ strong sample peaks in the blue cloud with a median colour of 1.36±0.04. The E+A sample peaks in the green valley with a median colour of 1.46±0.04. We find that the pure E+As predominantly reside in the red sequence with a median colour of 1.66±0.04.

Hogg et al. (2006) select E+A galaxies using a cut in Hα and find that E+As are located in the red sequence towards the green valley. While E+As have a significant connection to the green valley (Vergani et al. 2010), we find that by selecting E+As using Hα emission we

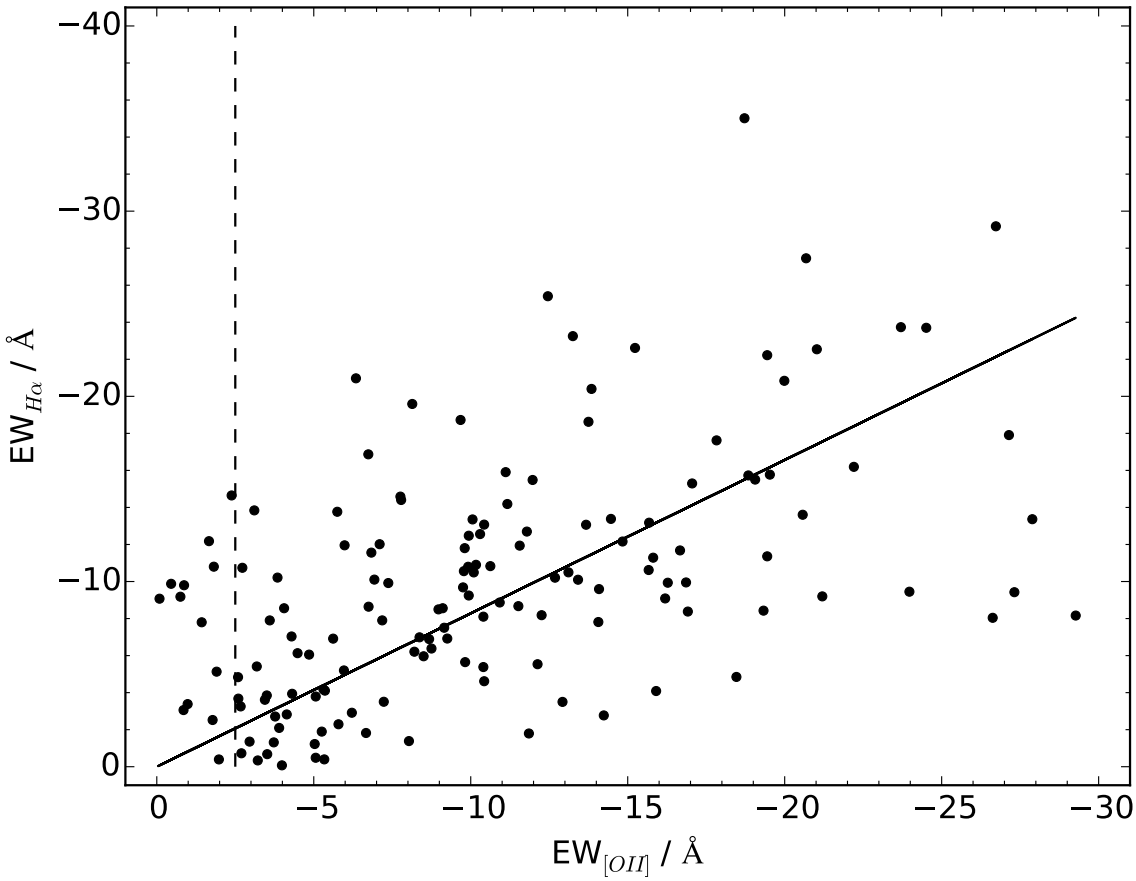

Figure 2.3: This plot shows the equivalent widths of [OII] and Hα. Note that positive/negative values for equivalent widths refer to absorption/emission respectively. The [OII] limit has been highlighted by the dashed line. The trend line (solid) has been fitted using a robust linear regression model (Huber 1981). This plot shows a significant amount of scatter in which R^2=0.30.

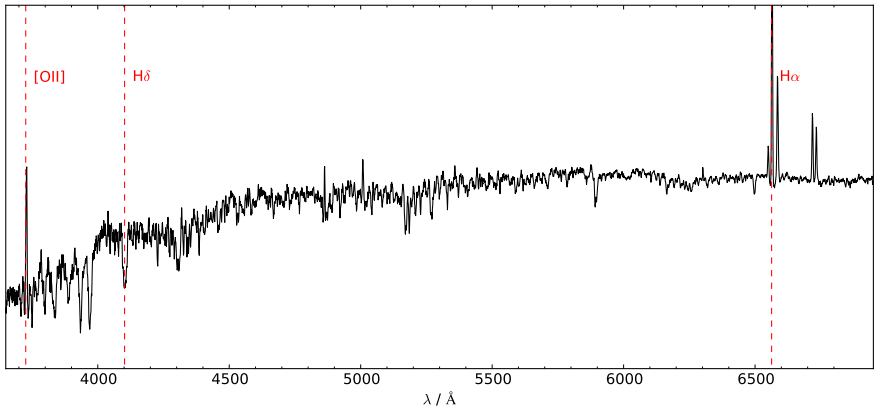

(a)

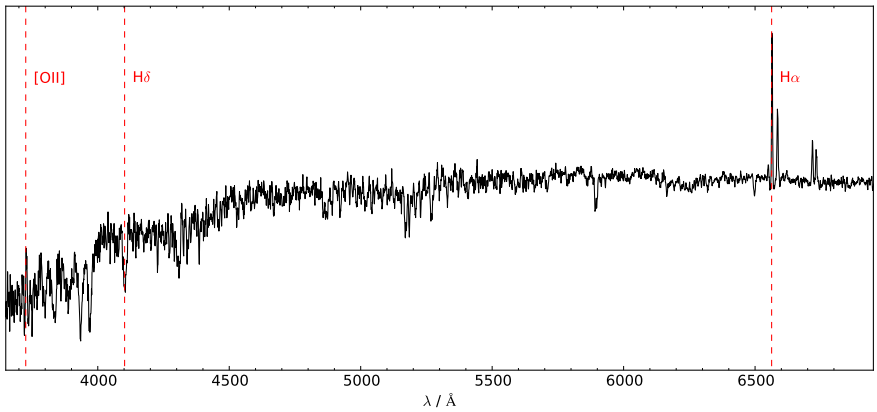

(b)

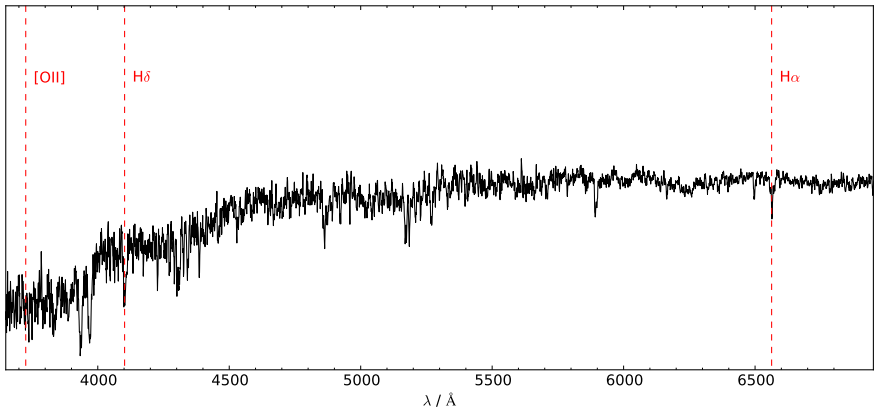

(c)

Figure 2.4: These are stacked median spectra for each of the populations of post-starburst galaxies in this study; Hδ strong (top), E+A (middle) and pure E+A (bottom). We have included the locations of the three spectral lines used for selection in this study (dashed lines). The y-axis is arbitrary flux units.

are predominantly selecting those towards the red sequence as star formation has ceased and the galaxies are truly passive.

To test whether the E+A and pure E+A samples are distinguishable we apply a two sample Kolmogorov-Smirnov statistical (abbreviated to KS onwards) test. When comparing the E+A sample with the pure E+As the KS test returns a p-value of 0.007 which demonstrated that E+As and pure E+As are unlikely to be drawn from the same parent distribution. In this study we consider any p-value less than 0.01 to be statistically different, whilst p-value over 0.1 we consider to be the same. P-values between these limits we consider to have a weak difference.

To test the distinguishability between the E+A sample and the Hδ strong sample, we apply the same test and output a p-value of 0.110. These distributions are likely to be from the same parent distribution. When we take Hδ strong galaxies that are not defined as E+As and compare to the E+A sample we get a p-value of 0.005. This means there is a statistical difference between non-E+A Hδ strong galaxies and E+A galaxies. Fig. 2.6 clearly shows that the pure E+A sample and the Hδ strong sample are statistically different. To quantify the distinguishability of the Hδ strong sample and pure E+As we include a p-value which is found to be 10^{-6}.

2.4 Morphology and Morphological Parameters

To explore the differences in findings on morphology we test the morphological fractions of each sample using the Galaxy Zoo (GZ) catalogue (Lintott et al. 2008, 2011). The GZ project provides an extensive catalogue of galaxy morphologies and is based on the data from SDSS. GZ is a citizen science project in which volunteers view images of galaxies and cast their vote as to whether the galaxy is elliptical, spiral, merger or unknown. We assign a classification of elliptical, spiral or merger to our galaxies if that classification takes 50% or more of the votes. The minimum number of votes per galaxy in our sample is 16 and the mean number of counts our sample has is 39.5. We note here that S0 galaxies are not easily distinguishable from the elliptical and spiral morphologies in the GZ catalogue. Whilst the majority of S0 galaxies are within the elliptical classification there will certainly be S0 contamination in the spiral classifications (Bamford et al. 2009). To ensure visual classifications are correct, we

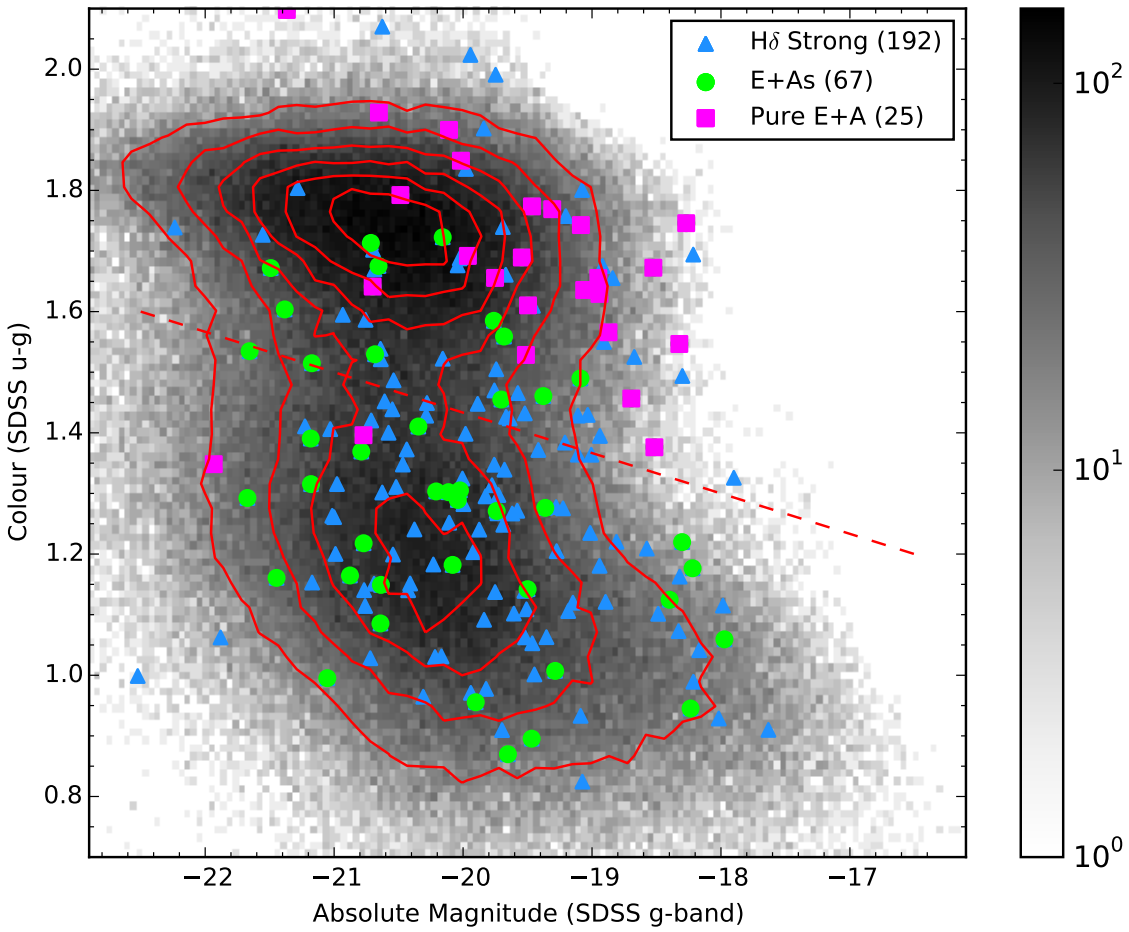

Figure 2.5: This plot shows a colour magnitude diagram with contour lines (red) that show the regions of the red sequence and blue cloud separated by a dashed line to guide the eye. These regions are based on the SDSS DR7 data shown in grey. The vast majority of pure E+As present predominantly lies in the red sequence whilst the remaining sample reside mainly in the blue cloud. We have included the number of galaxies in each sub-sample in brackets within the legend.

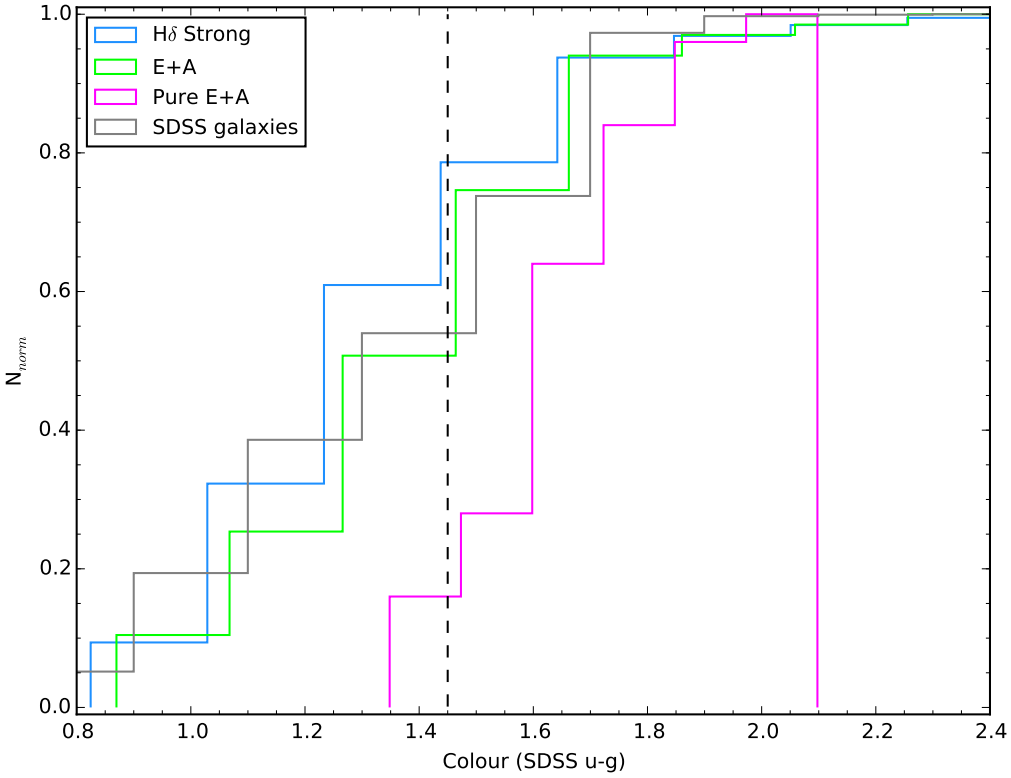

Figure 2.6: This histogram shows the cumulative distributions of colour between the three samples in this study and SDSS galaxies. From this we see there is a greater proportion of Hδ strong and E+A galaxies in the blue cloud compared to the pure E+As that are well established in the red sequence.

cross-check all the galaxies from our master catalogue and find the galaxy zoo classifications are in an agreement with our own.

We find that from our Hδ strong sample we are able to match 185 (96.4%) galaxies to the GZ catalogue. This in turn means we matched 62 E+As (92.5%) and 21 pure E+As (84.0%) to the catalogue. The morphology fractions for each of the samples are shown in Table 2.2. We find that there is no statistically significant merger fraction in either of the three samples, this is due to the very low numbers that were identified. We find that ~55% of the Hδ strong sample have a spiral morphology and ~30% have an elliptical morphology. There is a clear majority here for a preference of disk morphologies. This result somewhat changes in the E+A sample in which there is a ≈50/50 (42%/44%) split between the elliptical and spiral morphologies for those matched to GZ. However, in the pure E+A sample we see ~80% of the galaxies are classed as ellipticals and no significant spiral fraction. This is in agreement with the findings that pure E+As are redder than the Hδ strong and E+A galaxies and occupy the red sequence with the majority of early-type galaxies. Interestingly we note that mergers make up less than 5% of any of the post-starburst categories and therefore do not seem to be important for this phase of galaxy evolution.

As well as using the GZ catalogue to test morphology fractions we also look at the $fracDeV$ parameter, which corresponds to the Sérsic index (a generalization of the de Vaucouleur profile, de Vaucouleurs 1948; Sersic 1968) and links together galaxy shape with surface brightness profiles (Fig. 2.7). $fracDeV$ is the fraction of light fit by the de Vaucouleur profile versus an exponential profile. When $fracDeV$=1, this represents a pure de Vaucouleur profile and is appropriate for an elliptical morphology. When $fracDev$=0, this represents a pure exponential profile and is appropriate for a disk morphology as seen in spiral galaxies. The $fracDev$ parameter is listed in the SDSS database for all u, g, r, i, z filters (Abazajian et al. 2009).

Fig. 2.7 shows the normalised distribution of the $fracDeV$ parameter and broadly agrees with the morphological classifications in Table 2.2. For the pure E+A the $fracDeV$ distribution tends to one meaning an elliptical morphology. For the Hδ strong sample and the E+A sample we visually see little difference in distribution and that both distributions are domin-

ated by a disk-like profile. We calculate their median $fracDeV$ values to be 0.086±0.025 for Hδ strong galaxies, 0.238±0.046 for E+As and 0.779±0.063 for pure E+As.To test this statistically we apply a KS test to all samples so determine their distinguishability. We find that when comparing the Hδ strong sample to the E+A sample we obtain a p-value of 0.338; we conclude that these two samples are not statistically different. To determine whether the E+A sample and the pure E+As emission are distinguishable we apply the same test and obtain a p-value of 0.003. We can therefore claim that there is a significant difference between E+As and pure E+As. To complete these tests, a p-value of $\sim 10^{-6}$ was achieved when comparing the Hδ strong sample to the pure E+As.

We examine the radii of our samples to further quantify our morphology results and to compare to the trends found in Shen et al. (2003). Here we use the effective radii based on the deVaucouleur profile in the SDSS r-band. We note here we have included a first order seeing correction to the radii, as shown in Equation 2.1 assuming the average SDSS seeing of 2".

$$r_{corrected} = (r^2_{observed} - seeing^2)^{1/2} \tag{2.1}$$

Fig. 2.8 shows the normalised radius distributions of the three samples. The majority of the pure E+A galaxies are mainly under 10kpc in radius and are therefore relatively small galaxies. We find the following median radii for the Hδ strong, E+A and pure E+A galaxies respectively: 11.4kpc±0.5, 9.8kpc±0.8 and 4.1kpc±1.2. When a KS test is applied to the Hδ strong sample and the E+A sample we obtain a p-value of 0.176. When comparing the E+As and Hδ strong sample to the pure E+As we obtain the p-values 0.006 and $\sim 10^{-6}$ respectively. This results shows that our third sample are statistically smaller in radii than the other two samples. This is also shown in Fig. 2.9 which shows the relation between radius and absolute magnitude with the corresponding trends from Shen et al. (2003). We look at the median separation between the half-light radius, R_{50}, and the trends from Shen et al. (2003) to quantify which line fits which population. From the Hδ strong sample we find that the median separation from the early-type trend is 1.21kpc and 0.03kpc from the late-type trend. Looking at the E+A sample we find that the median separation is 0.48kpc from both the early-type trend and late-type trend, this demonstrate the finds from Table 2.2. Finally,

Sample	Elliptical	Spiral	Merger	Unclassified
Hδ Strong	0.297±0.040	0.541 ±0.054	0.005±0.005	0.157±0.029
E+A	0.419±0.082	0.435±0.084	0.016±0.016	0.130±0.044
Pure E+A	0.810±0.206	0.048±0.048	0.048±0.048	0.094±0.061

Table 2.2: This table shows the morphology fractions for each of the samples along with the Poisson error. These morphologies were assigned using the galaxy zoo catalogue in which a particular classification took 50% or more of the votes. Here we see the majority of Hδ strong galaxies take up a spiral morphology, whilst E+As are equally found as ellipticals and spirals. We see that pure E+As are predominantly elliptical.

we find that the median separation of the pure E+A sample to the early-type trend is 0.39kpc and 0.85kpc to the late-type trend. This shows the Hδ strong galaxies follow the trend for late-type galaxies, the E+As an even mix of early- and late-type and the pure E+As resemble an early-type relation. This again confirms our findings from the colour and morphology analysis.

2.5 Environment

Whilst there is little evidence in the literature that selection criteria affect the environmental results, we aim to test whether there are any environmental differences between our sub-samples.

In order to explore the environments of the galaxies in our samples we use the Yang group and cluster catalogue (Yang et al. 2007). We directly match 176 galaxies in our sample (91.2%); this corresponds to 64 E+As (94.0%) and 22 pure E+As (88.0%). The Yang catalogue is based on the 4th data release of SDSS and selects galaxies with a redshift completeness $C > 0.7$, so therefore may not match totally to the 7th data release.

First, we examine whether our galaxies are in groups/clusters, if so, we look at the membership of that group or cluster to determine the size. Our results are displayed in Table 2.3. We split our environment classifications into field galaxies, pairs, weak groups (3<N<10), rich groups (10<N<50) and clusters (N>50).

Table 2.3 shows that ~70% and ~60% of the Hδ strong galaxies and E+A galaxies respectively are field galaxies with a strong preference for this type of environment; this

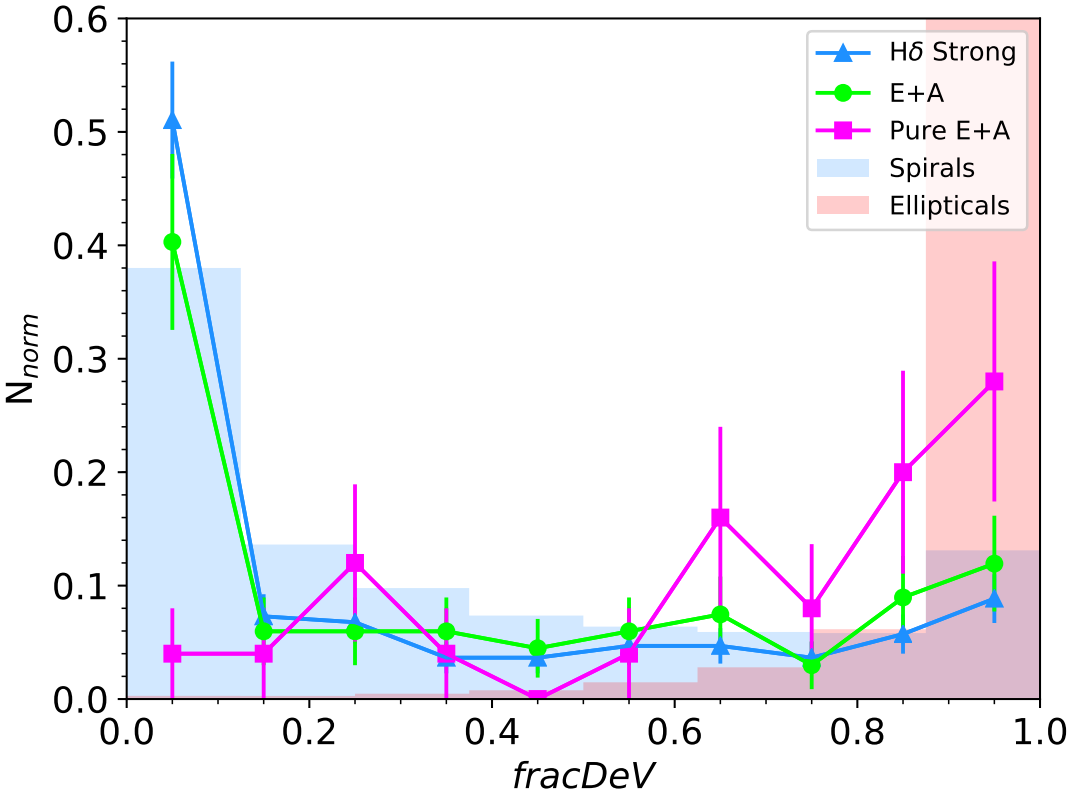

Figure 2.7: This plot shows the normalised distributions of the $fracDeV$ parameter for the three samples in this study, we include blue and red shaded regions to show the distributions of spirals and ellipticals respectively from our control sample. We see that the Hδ strong galaxies and E+A galaxies tend to a disk-like light profile whereas the pure E+As tend to an elliptical profile.

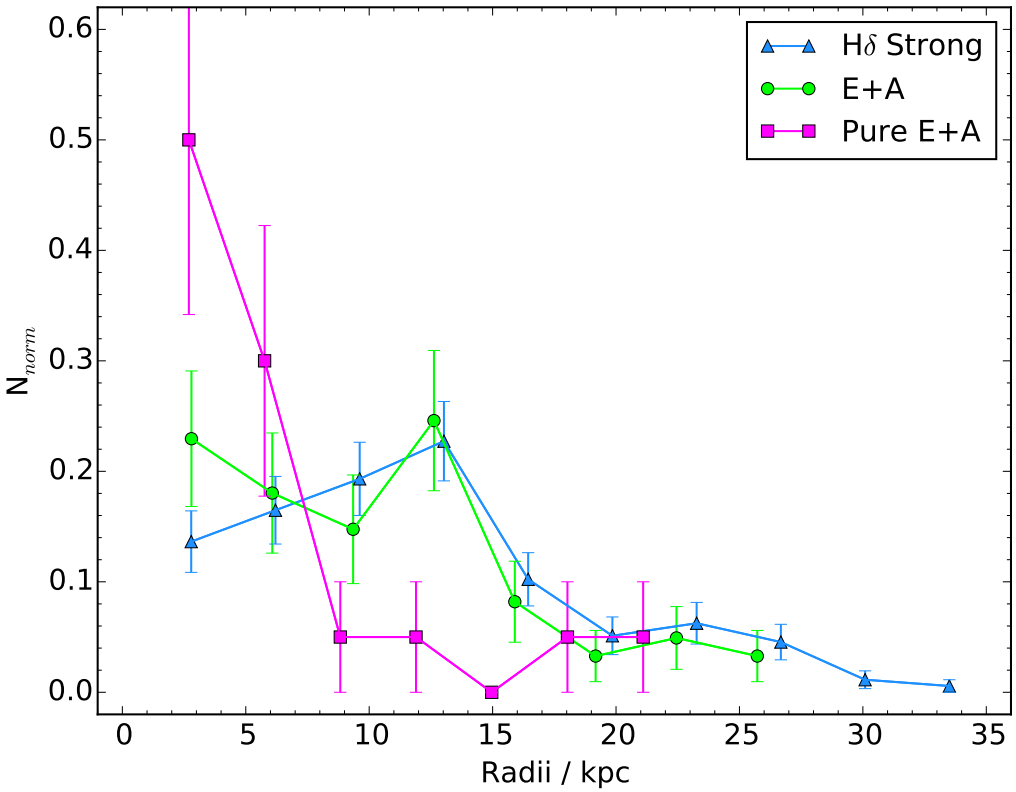

Figure 2.8: This plot shows this normalised distributions of radii for the three samples. The Hδ strong sample has a median radii of 11.4kpc±0.5, whereas the E+A population has a median radii of 9.8kpc±0.8. The median radii of the pure E+As is 4.1kpc±1.2.

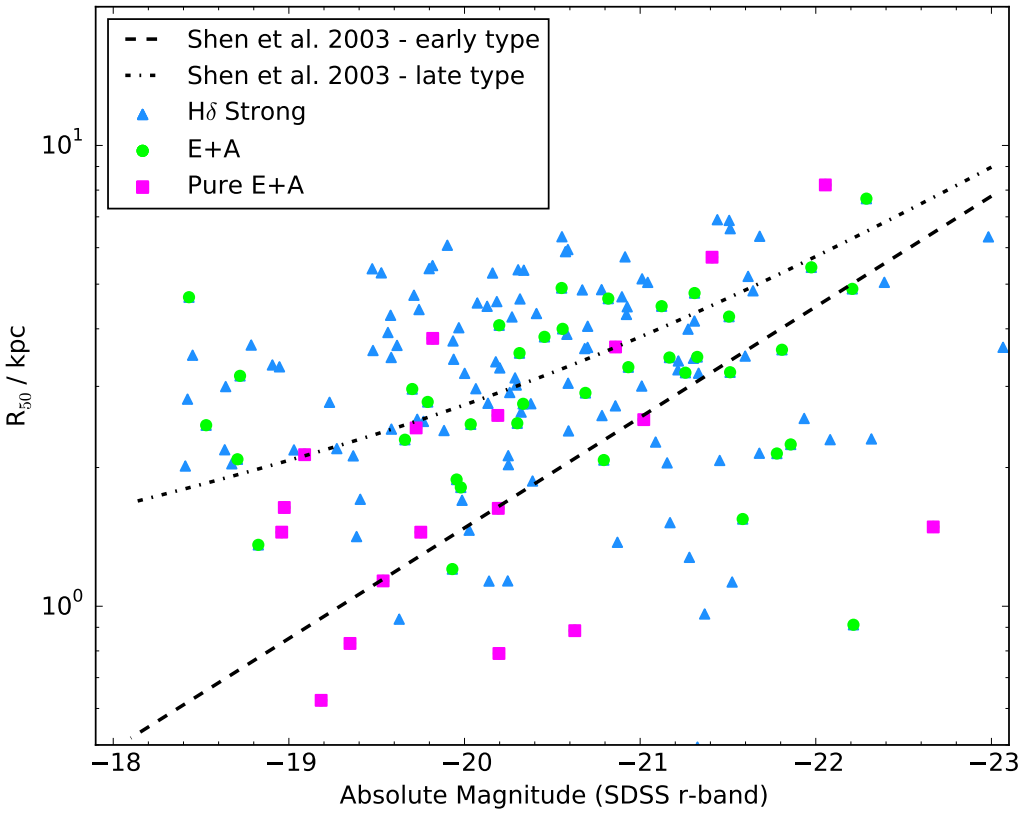

Figure 2.9: This plot shows the relation between absolute magnitude and the half light radius, R_{50}. For comparison we include the relationships found in Shen et al. (2003). We find that our Hδ strong and E+A galaxies follow the late-type trend whereas the pure E+As follow the early-type trend.

supports the findings of Zabludoff et al. (1996) who find that 75% of E+A galaxies to be in a field environment. We find that only~40% of the pure E+As are in the field environment whilst there is a significant amount of pure E+A galaxies in the group environments. When combining these environments together into all field (field and pair, where a pair is two galaxies that are gravitationally bound) and all cluster (weak groups, rich groups and clusters) environments we see the following splits in preference (field/cluster); 80/20, 70/30 and 50/50 for Hδ strong, E+A and pure E+As respectively. This suggests that pure E+As are more likely to be in denser environments than the other sub-samples of post-starburst galaxies.

2.6 AGN Connection

Hydrodynamical simulations show that major mergers of spirals contribute heavily to the populations of E+A galaxies (Snyder et al. 2011). When these gas-rich spirals merge, high levels of star-formation occur and to quench this star-formation a feedback mechanism is required, potentially AGN driven feedback.

During a merger gas is funnelled into the nucleus of a merging galaxy by tidal torques and can trigger a nuclear starburst (Mihos & Hernquist 1996; Hopkins et al. 2008a; Hopkins et al. 2008b) and therefore a potential progenitor of the E+A phase. With an excess of gas in the nucleus of the galaxy, this provides fuel for the supermassive black hole in the centre and can trigger an active galactic nuclei (AGN). AGN can produce jets, winds or radiation that heat or remove cold gas from galaxies, removing the fuel for further star formation.

De Propris & Melnick (2014) show in their study of 10 K+A galaxies that at any age there is no presence of AGN. They suggest, however, that a quasar phase immediately follows the quenching mechanism and this leads onto the K+A phase.

In this section we investigate the E+A/AGN link further by examining the AGN fractions within our samples and comparing to the fractions found in SDSS. We start by plotting a BPT diagram (Baldwin et al. 1981; Veilleux & Osterbrock 1987) shown in Fig. 2.10 which includes the Kauffman (Kauffmann et al. 2003), Kewley (Kewley et al. 2001) and Schawinski lines (Schawinski et al. 2014). Using these lines we locate the seyfert, LINER, composite and star formation regions. Starting with a control sample derived from SDSS we find that seyfert

Sample	Field	Pair	Weak Group	Rich Group	Cluster	All Field	All Cluster
Hδ Strong	0.69±0.06	0.08±0.02	0.11±0.03	0.09±0.02	0.02±0.01	0.77±0.07	0.23±0.04
E+A	0.59±0.10	0.10±0.04	0.14±0.05	0.13±0.05	0.05±0.03	0.68±0.11	0.32±0.07
Pure E+A	0.41±0.14	0.09±0.06	0.27±0.11	0.14±0.08	0.09±0.06	0.50±0.15	0.50±0.15

Table 2.3: This table shows the fractions of galaxies from each sample that reside in different environments. In this work we class field galaxies to be those that are not associated with any group or cluster in the Yang catalogue. We class weak groups as containing between 3 and 10 galaxies, rich groups 10-50 galaxies and clusters 50+ galaxies. The all field category includes galaxies which are in field and pair environments. The all cluster environment includes galaxies which are in groups with 3 or more members.

galaxies make up 10.8% of the general galaxy population, LINERs 11.5%, composites 20.7% and star formers 57.0%.

We plot the Hδ strong and E+A samples in Fig. 2.10 on the BPT diagram and find that the majority these two samples are within the star forming region (65.4%±6.4 and 57.1%±11.7 respectively). We find that composites makes up 23.0%±3.8 of the Hδ strong sample and 35.7%±9.2 of the E+A sample. Seyferts make up 8.2%±2.3 of the Hδ strong sample and 4.8%±3.4 of the E+As whilst LINERs make up 3.1%±1.4 of the Hδ strong sample and 2.4%±2.4 of the E+As. These results show similar fraction in both samples of star formers compared to the general galaxy population, however we witness an enhancement in E+A composite galaxies and decline in E+A AGN.

We also look at AGN fractions using a WHAN diagram (Fig. 2.11), described by Cid Fernandes et al. (2010, 2011) which unlike the BPT can identify 'fake' AGN (i.e. retired galaxies) from those with weakly active nuclei from the BPT LINER region. Using the SDSS control sample we find that 46.0% of the general galaxy population is made up of star forming galaxies, 27.2% passive galaxies, 19.3% strong AGN (sAGN) and 7.4% weak AGN (wAGN).

We find that the Hδ strong sample is comprised of 59.7%±6.1 star forming galaxies, 15.1%±3.1 passive galaxies, 16.4%±3.2 sAGN and 8.8%±2.3 wAGN. The E+A sample is found to be comprised of 54.2%±10.6 star forming galaxies, 27.1%±7.5 passive galaxies, 12.5%±5.1 sAGN and 8.3%±4.2 wAGN. These fractions are similar to those found in the SDSS control sample, however, we witness a decline in passive galaxies and slight enhancement of star formers within the Hδ strong sample compared to SDSS galaxies, which is to be expected.

2.7 Discussion

2.7.1 Links to Previous Studies

We have discussed in section 1 how different studies have used different selection methods to select post-starburst galaxies. There are two main methods for selection; the most common selecting on the lack of [OII] emission and the presence of Balmer absorption whilst the other selects on Hα emission, as well as [OII] emission and Balmer absorption.

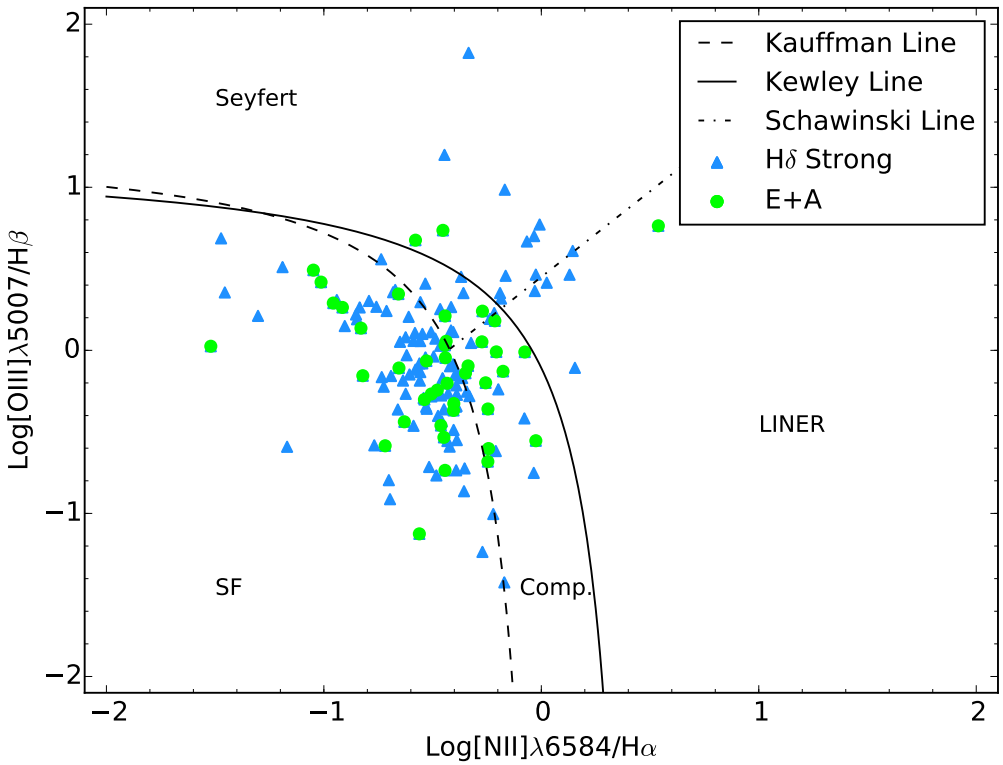

Figure 2.10: This BPT shows the classification of our samples using the Kauffman (Kauffmann et al. 2003), Kewley (Kewley et al. 2001) and Schawinski lines (Schawinski et al. 2014). We find the majority of the Hδ strong galaxies are located within the star forming region. We find that the E+A galaxies tend towards the star-forming and composite regions.

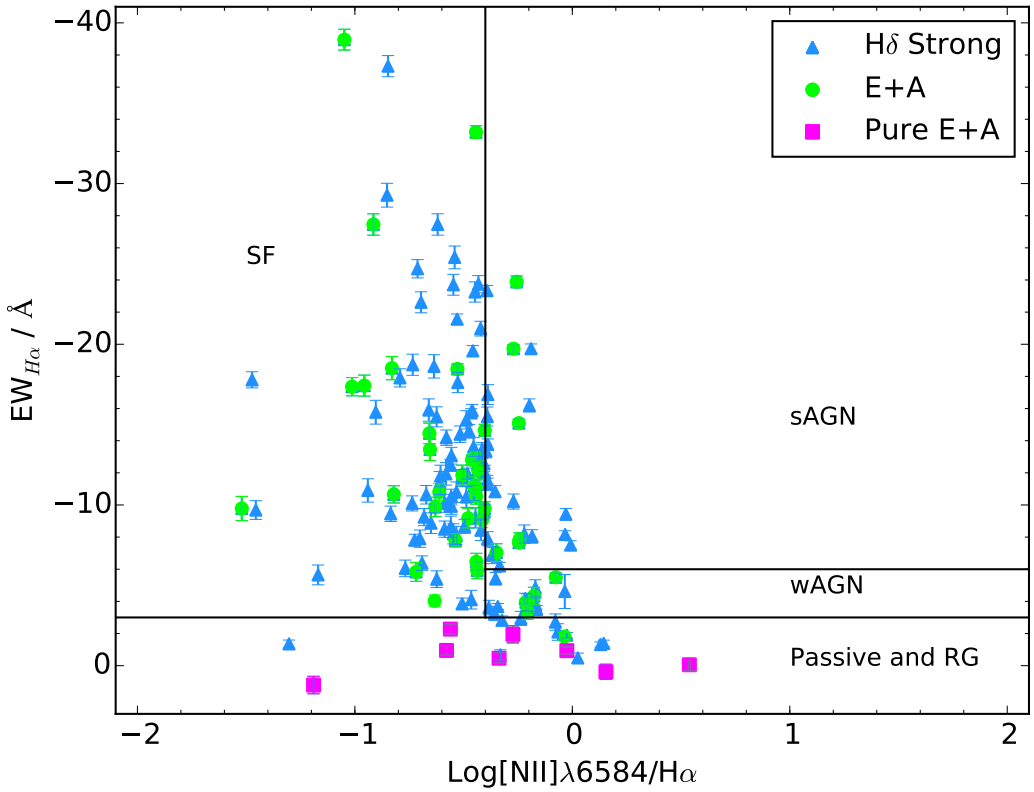

Figure 2.11: This WHAN diagram shows the majority of the Hδ strong and E+A galaxies are in the star-forming region (59.7%±6.1) with a small fraction residing in the AGN sections of the WHAN diagram (25.2%±4.0). Error bars are included on all points for the Hα line. Note that positive/negative values for equivalent widths refer to absorption/emission respectively.

Poggianti et al. (1999, 2009) find that there are two populations of E+As when they select using [OII] emission and Hδ Balmer absorption; these two populations can be classed as red and blue. We have seen from Fig. 3.8 and Fig. 3.9 that the Hδ galaxies peak in the blue cloud, the E+As peak in the green valley and the pure E+As peak in the red sequence. This result matches with that of Hogg et al. (2006) who place Hα selected E+As within the red sequence. This means the cut in Hα is removing galaxies with residual star formation, therefore, we are intrinsically selecting the red E+As mentioned in Poggianti et al. (1999) and Poggianti et al. (2009).

Along with colour we have also tested the morphologies of our three samples. The literature tells us E+As are bulge dominated with an underlying disk component (Tran et al. 2004; Quintero et al. 2004), similar to the S0 morphology. This was not seen to change with different selection methods mentioned above. We find in Table 2.2 and Fig. 2.7 that there are significant fractions in both the elliptical and spiral morphologies for Hδ strong galaxies and E+As. However, we see that pure E+As are predominantly elliptical.

Regardless of what selection method is used in the literature there is a great deal of discrepancy in the environmental preferences of post-starburst galaxies. Table 2.3 shows that ~70% and ~60% of Hδ strong galaxies and E+As are within the field, this result agrees with the findings of Zabludoff et al. (1996) at low redshifts $z < 0.1$. Lemaux et al. (2016) states that pure E+As have a higher fraction in clusters than E+As selected only on [OII] emission and Balmer absorption, we find the same trend when examining the fractions of post-starburst galaxies in various environments. Mahajan (2013) find that E+As prefer a weak-group environment, whilst we do see a systematically higher fraction in the weak-group environment compared with rich environments this result is not statistically significant.

2.7.2 Duty Cycle of Post-Starburst Galaxies

In section 2.3, we find that the colours of Hδ strong galaxies peak in the blue cloud, the E+As in the green valley and the pure E+As in the red sequence (Fig. 2.5 and Fig. 2.6). This result is backed up morphologically in section 4. We find that the majority of Hδ strong galaxies have a spiral morphology whereas the E+As have a mix of spiral and elliptical morphologies . The

majority of pure E+As display an elliptical morphology (Table 2.2). This is confirmed again by the light profiles of our samples (Fig. 2.7), we find that Hδ strong and E+A galaxies have a disky light profile whereas the pure E+As have a de Vaucouleur light profile, typical of an early-type morphology. This difference in morphology is seen in the radii of our galaxies (Fig. 2.8 and Fig.2.9), in which the Hδ strong and E+A galaxies follow the late-type relationship found by Shen et al. (2003) and the pure E+As follow the early-type relationship. The lack of merging morphologies suggests that major mergers do not play an important role in the post-starburst phase.

We speculate that the Hδ strong galaxies, E+A and pure E+As are part of an evolutionary sequence in which star forming galaxies are quenched into blue disky Hδ strong galaxies. They are then quenched further into green valley E+As before, finally, quenching fully into red elliptical pure E+As. If this is true, how does the morphology transition from disk to elliptical? This could be due to a fading disk with time as young stars die or possibly due to any mergers. We add here that we witness no evidence for mergers in the morphologies (Table 2.2) so the trigger would have to be a minor merger or a mergerless interaction.

Another factor we consider is environment, although we have low-number statistics, we see a higher proportion of pure E+As in denser environments than the Hδ strong and E+A galaxies. Whilst in the Hδ strong and E+A galaxies we see a strong preference for a field environment. We note this is not a migration of galaxies from the field to a cluster environment as the migration time scale is much longer than that of the evolution of our galaxies. Instead, this may point to an accelerated evolution from Hδ strong galaxies to pure E+As in dense environments (Hatch et al. 2011). A dense environment would enhance processes such as interactions and minor mergers. Also the hot atmosphere of the intracluster medium would help quench and fade the disk by starving the galaxy of the fuel to replenish its cold gas supply.

We see from looking at AGN fractions using BPT and WHAN diagnostics that there is a higher fraction of AGN in the Hδ strong sample compared with the E+As. This could suggest that E+As are the product of Hδ strong galaxies that have been quenched by AGN feedback, however, as the E+A cut selects against line emission this is purely speculative and we have no solid evidence that AGN are important in quenching star formation after a burst.

2.8 Conclusion

The post-starburst phase in galaxy evolution is an important and significant link between star-forming disks and quiescent early-type galaxies. Throughout the literature there are several different selection techniques. We split these different techniques into two categories; those that select on the presence of Balmer absorption and the absence of [OII] emission and those which also select against Hα emission. There are advantages and disadvantages in using either method, one includes those galaxies that have Hα due to the presence of AGN and the other excludes dusty starburst galaxies. In this work we have explored how the different selection techniques can affect the results found in colour, morphology, environment and AGN fraction. Here we list our principal findings and suggest what we feel is an ideal selection method:

1. By locating our samples on a colour magnitude diagram and colour histogram, we have been able to find where each population peaks. We find that Hδ strong galaxies peak in the blue cloud, E+A galaxies in the green valley and pure E+As in the red sequence.

2. Using the GZ catalogue we find that Hδ strong galaxies are predominantly spiral in morphology with a fraction of 54%. We find that E+As have approximately an even split between the elliptical and spiral morphologies and pure E+As have an elliptical fraction of 81%. These results are confirmed when we look at the $fracdev$ parameter which shows the Hδ strong galaxies and E+As have a disk morphology and the pure E+As have an early-type morphology. This is again demonstrated when we look at the radii of our galaxies, we see that the Hδ strong galaxies and E+As follow the late-type trend found in Shen et al. (2003), whilst the pure E+As follow the early-type trend.

3. We find that the majority of Hδ strong galaxies and E+A galaxies have a strong preference for the low density environment, however, there is an even split between the low and high density environments within the pure E+A population. We see that there is a higher fraction of pure E+As in denser environments than the other two populations.

4. In this study we have also tested the AGN fractions of our samples by using BPT and WHAN diagrams. Both diagrams suggest that the emission lines of the Hδ strong and

E+A populations are excited by star formation and not AGN activity. The AGN fraction of the Hδ strong galaxies is typical of the general galaxy population, so provides no evidence that AGN play a role in quenching star-formation in post-starburst galaxies. However, we see a significant decrease in AGN fraction compared with the general population which could be a consequence of AGN fading into the E+A phase assuming AGN feedback leads to the E+A phase. However, we note that the E+A sample is selected to not have strong emission lines (albeit in [OII]) and so it is not possible to draw strong conclusions.

We postulate that different selection criteria allow us to probe different stages of post-starburst galaxies. After the initial starburst has ended the galaxies are seen as blue spirals/disks with a young stellar spectra, indicated by deep Balmer absorption features. However, ~65% of these disks are still forming stars as seen by their [OII] and/or Hα emission lines. If we cut on [OII] emission (and therefore star formation) we see a population of green valley disk galaxies suggestive of the next stage in the post-starburst evolution as galaxies quench towards the red sequence. If we make a further cut on star formation using a lack of Hα emission then we find a population of early-type red sequence galaxies. These are galaxies that still show deep Balmer absorption but with no ongoing star formation and represent the final post starburst phase before the underlying stellar population becomes dominated by old stars.

The lack of any significant enhancement in the merger or AGN fractions for the post-starbursts indicates that, while we cannot rule out a scenario whereby the initial starburst was triggered by a major merger and then initially quenched by an AGN, it is not these processes that continue to quench the galaxies down to full quiescence. One puzzle in our proposed evolutionary sequence is how the morphologies have changed from disky to early-type without evidence of major merging. We speculate that this morphological evolution could be due to the secular fading of the star-forming disk leading to a bulge dominated system or to a series of minor interactions not detected in the imaging. There also seems to be a suggestion that the passive, pure E+As are more prevalent in denser environments, which perhaps suggests that the quenching that follows a starburst proceeds more quickly in dense environments perhaps

due to the enhancement of minor interactions in groups or the removal of a cold gas supply by the hot intracluster medium of the most massive systems.

Acknowledgements

JPS gratefully acknowledges support through the Hintze Research Fellowship.

Funding for the SDSS and SDSS-II has been provided by the Alfred P. Sloan Foundation, the Participating Institutions, the National Science Foundation, the U.S. Department of Energy, the National Aeronautics and Space Administration, the Japanese Monbukagakusho, the Max Planck Society, and the Higher Education Funding Council for England. The SDSS Web Site is http://www.sdss.org/.

The SDSS is managed by the Astrophysical Research Consortium for the Participating Institutions. The Participating Institutions are the American Museum of Natural History, Astrophysical Institute Potsdam, University of Basel, University of Cambridge, Case Western Reserve University, University of Chicago, Drexel University, Fermilab, the Institute for Advanced Study, the Japan Participation Group, Johns Hopkins University, the Joint Institute for Nuclear Astrophysics, the Kavli Institute for Particle Astrophysics and Cosmology, the Korean Scientist Group, the Chinese Academy of Sciences (LAMOST), Los Alamos National Laboratory, the Max-Planck-Institute for Astronomy (MPIA), the Max-Planck-Institute for Astrophysics (MPA), New Mexico State University, Ohio State University, University of Pittsburgh, University of Portsmouth, Princeton University, the United States Naval Observatory, and the University of Washington

2.9 Additional Results

Studies such as Poggianti et al. (2009) and Mahajan (2013) suggest that E+As are preprocessed before being accreted into cluster environments. If this is the case, we would expect to see a significant fraction infalling onto groups and clusters. We test this hypothesis by producing a phase space diagram, shown in Fig. 2.12, for the post-starburst galaxies that we find in groups and clusters.

To create the phase space diagram, we plot r/r_{200} against $\Delta V/\sigma_v$, where r is the projected

distance from the centre of the group/cluster and ΔV is the difference in radial velocity between the galaxy and the group/cluster centre. The virial radius, r_{200}, is calculated using Eq. 2.2 and Eq. 2.3 (Pimbblet et al. 2006), where σ_v is the cluster velocity dispersion (we calculate this to be one standard deviation of the radial velocities of the group/cluster members). In Fig. 2.12 we also include a 3 standard deviation caustic to determine whether the galaxies in this study are infalling or are well established in their group/cluster,

$$r_{200} = \frac{\sqrt{3}\sigma_v}{10H(z)}, \tag{2.2}$$

$$H(z) = H_0(1+z)\sqrt{1+\Omega_M z}. \tag{2.3}$$

We find that all of the post-starburst galaxies within groups and clusters are inside the caustic meaning they are well established within their environment, this disagrees with the findings of Poggianti et al. (2009) and Mahajan (2013). We also see no difference between the three samples in our study with relation to their location within a group environment, suggesting Hα has no or little effect on environment . This all suggests that whilst environment plays an important role in triggering starbursts, it is not the driving force behind the evolution of post-starburst galaxies.

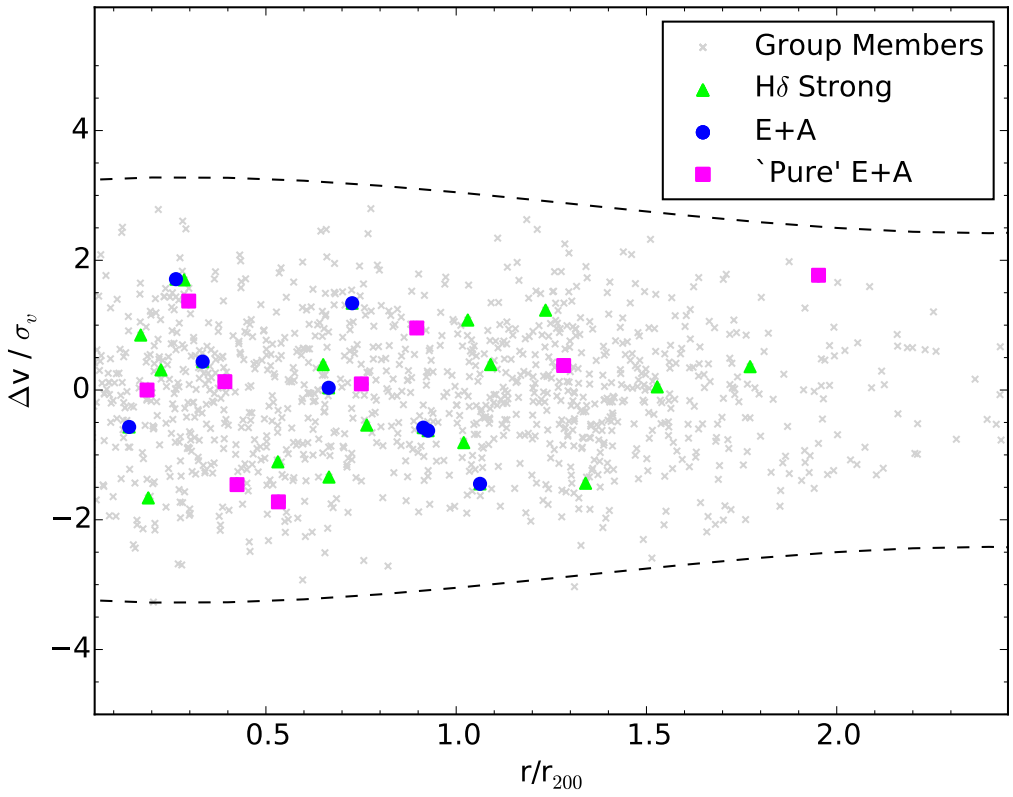

Figure 2.12: This plot shows a phase space diagram, along with caustics, were the group/cluster members are shown as grey crosses. All group/cluster post-starburst galaxies on this plot are within the caustic, so are well established in their group/cluster and not in the process of infalling.

3. The Evolution of Starburst Galaxies in the Illustris Simulation

Declaration

This Chapter consists of the published work 'The Evolution of Starburst Galaxies in the Illustris Simulation' (Wilkinson et al. 2018) in Sections 3.1-3.5. This work investigates the triggering mechanisms of starburst galaxies and determines how different triggers affect observational properties. In Sections 3.6, we build on this published work by including analysis that did not make it into the published work.

Abstract

There is a consensus in the literature that starburst galaxies are triggered by interaction events. However, it remains an open question as to what extent both merging and non-merging interactions have in triggering starbursts? In this study, we make use of the Illustris simulation to test how different triggering mechanisms can effect starburst events. We examine star formation rate, colour and environment of starburst galaxies to determine if this could be why we witness a bimodality in post-starburst populations within observational studies. Further, we briefly test the extent of quenching due to AGN feedback. From Illustris, we select 196 starburst galaxies at $z = 0.15$ and split them into post-merger and pre-merger/harassment driven starburst samples. We find that 55% of this sample have not undergone a merger in the past 2 Gyr. Both of our samples are located in low-density environments within the filament regions of the cosmic web, however we find that pre-merger/harassment driven starbursts are in higher density environments than post-merger driven starbursts. We also find that pre-merger/harassment starbursts are redder than post-merger starbursts, this could be driven by environmental effects. Both however, produce nuclear starbursts of comparable strengths.

3.1 Introduction

The star formation main sequence (SFMS) is a tight correlation (scatter ≈ 0.2 dex as reported by Speagle et al. 2014) between mass and star formation rate (SFR). It holds true at both low (Brinchmann et al. 2004; Salim et al. 2007) and high redshifts (Daddi et al. 2007) over multiple wavelengths (Elbaz et al. 2011; Rodighiero et al. 2014). Star-formation occurs in two modes: quiescently and star bursting (Pillepich et al. 2017), as revealed by the Kennicutt-Schmidt relation (Kennicutt 1998). Most galaxies situated in the SFMS can be considered star forming at a steady rate, whilst those significantly above the main sequence are considered to be in a starburst phase. Galaxies undergoing a starburst spend a very short amount of time in this phase ($\sim 10^8$ years) and because of this, they are rare, making up between only 5% and 10% of the global galaxy population (Rodighiero et al. 2011).

Throughout the literature there is a consensus about the possible triggers of starburst/post-starburst galaxies, namely mergers (Barnes & Hernquist 1991; Sparre & Springel 2016) and galaxy-galaxy interactions (Zabludoff et al. 1996). It is suggested that these mechanisms are responsible for transforming star forming spirals into quiescent ellipticals. Evidence of this can be seen in the morphologies of post-starburst galaxies. Zabludoff et al. (1996) finds that in a sample of 21 post-starburst galaxies from the Las Campanas Redshift Survey that 5 galaxies display tidal features. This is a consequence of galaxy interactions. Other studies such as Tran et al. (2004) and Quintero et al. (2004) find that the morphology of post-starburst galaxies are generally bulge dominated with underlying disk components, similar to the S0 morphology, reinforcing the evolutionary link between spiral and elliptical galaxies.

It is widely believed that major mergers contribute heavily to the production of elliptical galaxies (Cox et al. 2006). Using 112 N-body merger simulations of varying mass ratios, Naab & Burkert (2003) find that mergers with mass ratios of 1:1 - 1:4 mostly result in elliptical-like remnants. These remnants can be disky and resemble an S0 morphology, similar to the post-starburst morphologies found by Yang et al. (2004). Work by Sparre & Springel (2017), using the Illustris simulation (Genel et al. 2014; Vogelsberger et al. 2014a,b), find that merger remnants are able to regrow their disk and do not necessarily have to be quenched ellipticals.

However, spiral morphologies are found in 44–54% of post-starburst galaxies (Wilkinson

et al. 2017), meaning major mergers are not the only process triggering the starburst phase. Cales et al. (2013) suggests that non-merging galaxy interactions are more likely to maintain a spiral morphology. This could suggest why there is a significant fraction of post-starburst spiral galaxies. However, this is not the only alternative to mergers to trigger starbursts, other studies such as Dekel et al. (2009), Ceverino et al. (2010), Cacciato et al. (2012) and Porter et al. (2014) suggest that instabilities in the disk could also result in starbursts.

Further, the environment in which starburst galaxies are found supports the merger/galaxy-galaxy interaction connection. Mergers, particularly gas-rich major mergers, are found to be more prominent in low-density environments (Bekki et al. 2001; Lin et al. 2010; Sánchez-Blázquez et al. 2009). These results back up the findings by Hashimoto et al. (1998), who find that star formation is on average higher in field environments than in cluster environments. This in turn reveals that there is a higher fraction of starbursts in the field compared with clusters. Zabludoff et al. (1996) finds that 75% of post-starburst galaxies are located in the field, a similar result is found in Wilkinson et al. (2017). By combining these findings, it suggests that for the majority of starburst galaxies major mergers are the main trigger (Wild et al. 2009; Snyder et al. 2011) but not the only trigger (Sparre & Springel 2017) for driving galaxy transformation, with galaxy-galaxy interactions being the next major trigger.

Whilst starbursts are twice as common in the field than in cluster environments (Poggianti et al. 1999), they are present in some cluster environments (Balogh et al. 1999). Poggianti et al. (2009) find that post-starburst galaxies are predominantly in cluster environments at higher redshifts ($0.4 < z < 0.8$). At lower redshifts ($0.02 < z < 0.06$), Mahajan (2013) find that post-starburst galaxies prefer a weak-group environment containing 4 to 10 group members and that 86% of X-ray bright clusters contain sub-structure on the weak group scale. Of these weak groups, 91% contain post-starburst galaxies. This suggests pre-processing is occurring, in which the starburst is triggered in a weak group environment which then infalls into a denser cluster environment. This results in ram pressure stripping that quenches star formation.

In both cases, mergers and interactions have the potential of triggering a starburst (Zabludoff et al. 1996; Bekki et al. 2001, 2005; Hopkins et al. 2006, 2008a) in which tidal torques funnel gas into the galactic centre (Barnes & Hernquist 1991; Barnes & Hernquist

1996). The increased build up of gas in the galactic centre then begins to fuel a rapid burst of star formation known as a nuclear starburst. Sparre & Springel (2016) suggests that head-on mergers are likely to produce a strong nuclear burst where the strength of the burst is directly proportional to the speed of the collision. Due to the regulatory processes within galaxies, this elevated rate of star formation is not sustained for a prolonged period of time and is quenched.

The literature suggests many potential mechanisms that could quench star formation after a starburst such as AGN feedback, stellar feedback, ram pressure stripping, and gas depletion. AGN feedback is a form of rapid quenching and has been discussed extensively within the literature (Springel et al. 2005; Goto 2006; Feruglio et al. 2010; Cicone et al. 2014) and is typically attributed to gas-rich major mergers (Di Matteo et al. 2005; Hopkins et al. 2006). When the merger occurs, gas is funnelled into the centre of the galaxy and activates the AGN, causing 'quasar mode' feedback which ejects remaining gas away from the star forming central region via strong galactic winds. After the quasar phase, 'radio mode' feedback takes over in which the AGN heats up surrounding gas preventing it from forming stars (Croton et al. 2006). Whilst AGN feedback is a powerful tool in suppressing star formation, gas falling back from the initial blow-out is capable of reigniting star formation (Faucher-Giguère 2018).

Star formation triggered by either minor mergers or galaxy-galaxy interactions are found to quench on an intermediate time-scale, $1.0 \lesssim \tau/\mathrm{Gyr} \lesssim 2.0$ (Smethurst et al. 2015). Mechanisms that could quench on an intermediate time-scale include ram pressure stripping, gas depletion or harassment. The morphology of such a remnant would resemble an S0 morphology, similar to the post-starburst galaxies found by Tran et al. (2004), Quintero et al. (2004) and Yang et al. (2004).

There has been many studies focusing on the link between starburst and mergers. However, there is little investigation in the literature that examines the links between non-merging events and starburst and how they compare to post-merger starbursts. In this study we use hydrodynamical simulations from Illustris (Vogelsberger et al. 2014a; Nelson et al. 2015) to track the evolution of starburst galaxies. We explicitly aim to determine their main trigger and make a comparison between post-merger and pre-merger/harassment driven starbursts.

In section 3.2, we give a brief description of the Illustris simulation and how we derive

our sample. In section 3.3, we discuss our findings on the triggering mechanisms of starburst galaxies, their properties and what quenches their star formation. In section 3.4, we will discuss our main findings and in section 3.5, we will make our conclusions.

3.2 Sample Selection

3.2.1 Illustris

In order to address the questions above, we use the Illustris simulation to track and compare starbursts driven by differing triggers. Illustris is a hydrodynamical simulation that tracks cosmological evolution from $z = 127$ to $z = 0$ in a box of comoving size 106 Mpc^3 (Genel et al. 2014; Vogelsberger et al. 2014a,b). The following cosmological parameters are adopted: $\Omega_m = 0.2726$, $\Omega_\Lambda = 0.7274$, $\Omega_b = 0.0456$, $\sigma_8 = 0.809$, $n_s = 0.963$ and $H_0 = 100\,h$ km s^{-1} Mpc^{-1} where $h = 0.704$. The initial conditions are generated at $z = 127$ and achieves a dark matter resolution of 6.26×10^6 $\mathrm{M}_\odot$ and baryonic matter mass resolution of 1.26×10^6 $\mathrm{M}_\odot$. The smallest radii of a cell achieved is 48 pc (Vogelsberger et al. 2014a).

Illustris uses the moving-mesh code AREPO (Springel 2010) that provides a hydrodynamical treatment of gas and works alongside gravitational forces (calculated using a Tree-PM scheme; Xu 1995) to create realistic galaxy formation. Phenomenological models are also included to allow for processes that regulate stellar mass growth within galaxies such as AGN feedback, stellar mass loss and SMBH growth. The simulation is capable of resolving gravitational dynamics down to ranges of 710 pc at $z = 0$ whilst following large-scale evolution (Vogelsberger et al. 2014a).

Illustris uses the star formation and feedback model from Springel & Hernquist (2003). The model describes the multiphase nature of star formation, accounting for both self-regulating, 'quiescent' star formation and 'explosive' star formation. Springel & Hernquist (2003) use a sub-resolution model that uses spatially averaged properties to describe the ISM; this includes the growth of cold gas clouds, radiative cooling and supernova feedback in the form of galactic winds, radiative heating and outflows. During a starburst the gas density is much higher than the star formation threshold and this allows for efficient star formation. However, in the self-regulating model, galactic winds can reduce the efficiency of star

formation producing results that are consistent with observations.

We make use of the publicly available merger trees (Nelson et al. 2015) created using the SUBLINK code (Rodriguez-Gomez et al. 2015). These trees allow us to track our selected galaxies through subsequent and previous time steps and give details about their merger histories. This will allow us to compare the driving forces behind starburst galaxies.

3.2.2 Starburst Selection

We begin by selecting starburst galaxies at a lookback time of 1.912 Gyr ($z = 0.15$) with the aim of tracking them forward through time to $z = 0$. By starting at this point in the simulation we are able to track the galaxies through 12 snapshots to $z = 0$ which covers the 2 Gyr duration of the post-starburst phase (Kaviraj et al. 2007). Selecting galaxies in one snapshot simplifies the analysis as the time between snapshots is not uniform. Working in a low-z regime allows for the minimum time difference between snapshots, allowing us to monitor the evolution of low-z galaxies more closely and provides ease of comparison to SDSS studies like Wilkinson et al. (2017).

To select starburst galaxies we first plot the star formation main sequence, as shown in Fig. 3.1. We exclude passive galaxies at $z = 0.15$ from our fit by fitting our trend line to main-sequence galaxies with specific star formation rates above 2.5×10^{10} yr^{-1}. Further, we apply a minimum mass of 10^9 M$_\odot$ for ease of comparison to observational studies. We identify galaxies 0.6 dex above the main sequence line as starburst galaxies, as defined by Zhang et al. (2016). Using this method, we select 196 starburst galaxies (0.82% of Illustris galaxies in this snapshot within the mass range given above).

We add the caveat that within our analysis of the Illustris simulation, starbursts are under-produced (Sparre et al. 2015), this is due to the temporal resolution of the available snapshots (Sparre & Springel 2016). For example, if the peak of the starburst is in the middle of two snapshots, this starburst would be be invisible or the measured SFR would be lower than expected. This problem reduces the star formation that is measured and therefore hides the bursty nature of starbursts. This could cause some starbursts to be hiding within the main sequence. The star formation main sequence becomes less defined at higher masses and as a

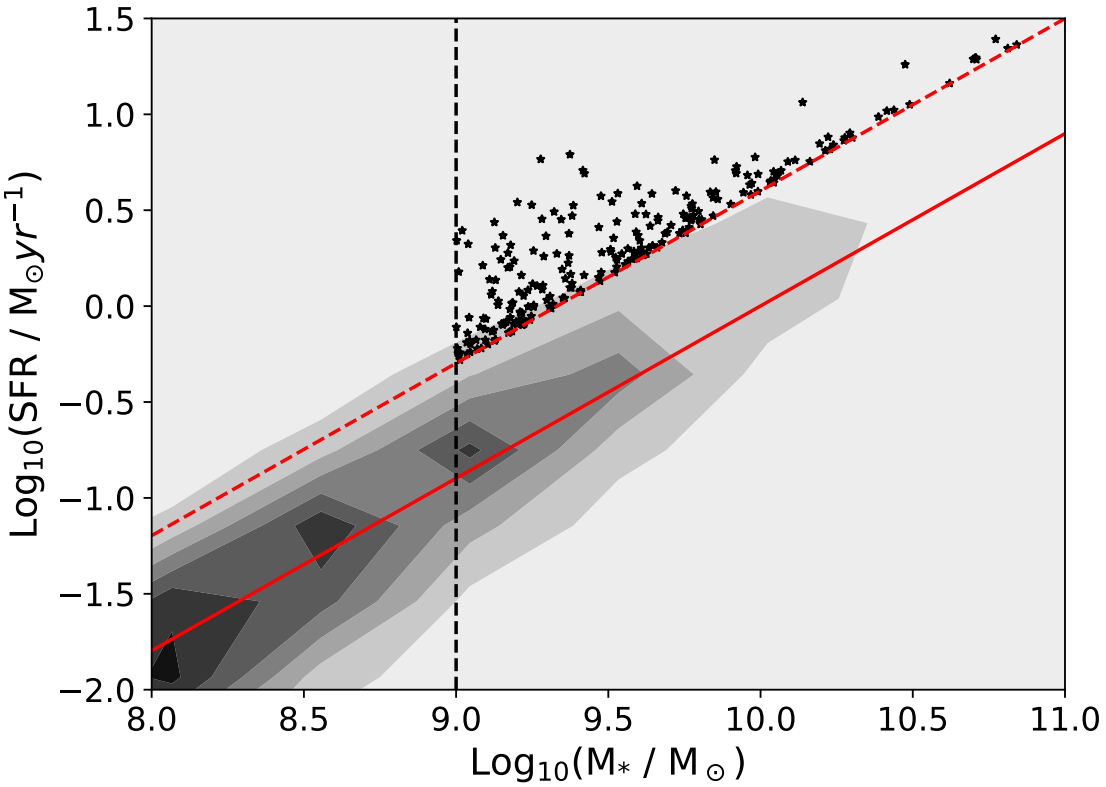

Figure 3.1: This plot shows the star formation main sequence at a lookback time of 2 Gyr. The red solid line denotes the star formation main sequence fitted using linear regression. We select starburst galaxies above the red dashed line 0.6 dex above the main sequence. We select galaxies with masses above $10^9 M_\odot$. Using this criteria we select 196 starburst galaxies.

result the average star formation rate drops as masses surpass $10^{10.5}$ $M_\odot$ (Sparre et al. 2015). This results in fewer starburst galaxies being identified at higher masses.

3.3 Results

3.3.1 Triggering Mechanisms of Starbursts

Zabludoff et al. (1996) suggested that the main mechanisms responsible for triggering the starburst phase are galaxy-galaxy interactions and mergers. Studies such as Wild et al. (2009) and Snyder et al. (2011) suggest gas rich major mergers are responsible for triggering starburst galaxies. Other studies have reported non-merging galaxy-galaxy interactions are more likely to maintain spiral structure post starburst (Cales et al. 2013; Wilkinson et al. 2017). There are

		$\log_{10}(M/M_{\odot})$			
Sub-Sample	Total	9.0-9.5	9.5-10.0	10.0-10.5	10.5-11.0
Major	35	20	12	2	1
Intermediate	24	5	12	5	2
Minor	30	9	15	4	2
Post-Merger	89	34	39	11	5
Pre-Merger/ Harassment	107	58	31	15	3

Table 3.1: Here, we explore the merger histories of our starburst sample by determining how many have had a merger in the past 2 Gyr and the mass ratios of such mergers. The mass ratios are as follows: 1:1-1:4 (major), 1:4-1:10 (intermediate) and 1:10-1:100 (minor). We also separate our findings by mass. We find that just over half of the starburst galaxies in this sample (55%) have not had a merger in the previous 2 Gyr.

an extensive number of studies researching the link between mergers and starbursts but to what extent do non-merging interactions play on triggering starbursts? In this section we explore the potential triggers of starbursts by making use of the SUBLINK merger trees in Illustris.

We examine the merger histories of our starburst galaxies and split our primary sample into two sub-samples based on whether they have undergone a merger in the previous 2 Gyr. Those starbursts that have had a merger in the past 2 Gyr we call post-merger starbursts and those that have not we call pre-merger/harassment starbursts, we note that this sample may or may not have a harassing neighbour that could or could not lead to a merger. However, at the snapshot in which these galaxies are selected, there has been no coalescence in the previous 2 Gyr and it is in this way that our two samples differ. We explore the post-merger scenario further by examining the types of merger that have occurred by splitting our post-merger driven starburst sample by mass ratio; 1:1-1:4 (major mergers), 1:4-1:10 (intermediate mergers) and 1:10-1:100 (minor mergers) as shown in Table 3.1. Mass ratio is defined as the ratio of stellar mass of the merger, calculated at a time when the secondary progenitor reaches its maximum stellar mass (Rodriguez-Gomez et al. (2015, 2016)). We find that 35 (15%) have had a major merger, as defined by Bournaud et al. (2005). We use this definition as it has been shown to produce remnants with similar morphologies to the post-starburst galaxies found by Naab &

Burkert (2003) and Tran et al. (2003).

We separate out intermediate mergers (those with ratios between 1:4 and 1:10) because Bournaud et al. (2005) finds that this type of merger can form remnants with S0 morphologies. We find that 24 galaxies (10%) in our sample have had this type of merger in the previous 2 Gyr. When examining minor mergers, those with mass ratios less than 1:10, we find that 30 starbursts (34%) have had minor mergers, i.e. those with ratios less than 1:10 in the past 2 Gyr. We also split these fractions by mass in Table 3.1, that shows minor mergers are more prevalent at higher mass regimes whilst major mergers are more likely to occur at lower mass regimes because the number density of galaxies drops as mass increases.

In total 89 (45.4%) starburst have had at least one merger in the past 2 Gyr which suggests mergers do have a significant impact on triggering starbursts. However, mergers are not the only trigger as suggested by Sparre et al. (2017); what is triggering the remaining 107 (54.6%) starbursts? Perhaps, another likely trigger is harassment interactions which can cause rotational instabilities that lead to tidal torques capable of tunnelling gas and dust into the galactic centre Barnes & Hernquist (1992).

To determine how starbursts in the pre-merger/harassment sample are being triggered, we examine the locations and track the movements of galaxies within a 100 kpc radius surrounding the pre-merger/harassment starburst sample. We find that 52 pre- merger/harassment starbursts (~49% of the pre-merger/harassment starburst sample) have a neighbour with a stellar mass at least 10% that of the starburst galaxy. This could indicate that harassment events are triggering starbursts whether it be a pre-merger harassment or a pure harassment event with no consequent merger. By examining the merger trees for future mergers, we find that 33 starbursts (31%) in our pre-merger/harassment sample have a future merger with a minimum mass ratio of 1:10 in subsequent snapshots. However, without the full raw data from Illustris we are unable to get a quantitative measure of tidal gravity. In 8 (~7%) of the pre-merger/harassment starburst galaxies, there are no surrounding galaxies or mass. In these galaxies, gas could be accreted from the intergalactic medium fuelling a starburst or instabilities in the galactic disk could be driving the rapid burst of star formation. Only a higher resolution simulation would allow us to determine what is causing bursts of star formation. These results could suggest that

interactions play a role in triggering starbursts.

For starbursts in the pre-merger/harassment sample that have neighbouring galaxies within a 100 kpc radius and are greater than 10% of the starburst mass, we investigate the harassment scenario by determining the relative distance to the closest neighbour. Fig. 3.2 shows the distribution of relative distances normalised to the total sample size. We define relative distance, D_{rel}, below in Eq. 3.1, where D is the distance from the centre of the starburst galaxy to the centre of its closest neighbour, R_1 is the half mass radii of the starburst and R_2 is the half mass radii of the closest neighbour. This method allows us to determine how close galaxies get regardless of their size,

$$D_{rel} = D / (R_1 + R_2). \tag{3.1}$$

In Fig. 3.2 we include a non-starburst control sample that is composed of 500 randomly selected galaxies from the Illustris simulation with masses above 10^9 $M_\odot$. We find that ~40% of the pre-merger/harassment starburst sample have a neighbour with $D_{rel} < 1$ which quickly drops to $\ll$10% for neighbours with relative distances greater than 1. Fig. 3.2 shows the control sample peaks at a higher D_{rel} values and has a much lower fraction at $D_{rel} < 5$ than our pre-merger/harassment starburst sample. This shows that starbursts are closer to their neighbours than non-starbursts. This is strong evidence for an interaction driven starburst. Due to the close proximity it is not unreasonable to predict that a merger will eventually follow, providing that the relative velocities are low enough to allow the galaxies to coalesce.

3.3.2 Environments

As we find in our previous study (Wilkinson et al. 2017), post-starburst galaxies predominantly reside in, but not restricted to, low-density environments. We find that those in high-density environments are redder and more elliptical in morphology than those in low-density environments. This suggests that environment could be enhancing the evolution in clusters and rich-groups. To discover more about the effects of environment on the post-starburst phase we look at the locations of our starburst galaxies in the Illustris simulation.

Firstly, we explore the global environments of starburst galaxies in the Illustris simulation.

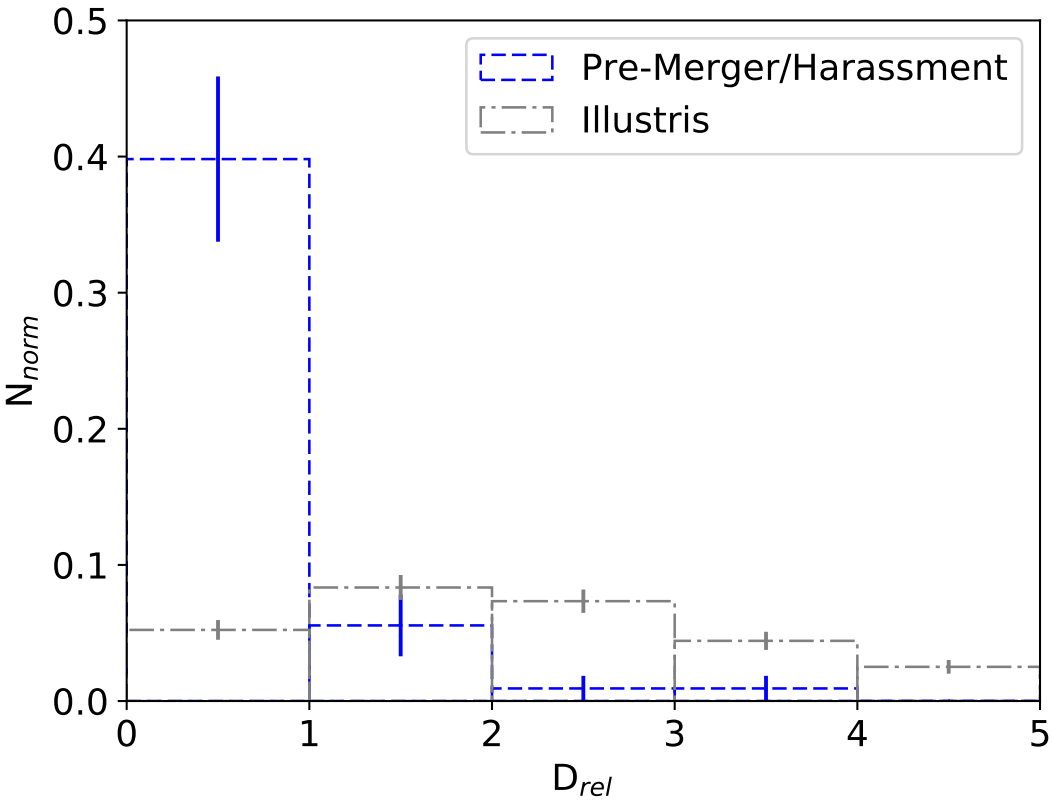

Figure 3.2: The distribution of relative distances of pre-merger/harassment starbursts and Illustris control galaxies to their closest neighbour, normalised to their relative total sample size. For ≈40% of the pre-merger/harassment starbursts, they have a neighbour within a relative distance of 1. This means that for these galaxies, the distance between the two galactic centres is less than the sum of their radii. We note here that there are galaxies within our sample were D_{rel} is greater than 5, however as the amount in each bin is negligible we exclude these from this plot.

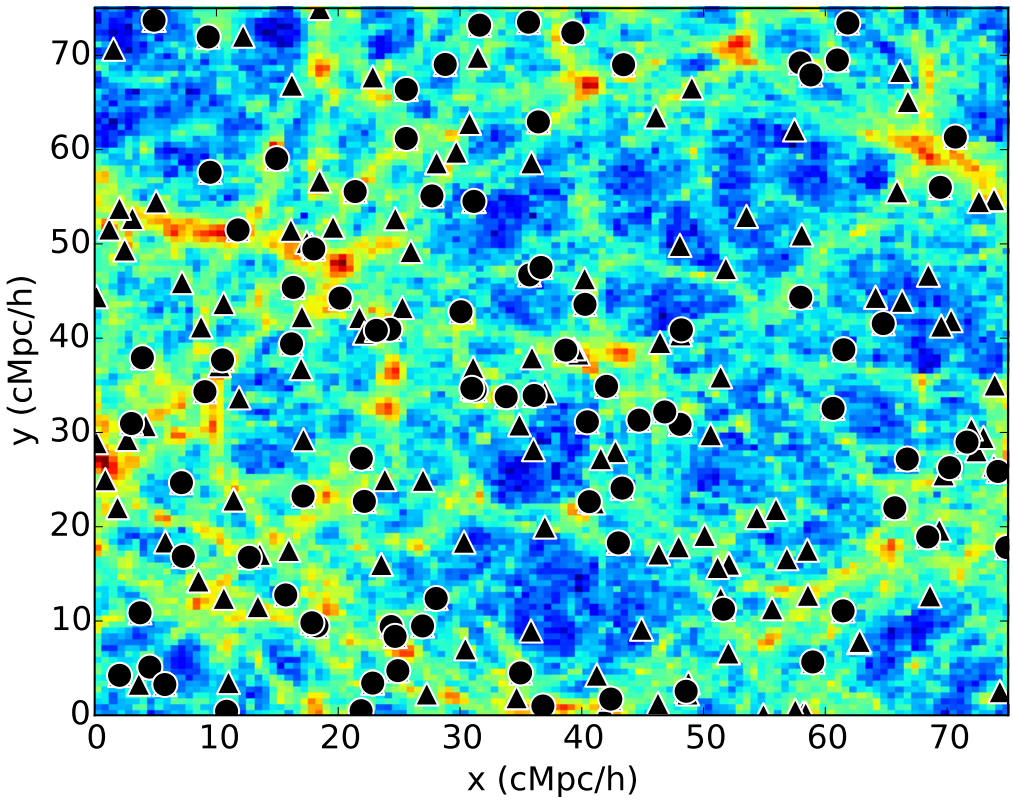

Figure 3.3: A projection view of the Illustris simulation highlighting the locations of starburst galaxies with mergers in the previous 2 Gyr (circles) and pre-merger/harassment starbursts (triangles). The redder regions of the plot represent the densest (by number of subhalos) areas within Illustris, whilst the blue regions are the least dense. We find that starbursts are predominantly in low-density regions around filaments within the cosmic web.

Fig. 3.3 shows the locations of starburst galaxies against the number density of galaxies in Illustris. We highlight the locations of starbursts that have had some sort of merger in the last 2 Gyr. We can see that the majority of the starbursts are located in the lower density environments around the filament regions.

To quantify the environments of starburst galaxies in Illustris, we determine the number of galaxies with a minimum mass of $10^5 M_\odot$ (this is the minimum stellar mass of a resolved subhalo) surrounding our starburst and control samples within 500 kpc and 1 Mpc as shown in Fig. 3.4. Using the same approach in section 3.1, we compose our control sample by selecting 500 random non-starburst galaxies. We find that the distribution in both samples peaks in the least dense environments, this confirms the findings of Wilkinson et al. (2017) and Zabludoff

et al. (1996) that suggest post-starbursts and therefore starbursts have a preference for low-density environments. We find that the distribution of the pre-merger/harassment starburst sample tends to the right of the post-merger starburst sample towards denser environments, suggesting starbursts in denser environments are more likely to be driven by harassment events rather than mergers. The distribution of non-starburst galaxies is shifted towards denser environments meaning that starburst galaxies are in less dense environments than pre-merger/harassment starburst environments. We quantify this by performing a KS test and obtain a p-value much less than 1% when comparing the pre-merger/harassment starburst sample to the post-merger sample at distances of 500 kpc and 1 Mpc.

When examining the halos our galaxies are in, we find the mean halo mass for the pre-merger/harassment starburst sample is $6.1\pm2.1\times10^{12}$ $M_\odot$ compared with $3.4\pm2.0\times10^{12}$ $M_\odot$ for the merger starburst sample. This result adds further evidence that starbursts without a previous merger are in denser environments to post-merger starbursts.

3.3.3 Nuclear or Global Starbursts?

In an extreme case, a starburst will use up all available cold gas throughout the galaxy, but as starbursts typically occur on a very short timescale, ~50 Myr, these cases are very rare (Mihos & Hernquist 1994). It is more likely that gas is funnelled into the galactic centre, triggering a nuclear starburst (Barnes & Hernquist 1991, 1996). It is unknown to what extent gas is consumed in this scenario because molecular hydrogen has been found in some post-starburst galaxies (Zwaan et al. 2013; French et al. 2015).

We start by examining the Star Formation Rates (SFR) of our samples (Fig. 3.5) from z = 0.36 to z = 0.00 (this is 2 Gyr either side of the snapshot used for selection). We split each sample by the mass bins as defined in Table 3.1. We include the total SFR (orange and aqua) and the SFR within the stellar half mass radius (red and blue). In the legends we include the significance of the peaks in terms of σ which is calculated by subtracting the median SFR before the peak from the height of the peak and dividing by the standard deviation of the pre-starburst SFRs. The peaks of the starbursts in these plots appear milder than expected, this is likely due to the time spacing between snapshots as starburst duration

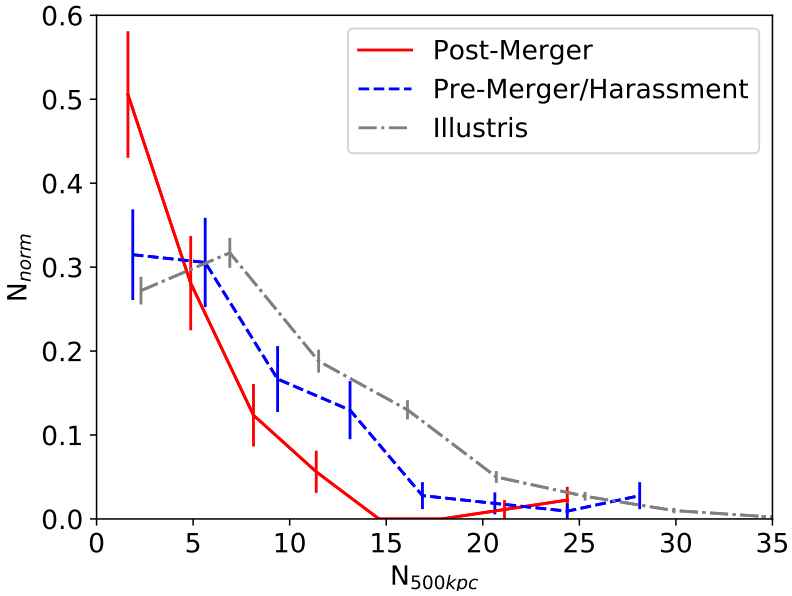

(a)

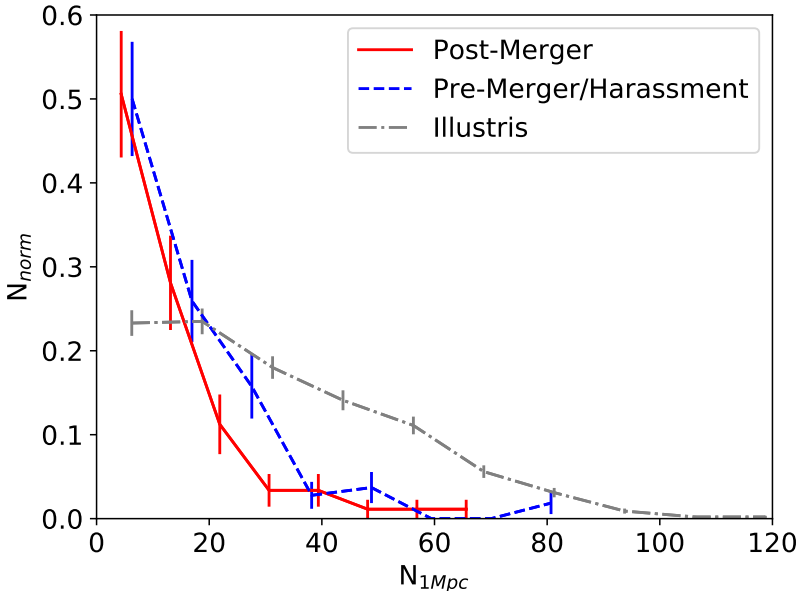

(b)

Figure 3.4: These plots show the number density of galaxies with a minimum mass of $10^5 M_\odot$ (the minimum stellar mass of a resolved subhalo) surrounding our samples within a volume of radii 500 kpc and 1 Mpc. Within a 500 kpc radius, we see the number density distribution for the pre-merger/harassment starburst sample (blue) shifts significantly to the right of the post-merger sample which indicate their locations in higher density environments, whilst merger driven starbursts reside in much weaker environments. In a 1 Mpc radius, we see less of a separation in distribution suggesting local environment could play a role in determining starburst triggers. In both plots, control galaxies from Illustris are in denser environments than both starburst samples.

(few 10^8 yr; Di Matteo et al. 2008) being comparable to snapshot time separation (0.158 Gyr) and therefore if the peak of the starburst does not occur when the snapshot is taken then SFR will be lower than expected. On average we find that the significance of the peak in SFR is higher in the pre-merger/harassment starburst sample (5.7σ at the half mass radius and 5.7σ at the total mass radius) than in the post-merger starburst sample (9.9σ at the half mass radius and 11.6σ at the total mass radius). We don't see a significant difference between the total and stellar half mass radius.

We also investigate the specific Star Formation Rates (sSFR) of our starburst galaxies. We plot sSFR against lookback time in Fig. 3.6, again split by mass bin and radii. In both samples we witness an offset between the total sSFR and sSFR within the stellar half mass radius, in which the sSFR in the stellar half mass radius is higher. For the post-merger sample, the average offset is $\log_{10}$(sSFR)=0.08 in which the sSFR in the total stellar mass radius is higher and for the pre-merger sample, we find this offset is $\log_{10}$(sSFR) = 0.1. When focusing on the enhancement at the time of the starburst, on average there is a higher enhancement in the stellar half mass radius. These results suggest that starbursts occur towards the galactic centre as noted by Barnes & Hernquist (1991) and Barnes & Hernquist (1996).

We can also see that the enhancement in sSFR is 0.1 dex higher in the pre-merger/harassment starburst sample compared to the post-merger sample. However, this could be a consequence of the resolution of Illustris; this means that burstier star formation would be averaged out into the background star formation as the measure of time used to calculate star formation is greater at the time duration of the starburst. Therefore, this could be the result of post-merger starbursts being burstier than the pre-merger/harassment starburst which would explain a lower peak in star formation.

When mergers and interactions occur, tidal torques funnel gas into the galactic centre (Barnes & Hernquist 1991, Barnes & Hernquist 1996). This build up of gas then acts as a fuel for a rapid burst of star formation. In this section we explore the extent of this increase in gas and test whether there is an infall to the galactic centre.

We plot the median stacked gas fractions within the stellar half mass radius and total gas fractions against lookback time in Fig. 3.7. We calculate gas fraction to be $M_{gas} / (M_{gas} + M_{stars})$,

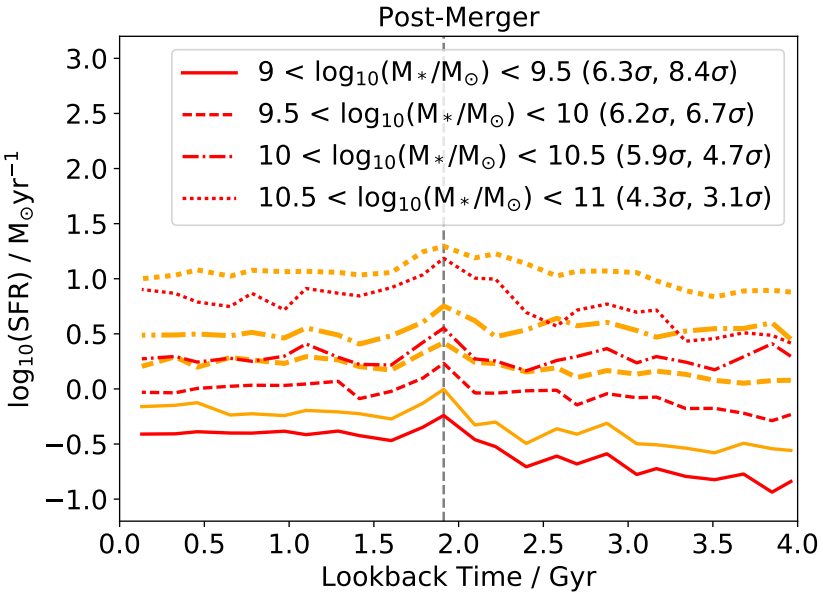

(a)

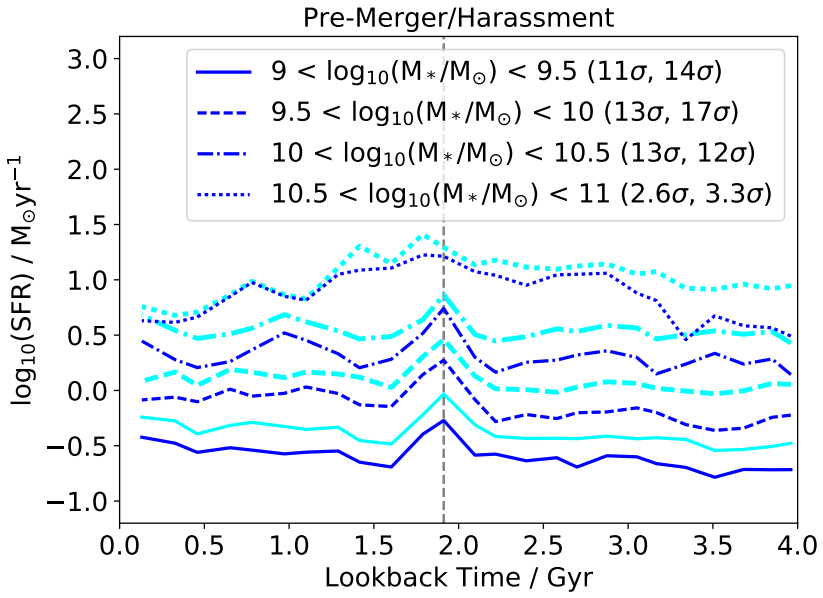

(b)

Figure 3.5: Median stacked star formation rates (SFR) as a function of lookback time for post-merger starbursts (above) and pre-merger/harassment drivenrbursts (below). We include a grey dashed vertical line that denotes the temporal location of the starburst. We split our two samples by mass as given in Table 3.1. The lighter colours (orange and aqua) are correspondent to the total SFR, whereas the bolder colours (red and blue) are representative of SFR within the stellar half mass radius. In all cases the starburst can be witnessed as a peak in the middle of the plots. In the legends we include the significance of the peaks in terms of σ (refer to main text for a description of how the significance is calculated) for the SFR in the stellar half mass radius and the total SFR respectively.

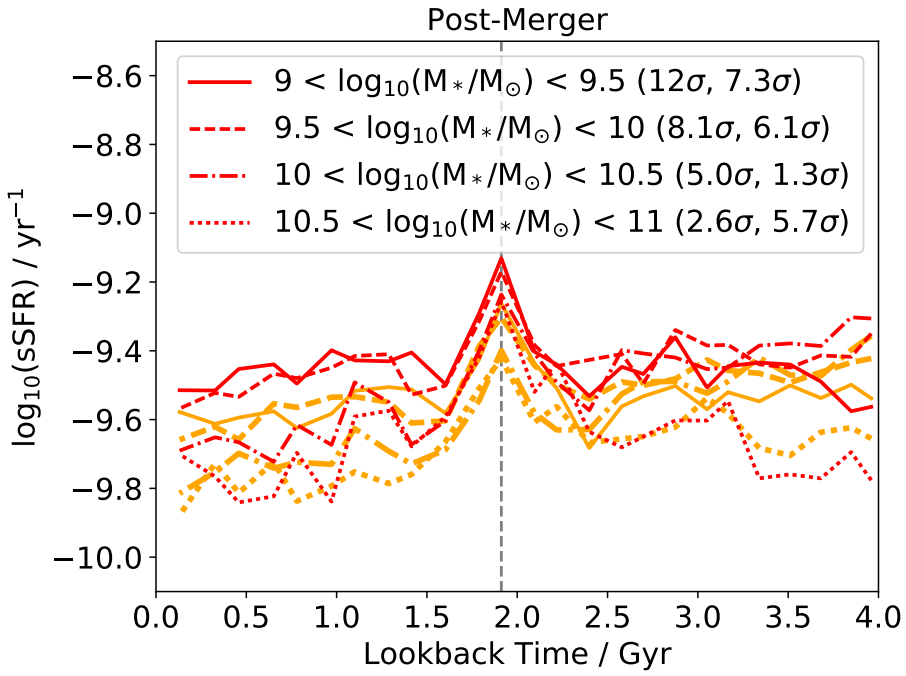

(a)

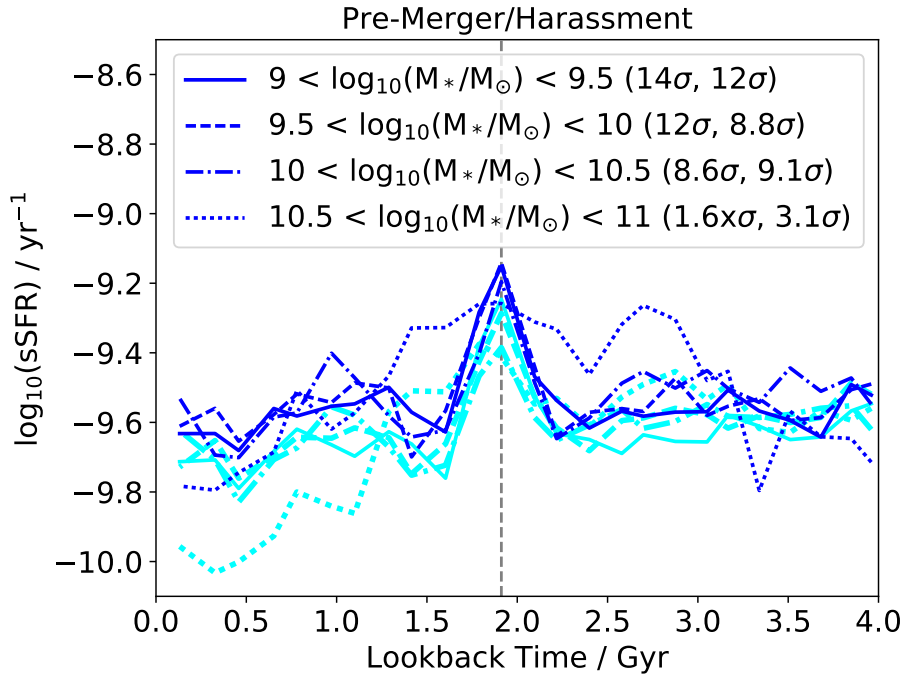

(b)

Figure 3.6: Median stacked sSFR as a function of lookback time. The sSFR in both samples is higher in the stellar half mass radius when compared to the total radius. Again, we include the significance of all peaks within the legends for the stellar half mass radius and total radius respectively. A description of how the significance is calculated can be found in the main text.

where M_{gas} is the mass of the gas and M_{stars} is the stellar mass. We see that there is a very mild downwards trend towards z=0 throughout each gas fraction calculated which is attributed to steady rates of star formation. Whilst we see no significant change in gas fraction within either sample at both the half mass and total radii, for both samples we see a slight fluctuation within the stellar half mass radius at the time of starburst. Due to the insignificance of this fluctuation, it could suggest that star formation in Illustris is very efficient. In the model described by Springel & Hernquist (2003), quiescent star formation rates increase with gas density, however if gas density surpasses a threshold value the gas consumption time scale becomes very rapid producing a burst of star formation. This increase in star formation efficiency in the galactic centre means that gas is quickly converted to stars. The insignificance of the peak in gas fraction could also be because the cold to hot gas ratio has increased during the starburst therefore increasing the star formation efficiency. We add the caveat that whilst it is possible to calculate the temperature of gas in Illustris, the resolution is not high enough to allow the probing of molecular gas clouds and therefore we are unable to locate the cold gas reservoirs in our galaxies.

By using a simulation that has shorter time intervals between snapshots, we may be able to witness a more significant rise and fall of the gas fraction within the stellar half mass radius. Because this fluctuation only appears in the half mass radii, this could indicate that the starburst event affects mainly the nuclear regions with a greater effect further afield only in extreme cases. A nuclear starburst would mean there is negligible change to gas fraction outside of the central region, which is what we see in Fig. 3.7.

3.3.4 Colour

Poggianti et al. (1999), Poggianti et al. (2009) and Wilkinson et al. (2017) find there is bimodality in colour when studying the properties of post-starburst galaxies. We explore this further by using the mock stellar photometry measurements Illustris provides. Fig. 3.8 shows a colour-magnitude diagram at the time of the starburst. We include the separation lines from Vogelsberger et al. (2014b) and Bray et al. (2016) that denote the locations of the blue cloud and the red sequence. We add the caveat that the red sequence is not well defined in Illustris

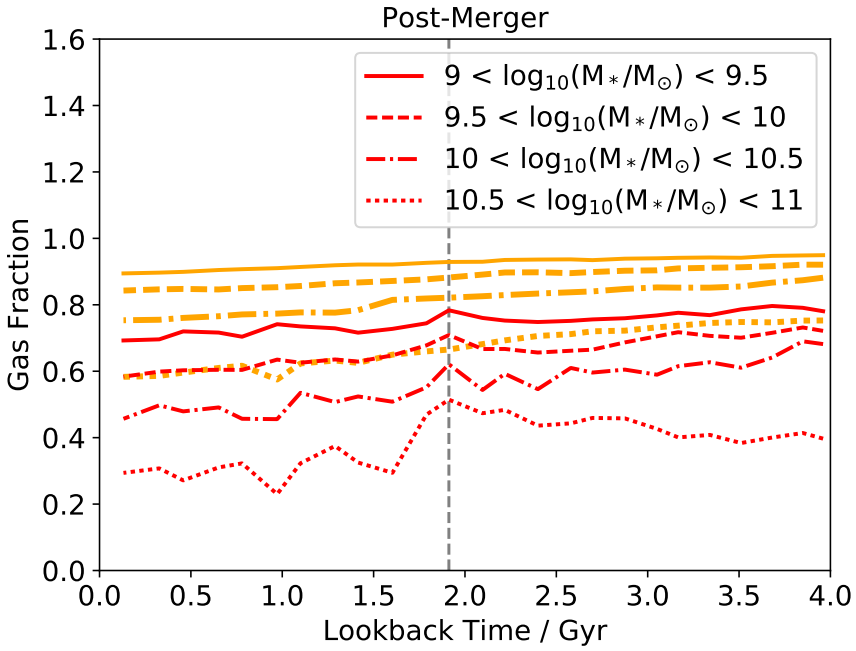

(a)

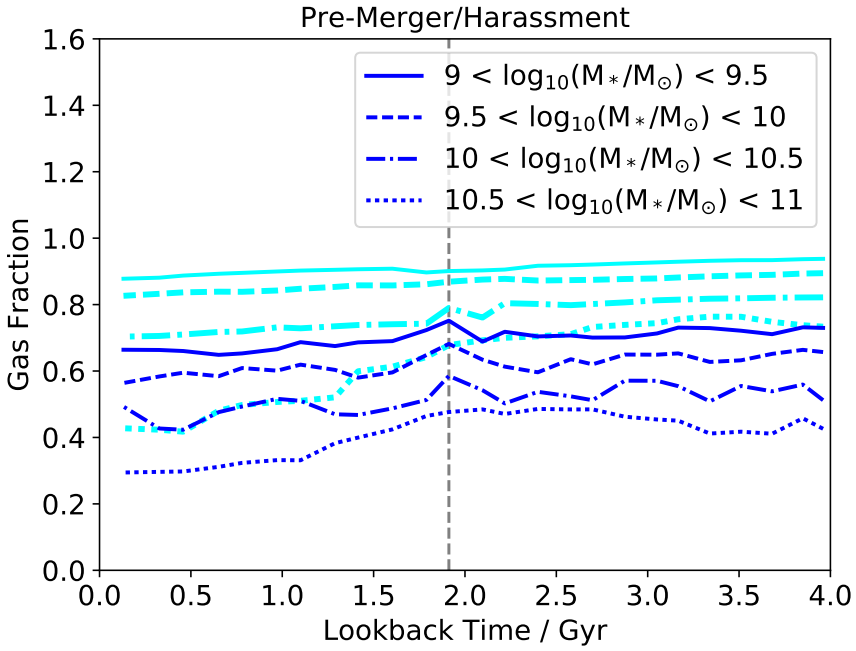

(b)

Figure 3.7: Median stacked gas fractions against lookback time for post-merger starbursts (above) pre-merger/harassment triggered starbursts (below). Gas fraction is calculated as M_{gas} / (M_{gas}+M_{stars}). There is no visible change in gas fraction within the total radius. However there is a slight but not significant change in gas fraction within the stellar half mass radius, this suggests star formation in Illustris is very efficient.

using photometry measurements, as there is no clear bimodality in colour. However, by plotting a colour-magnitude diagram, it allows us to determine whether one sample is bluer or redder than the other. Comparing to observational colour magnitude diagrams (Lorenzo et al. 2012), we find that in observations the red sequence and blue cloud tend to higher g-r values and the two red and blue populations more pronounced, whilst in Fig. 3.8, we see a flattened red sequence, making the two populations somewhat indistinguishable. These differences in observational and Illustris colour magnitude diagrams stem from the lack of dust in Illustris and therefore only the intrinsic colours are able to be calculated (Vogelsberger et al. 2014b).

From Fig. 3.8, we see that all starbursts are located well within the blue cloud region of the colour-magnitude diagram; situated under both the Vogelsberger and Bray lines (Vogelsberger et al. 2014b and Bray et al. 2016 respectively). The Illustris simulation does not include dust and therefore this is why there is no large range in the colour of starbursts. Instead, starbursts are 'ultra-blue' in colour.

We explore how colour changes over time in Fig. 3.9 by plotting the colour distribution at 0.5 Gyr intervals before, during and after the starburst event. We find that within the 4 Gyr range the vast majority of starbursts are below g-r = 0.6 and can be considered blue (Vogelsberger et al. 2014b). At the snapshot containing the starburst we can see that the colours of both samples become bluer and then shift to approximately their original positions after the starburst. However, we find that the pre-merger/harassment sample has an extended tail towards redder colours which becomes more pronounced as the galaxies progress through the post-starburst phase. We have seen previously in section 3.2. pre-merger/harassment starbursts have an extended tail into denser environments which suggests environment has an impact on the colour of starburst galaxies.

3.3.5 Quenching and Feedback

Active galactic nuclei (AGN) have been linked with post-starburst galaxies in many studies such as Trouille et al. (2011), Melnick et al. (2015) and Baron et al. (2017) to name a few. It is heavily reported in the literature that mergers, particularly gas-rich major mergers, could be the main trigger behind AGN activity (Di Matteo et al. 2005; Hopkins et al. 2006). This

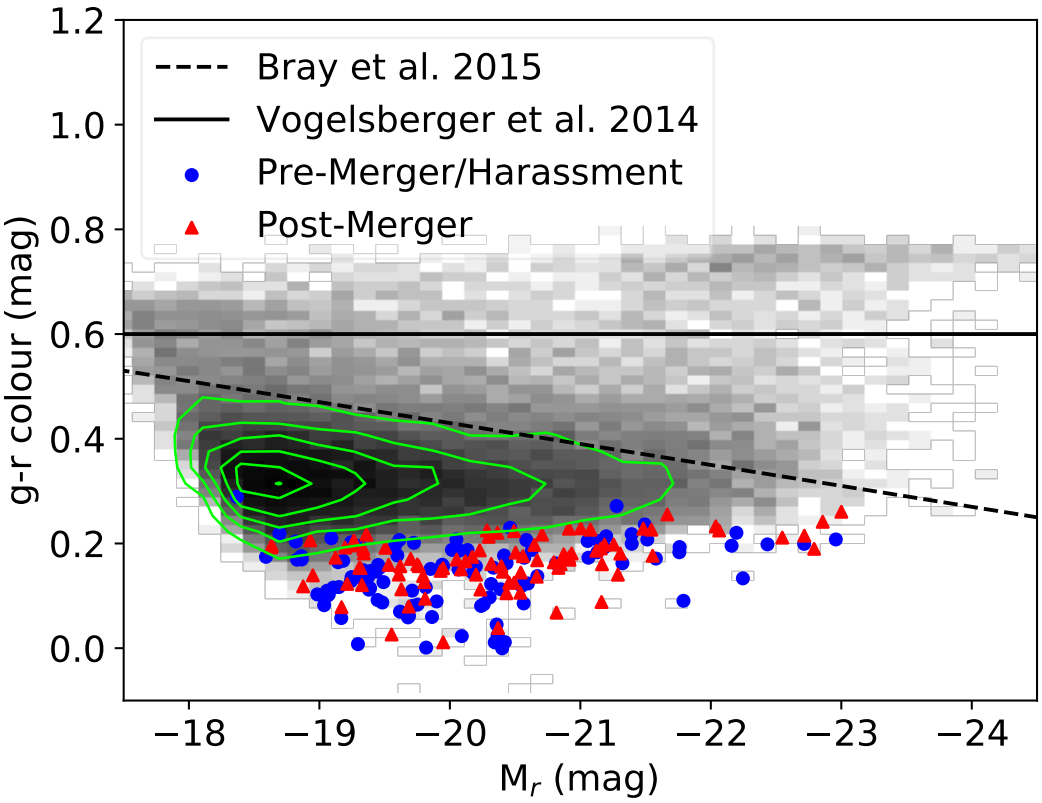

Figure 3.8: Colour-magnitude diagram at the time of starburst. We include the separation lines from Bray et al. 2016 (dashed line) and Vogelsberger et al. 2014b (solid line) that denote the locations of the blue cloud and red sequence. Illustris galaxies are denoted by the grey colour map and green contour lines. The darkest areas of the plot are the densest regions of the colour-magnitude diagram. It is clear from the distribution of Illustris galaxies, the red sequence is not well defined and hence the majority of galaxies reside in the blue cloud, this could be due to the absence of dust in the Illustris simulation. We find that both the post-merger (red triangles) and pre-merger/harassment (blue circles) starburst samples are located at the farthest regions of the blue cloud.

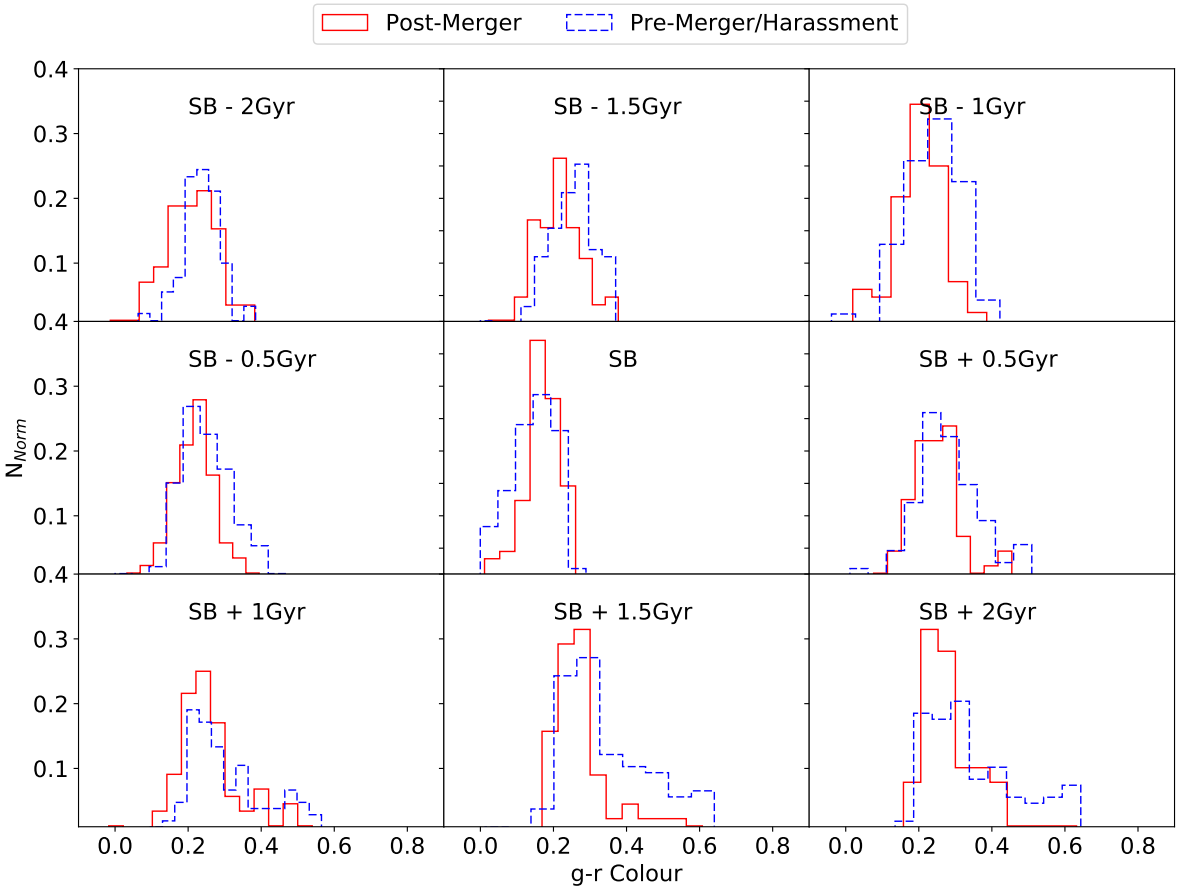

Figure 3.9: The g-r colour distributions 2 Gyr before and after the starburst event at intervals of 0.5 Gyr. We can see both populations are within the blue cloud and at the time of starburst (central plot) the distributions shift further into the blue cloud. After the starburst, the colour distributions shift to the right, slightly reddening.

is the same trigger that is believed to ignite the starburst phase and hence post-starburst phase (Zabludoff et al. 1996; Bekki et al. 2005; Hopkins et al. 2006). In this section we briefly test to what extent AGN feedback plays in quenching star formation by examining black hole masses of the galaxies in this study.

In Fig. 3.10, we plot black hole mass against lookback time. Here, black hole mass is described at the sum of the masses of all black holes in a subhalo. In both samples we see there is a gradual increase in black hole mass. For higher mass galaxies in the post-merger sample, there is on average a greater growth in black hole mass which could indicate there is a larger level of AGN feedback, although there is no significant difference towards lower masses.

3.4 Discussion

Whilst previously thought that mergers are required to trigger a starburst, we find in this study, that harassment events can also trigger a starburst that is comparable in strength. We see that 55% of the starbursts in this study have not had a previous merger in the past 2 Gyr. These starbursts appear to have been triggered by harassment events (that may or may not lead to a future merger), galactic instabilities (Sparre et al. 2015) or the accretion of gas from the surrounding intergalactic medium. Without the raw Illustris data we are unable to measure the tidal gravity between surrounding galaxies to test directly whether harassments are the main trigger for the pre-merger/harassment starbursts; this would be a suitable subject for future study. However, to get an indication of whether harassments could be a significant trigger, we test how close galaxies get to one another by studying their relative distances, as defined in Eq. 3.1. We find that ~40% are within distances equivalent to the sum of their half mass radii, this means galaxies become very close, possibly to the extent in which their disks directly interact. At these distances it is likely that this could trigger a starburst.

In the literature, post-starburst galaxies have been shown to reside in low-density environments (Zabludoff et al. 1996; Bekki et al. 2001; Sánchez-Blázquez et al. 2009). We have seen that the starburst galaxies in this study are found to reside along the filament regions in low-density environments. When comparing the post-merger starbursts to the

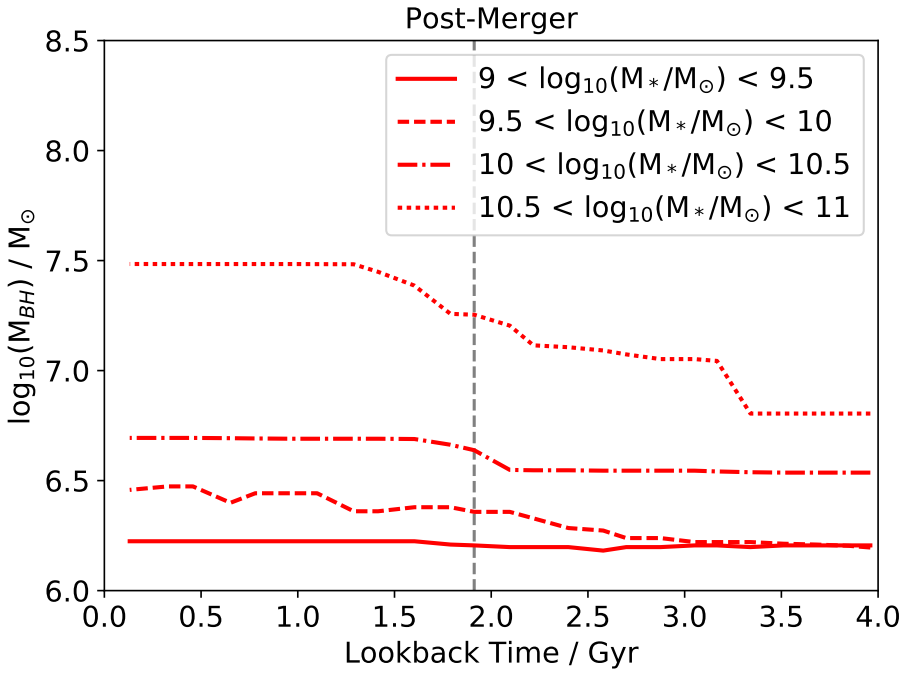

(a)

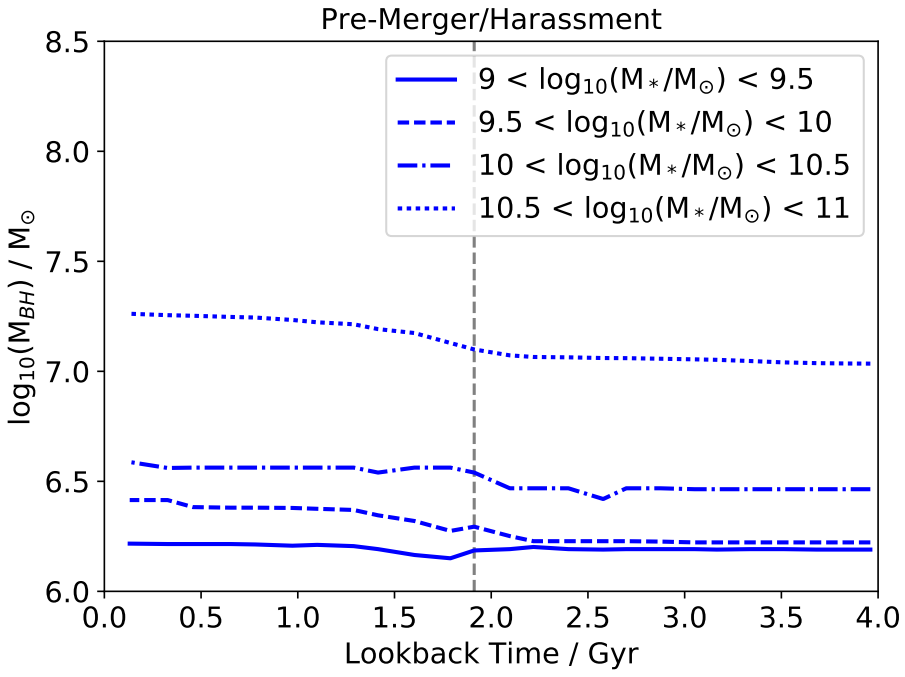

(b)

Figure 3.10: Median black hole masses over lookback time for both samples. We have split each sample into the mass bins defined in Fig. 3.1. We see that for higher mass galaxies there is a slight gradual increase in black hole mass.

pre-merger/harassment starbursts we find that the pre-merger/harassment sample has a preference for denser environments. As denser environments have higher velocity dispersions, galaxies in close proximity are more likely to harass and fly-by than merge directly. We also compare the colours of both samples before, during and after the starburst and find the colour distribution of pre-merger/harassment starburst sample to be slightly redder than post-merger driven starbursts. We believe this is linked to environment and therefore starbursts that occur in denser environments are likely to be redder than low-density environments.

To examine the strength of the starbursts, we test SFR and sSFR and find that starbursts occur on timescale of <0.5 Gyr. With a higher resolution simulation and shorter time intervals between snapshot we would be able to make a more accurate measurement of starburst duration. Further, we see there are higher sSFR within the stellar half mass radius compared to the total sSFR. This suggests that starbursts occur more in the central regions as suggested by Barnes & Hernquist (1991) and Barnes & Hernquist (1996) rather than affecting the whole galaxy. This is also visible when we test gas fractions: while there is no significant enhancement in gas fraction due to efficient star formation within the entire halo, we do witness a slight change within the stellar half mass radius which supports the nuclear starburst hypothesis.

We also find that the enhancement in sSFR at the time of the starburst is on average higher in the pre-merger/harassment starburst sample, which would suggest that starbursts are stronger when not driven by a merger. However, due to the resolution of the Illustris simulation, it is more likely that starbursts in the merger driven sample are burstier than pre-merger/harassment starbursts and hence appear to be lower when averaged over time (Sparre & Springel 2016).

We briefly investigate the extent AGN feedback could play in quenching star formation by measuring black hole masses over lookback time. We find there is on average more growth in black hole mass in the post-merger sample than there is in the pre-merger/harassment sample. This could indicate that there is more AGN feedback post-merger.

Illustris is a state of the art simulation capable of generating a partial Universe that resembles the large scale structure visible in the observable Universe. Whilst our findings on

environment match the observational findings in our previous work (Wilkinson et al. 2017), there are still parameters than can be improved on, for example, the presence of dust, which has a significant effect on colour. While we have been able to make meaningful predictions on the properties of starburst galaxies, improvements in temporal and spatial resolution would give us a larger sample size and allow us to probe deeper into a starburst kinematics so we can make better predictions for the properties of observable starbursts.

3.5 Conclusions

Starburst galaxies and the events that trigger them play an important role in transforming star forming spirals into quiescent ellipticals. The literature has many discrepant findings concerning the role of environment and triggering mechanisms. In this chapter we have utilised the Illustris simulation to explore the possible triggering-mechanisms and making a comparison between post-merger and pre-merger/harassment triggered scenarios. We list here our principal findings:

1. We find that 55% of the starbursts identified in this study have not been triggered by a merger. The majority of this sample we believe to have been harassment driven due to their very close relative distances between surrounding galaxies, < 1.

2. We find that in both of our samples, starburst galaxies are located within low-density regions in the filament regions of the cosmic web. The pre-merger/harassment driven starbursts have been found to have an extended tail in denser environments compared to post-merger starbursts.

3. sSFR is on average larger within the stellar half mass radius which suggests a nuclear starburst rather than a galaxy wide starburst.

4. Pre-merger/harassment starbursts have a slight extended tail towards redder colours in their colour distribution compared to post-merger starbursts. This is driven by environment and therefore denser environments produce redder post-starburst galaxies.

5. These results suggest that mergers not only trigger bursty star formation but they could also trigger higher rates of feedback.

These findings suggest that whilst there are two significant processes that can trigger a starburst of comparable strength, environment has an impact on which process a galaxy takes to enter the starburst phase. This also has an effect on the colour of the galaxy which in turn could contribute to the bimodality of colour of post-starburst galaxies we see in observational studies such as Poggianti et al. (1999). Further work using the latest IllustrisTNG (Nelson et al. 2018b; Naiman et al. 2017; Springel et al. 2017; Pillepich et al. 2017; Marinacci et al. 2017) will allow us to probe starburst galaxies in further detail with a higher temporal and spacial resolution.

Acknowledgements

We thank the anonymous referee for their useful report that has helped improve the quality of this work. We would like to thank Sugata Kaviraj for his advice and useful discussions during this study. KAP and BKG acknowledge support of STFC through the University of Hull Consolidated Grant ST/R000840/1. This research has made use of the Illustris database. The Illustris project acknowledges support from many sources: support by the DFG Research Centre SFB-881 “The Milky Way System” through project A1, and by the European Research Council under ERC-StG EXAGAL-308037, support from the HST grants program, number HST-AR-12856.01-A, support for program #12856 by NASA through a grant from the Space Telescope Science Institute, which is operated by the Association of Universities for Research in Astronomy, Inc., under NASA contract NAS 5-26555, support from NASA grant NNX12AC67G and NSF grant AST-1312095, support from the Alexander von Humboldt Foundation, NSF grant AST-0907969, support from XSEDE grant AST-130032, which is supported by National Science Foundation grant number OCI-1053575. The Illustris simulation was run on the CURIE supercomputer at CEA/France as part of PRACE project RA0844, and the SuperMUC computer at the Leibniz Computing Centre, Germany, as part of project pr85je. Further simulations were run on the Harvard Odyssey and CfA/ITC clusters, the Ranger and Stampede supercomputers at the Texas Advanced Computing Center through XSEDE, and the Kraken supercomputer at Oak Ridge National Laboratory through XSEDE.

3.6 Additional Results

In this section, we present extra findings that were not included in the published work Wilkinson et al. (2018). As described in section 3.3.5, AGN have been linked quite heavily with post-starburst galaxies and to extend this work we investigate how accretion rate varies over lookback time for our starburst sample. In addition, we also examine the presence of stellar winds. In Illustris, stellar winds are driven by supernova feedback in which gas can be blown out suppressing star formation. This process could have significant impact on quenching star formation in starburst galaxies.

3.6.1 Accretion Rates and Stellar Winds

We begin by plotting accretion rate against lookback time in Fig. 3.11. Whilst the data are noisy, we do witness some significant peaks in the merger sample in the lowest two mass bins and the highest mass bin. In the non-merger starburst sample we see that the $10^{9.5}$-10^{10} $M_{\odot}$ and $10^{10.5}$- 10^{11} $M_{\odot}$ mass bins show a significant rise in accretion rate. We display the significance of the peaks in Fig.3.11 in terms of σ. However, because both samples are too noisy (i.e. other peaks of similar height to the starburst peak) we cannot formulate a conclusive result from these plots. Higher resolution simulations will allow us to investigate the effects of AGN feedback with greater precision. If AGN feedback operates within a relatively small radius in the galactic core, then we need to be able to resolve this area. Starburst galaxies are under-produced in Illustris (Sparre et al. 2015), therefore a better resolved simulation would tackle this problem leading to larger samples of starbursts to be produced and the amount of noise witnessed in Fig. 3.11 would be reduced.

Finally, we test whether the stellar winds from supernova suppress star formation as found by Faucher-Giguère (2018). To do this we plot wind mass against lookback time in Fig. 3.12. In the non-merger starburst sample we find that in each of the mass bins there is a >2 σ peak which suggests stellar winds have a significant impact on quenching star formation. In the merger sample, we see some enhancement in wind mass around the point of starburst. This could mean that mergers are capable of triggering greater galactic winds than non-merger interactions and therefore winds play a greater role in quenching star formation

in merger driven starbursts compared with non-merger driven starbursts. Greater resolved single study simulations would allow us to trace the galactic winds generated as a result of merger interactions to determine whether winds are responsible for quenching star formation and whether their role is greater in merger driven starbursts compared to harassment driven starbursts.

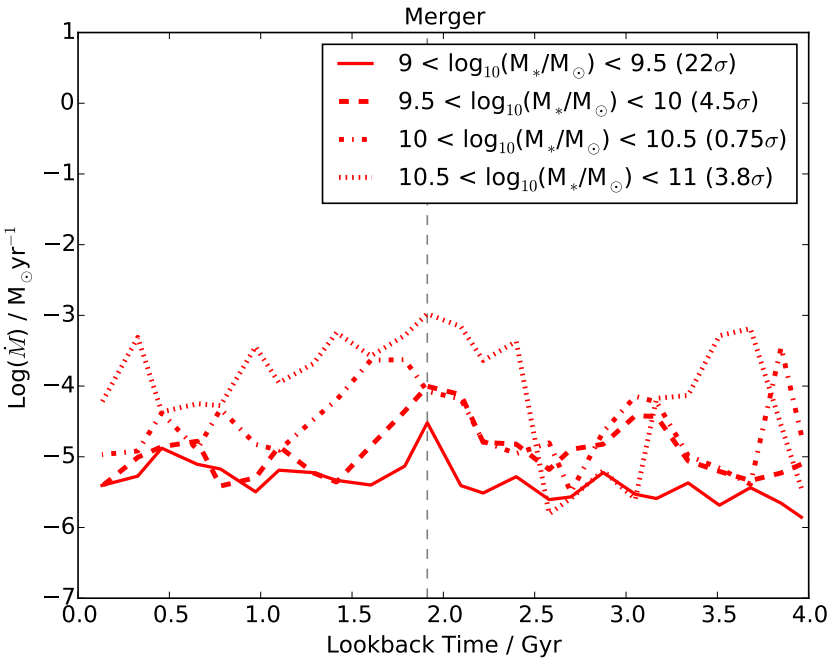

(a)

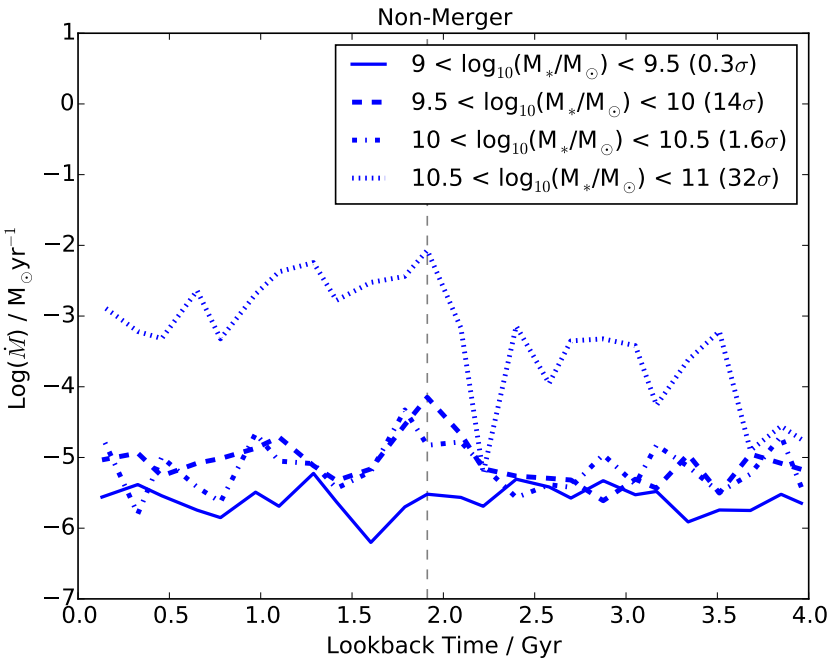

(b)

Figure 3.11: Stacked median instantaneous black hole accretion rates over lookback time for both samples. Whilst there is a large amount of scatter in both plots, we see significant peaks (listed in the legend of the plots) in the merger sample for all but the third mass bin. In the non-merger starburst sample we only see significant peaks in the second and fourth mass bins. Due to the noise we cannot make a comparison between the two samples.

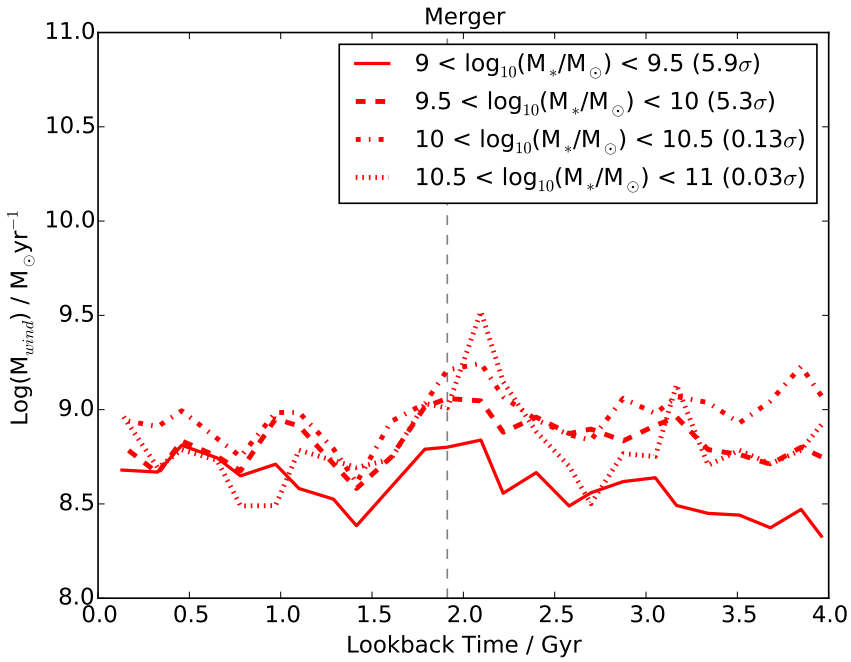

(a)

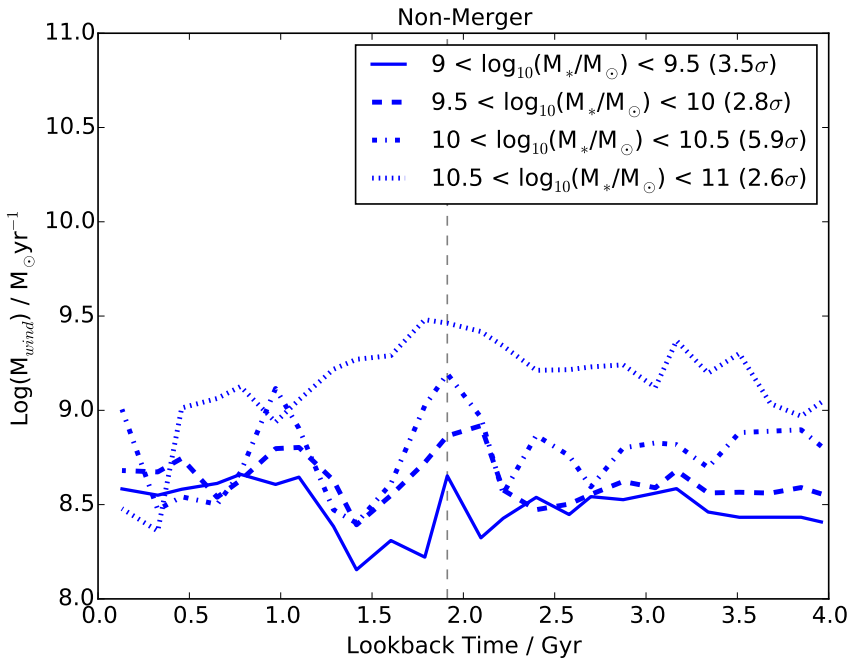

(b)

Figure 3.12: These plots shows the stacked median masses of the total wind particles in our galaxies. These kinetic winds are caused by supernova expelling the surrounding gas. We find that wind is present in both samples suggesting it plays a significant role in quenching star formation in Illustris, although for lower mass galaxies we find that the winds are stronger in the merger sample.

4. The Radio Properties of Starburst Galaxies

Declaration

This chapter represents work in preparation for publication as a letter in the MNRAS journal. It has been led by myself and co-authors are Dr Kevin Pimbblet and Dr John Stott.

Abstract

There are multiple pathways in which star formation in bursts can be quenched. These include AGN feedback, stellar winds, ram pressure stripping etc. Here we attempt to determine whether or not AGN play the primary role in quenching starbursts. We do this by comparing the fractions of optical and radio AGN in our starburst sample to a control sample comprised of 'normal' star forming main sequence galaxies. We find that 1.7±0.4% of starbursts contain optical AGN whereas 6.1±0.2% of star forming galaxies have an AGN. This suggests that either AGN do not play significant role in the primary quenching of the burst, the starburst phase is not well regulated by AGN feedback or that the overlap time between the starburst and AGN phase is very short such that detecting galaxies with both signatures is very rare.

There are many studies that suggest the IMF in starburst galaxies is top-heavy. If the IMF is top-heavy, then more higher mass OB stars are produced and thus more supernova explosions. However, if the IMF is bottom-heavy, then more lower mass stars are produced and fewer supernovae resulting in a lower radio emission. In this study we aim to test these scenarios by comparing optical emission, using the Hα line which traces massive stars greater than 20 $M_\odot$, to radio emission which traces stars approximately 8 $M_\odot$ and greater. We select a sample of starburst galaxies from SDSS DR7 and match to the radio catalogue FIRST and compare their emission to a control sample of galaxies that are quiescently star forming. We find that there is an excess in Hα emission in the starburst sample which suggests there are more higher mass stars formed in a burst compared with quiescent star formation, this could indicate a top-heavy IMF in starbursts galaxies, although this could also be caused by other phenomena such as low-level AGN.

4.1 Introduction

4.1.1 AGN in Starbursts

The connection between starburst galaxies and AGN has been extensively studied with inconclusive results. Some studies such as Coil et al. (2011), Cicone et al. (2014), Yesuf et al. (2014) and Wilkinson et al. (2017) suggest that starbursts are not explicitly quenched by AGN whilst studies such as Smith et al. (1998), Goto (2006), Melnick et al. (2015) and Baron et al. (2017) support the idea that AGN play an important role in quenching bursts of star formation.

Goto (2006) use spatially resolved spectroscopy to examine the properties of post-starburst (PSB) galaxies with AGN signatures. They find that the post-starburst region is centrally located around the AGN such that the spatial proximity is close enough that the AGN could affect the PSB region. They find that AGN outlive the starburst phase indicating that AGN feedback plays a role in quenching the burst of star formation. More recent work by Baron et al. (2017) find evidence of on-going AGN feedback in the post-starburst galaxy SDSS J132401.63+454620.6. They find gas with a velocity dispersion greater than the escape velocity, this indicates strong evidence of an AGN-driven outflows in post-starburst galaxies. If AGN are responsible for quenching the starburst phase, we would expect to detect an enhanced fraction of AGN within our starburst sample.

Coil et al. (2011) examine spectra for 10 AGN and 13 post-starburst galaxies to see if the observed extreme winds found by Tremonti et al. (2007) are apparent in AGN and post-starburst galaxies. Whilst they find that both samples contain winds, these winds are not strong enough to suppress star formation and are likely to originate from supernova not AGN. This supports the idea that AGN do not quench star formation in starbursts. Meanwhile, Cicone et al. (2014) finds that outflows in starbursts without AGN are 'momentum-driven' caused by the radiation pressure of young stars. These outflows are powerful enough to quench star formation and can be enhanced by the presence of AGN increasing the efficiency at which cold gas is removed from the star forming region.

Whilst Yesuf et al. (2014) finds that post-starburst galaxies have a higher fraction of AGN compared to normal star forming galaxies (>36% more than other galaxy types), they find there is a time delay of ≈200 Myr between the peak of the starburst and the AGN. Yesuf

et al. (2014) compare the dust content between starbursts and post-starburst and find starburst galaxies have higher dust contents than post-starbursts indicating the AGN removes dust at a later stage and may not be involved with the primary quenching of the starburst but minimise the low-level star formation after the burst.

It is clear from the literature that AGN play a significant role in the life cycle of galaxies, however, there is still much debate as to what extent their role is in quenching starbursts. In this study, we aim to compare the fraction of AGN found in starburst and 'normal' main sequence star forming galaxies to determine whether AGN feedback is the main quenching pathway of star formation in bursts. If AGN really are responsible for quenching the starburst then we may expect to see a significant fraction of AGN in our starburst population. We investigate the presence of AGN in starburst galaxies using both optical and radio techniques to determine whether AGN play a significant role in quenching the starburst phase.

4.1.2 Top Heavy IMF in Starbursts

The IMF connects the distributions of high mass stars, detected through Hα, UV, IR and radio tracers, and low mass stars which dominate the galactic stellar populations (Kennicutt 1998). Understanding the form of the initial mass function (IMF) is critical when studying the spectral and chemical evolution of galaxies. Whether starburst galaxies have a top-heavy IMF (i.e. the slope of the IMF is flatter than that of the Salpeter slope which is based on a simple power-law model; Salpeter 1955) has been heavily debated in recent years (Baugh et al. 2005; Gunawardhana et al. 2011; Marks et al. 2012). Very recently, Schneider et al. (2018) gathered optical spectra for ~800 stars within the starburst region of the Large Magellanic Cloud, 30 Doradus (30 Dor). They find an excess of massive stars (> 30 $M_\odot$) and a shallower IMF slope above 15 $M_\odot$ meaning the IMF in 30 Dor could be top-heavy. However, they add that measuring the IMF above 30-60 $M_\odot$ is difficult (Bastian et al. 2010) and suggest mass accretion in binary systems cause stars to appear younger than they are. Other observational studies such as Rieke et al. (1993), Figer et al. (1999), McCrady et al. (2003), Stolte et al. (2005), Parra et al. (2007) and Harayama et al. (2008) find observational evidence of a top-heavy IMF within the starburst regions of galaxies M82, Arp 220 and the Milky Way.

At higher redshifts (z~2–4), sub-millimetre galaxies are found to have extremely high rates of star formation, particularly that of massive O-class stars which infer the presence of a top-heavy IMF. Their spectral energy distribution is dominated by the thermal emission of stars and therefore are good tracers for optically obscured star formation (Hayward et al. 2011). Baugh et al. (2005) investigate how sub-millimetre galaxies fit into current theories of galaxy formation. They combine semi-analytical modelling of galaxy formation with radiative transfer modelling to estimate the number of sub-millimetre galaxies at high redshifts. Baugh et al. (2005) find that by including a top-heavy IMF in their model, they better predict the number of sub-millimetre galaxies. Following on from Baugh et al. (2005), Lacey et al. (2008) use a combination of semi-analytical galaxy formation models and spectrophotometric code to calculate the galactic spectral energy distributions. They incorporate two IMFs into their model; normal IMF for quiescent star formers and top-heavy for merger triggered starbursts. By incorporating two IMFs into their model, their results strongly match to observational data gathered by the Spitzer telescope at mid- to far-IR wavelength. Lacey et al. (2008) find that their model under predicts the evolution in the mid-IR luminosity function compared to observations if using a normal IMF in starbursts supporting the idea that a top-heavy IMF is required in starburst galaxies.

Scalo (1990) review the use of the ratio of equivalent widths of silicon (λ1400) and carbon (λ1550) (Sekiguchi & Anderson 1987) to determine the IMF. Silicon originated from early B-class stars whereas carbon originates from the stellar winds of more massive O-class stars (Leitherer & Lamers 1991) and therefore the ratio of these lines allow us to infer the IMF. They find that not all starburst galaxies require a top-heavy IMF to explain their properties and between 10 and 50% of starbursts have an excess of massive stars, depending on whether the upper mass limit is no larger than 80-100 $M_{\odot}$.

In this study we use radio and optical data to infer the IMF of starburst galaxies. Parra et al. (2007) observe radio spectra for 18 radio sources within the Arp 220 starburst galaxy with the aim of determining the shape of the IMF. They find that the IMF in Arp 220 could overproduce high mass stars, however due to large uncertainties they cannot confidently claim starbursts have a top-heavy IMF. High mass stars (>8 $M_{\odot}$; Condon 1992) end their lives with

core collapse supernova explosions. Supernova and their remnants (excluding type-1a which are instead a thermonuclear detonation) emit synchrotron radiation at radio wavelengths due to the acceleration of relativistic electrons. Supernova remnants also ionize surrounding HII regions. Massive stars produced in a starburst can live up to $\gtrsim 3\times10^7$ yr whilst the relativistic electrons can live up to $\gtrsim 10^8$ yr (Condon 1992) therefore radio observations probe very recent star formation. Meanwhile, Hα emission traces the ionization of nebula caused by the UV radiation emitted by massive stars (>20 $M_\odot$; Calzetti 2013). Therefore, if a top-heavy IMF is present there should be an excess in Hα emission.

We aim to test the results of Parra et al. (2007) by comparing the observed to the predicted radio luminosities of a statistically significant sample of starburst galaxies to their optical emission in order to assess their IMF. We use SDSS selected starbursts with radio emission from the FIRST catalogue and compare to 'normal' star forming galaxies. If starbursts have a top-heavy IMF they should have a higher than expected Hα emission for a given radio luminosity compared to 'normal' star forming galaxies.

In section 4.2, we describe how we select the starbursts in this study and how we derive radio luminosity and radio star formation rates. In section 4.3, we describe the Starburst-AGN relationship. In section 4.4, we discuss the radio properties of starburst galaxies and discuss our overall findings in section 4.5. Our conclusions are presented in section 4.6. We assume the following cosmological parameters for a flat Universe: H_0 = 69.3 km s^{-1} Mpc^{-1}, Ω_M = 0.238 and Ω_Λ = 0.762 (Spergel et al. 2007).

4.2 Sample Selection

We use the MPA/JHU valued-added catalogue from SDSS DR7 (Abazajian et al. 2009) to create a volume limited sample of starburst galaxies. We begin by ensuring our sample is complete by using the same method displayed in Fig. 2.1 (Wilkinson et al. 2017). To create a volume and mass limited sample of starbursts, we select galaxies with redshift between 0.05 and 0.13, and stellar masses above $10^{10.5} M_\odot$ yr^{-1}. We explicitly select starbursts in the high mass regime, as at these masses AGN are thought to play a more dominant role in feedback as opposed to supernova, which are not energetic enough to deplete the cold gas reservoir needed

for star formation (Kaviraj et al. 2007). Using star formation rates and masses derived from Brinchmann et al. (2004) and Kauffmann et al. (2003) respectively, we plot the star formation main sequence, shown in Fig. 4.1. We note here that the SFR derived by Brinchmann et al. (2004) are based on a Kroupa IMF. To ensure we only fit our main sequence to the star forming galaxies, we explicitly remove quiescent galaxies by placing a cut in specific star formation rate at sSFR = $10^{-10.5}$ yr^{-1}. We repeat the method shown in Fig. 3.1 (Wilkinson et al. 2018), using linear regression to fit to the SFMS and selecting starbursts 0.6 dex above this line and above the mass limit stated above. Using this method we select 943 starburst galaxies.

Based on the same cuts in redshift and mass we form a control sample of star forming galaxies. We select star forming galaxies to be within ±0.6 dex of the main sequence, represented by the solid line shown in Fig. 4.1. This gives us a control sample size of 41288.

4.2.1 FIRST

In this study we make use of the radio survey FIRST (**F**aint **I**mages of the **R**adio **S**ky at **T**wenty-cm; Becker et al. 1995). FIRST is run from the Very Large Array (VLA), a component of the National Radio Astronomy Observatory (NRAO) and operates over the 1.4 GHz continuum. We choose this particular survey as it coincides with the survey area of SDSS and provides a larger sample size compared with the NVSS survey.

We match our starburst and control star forming sample to a matching radius of 15". If multiple matches occur, we select the closest match. This methods gives us 598 (63%) starbursts and 3566 (8.6%) star forming galaxies with radio data in the FIRST catalogue. Those galaxies without FIRST data were either not in the search radius of FIRST or the radio emission fell below the detectable limit of FIRST.

Before gaining any insights into the radio data, we must first calculate the radio luminosity, $L_{1.4\ GHz}$, from the radio flux density, S_{obs}. To do this we use Eq. 4.1, where D_L is the luminosity distance and α is the radio spectral index for which we adopt a value of 0.7 (Condon et al. 2002). The denominator in this equation adds a K-correction to the calculation.

$$L_{1.4\ GHz} = \frac{S_{obs} 4\pi D_L^2}{(1+z)^{1+\alpha}} \tag{4.1}$$

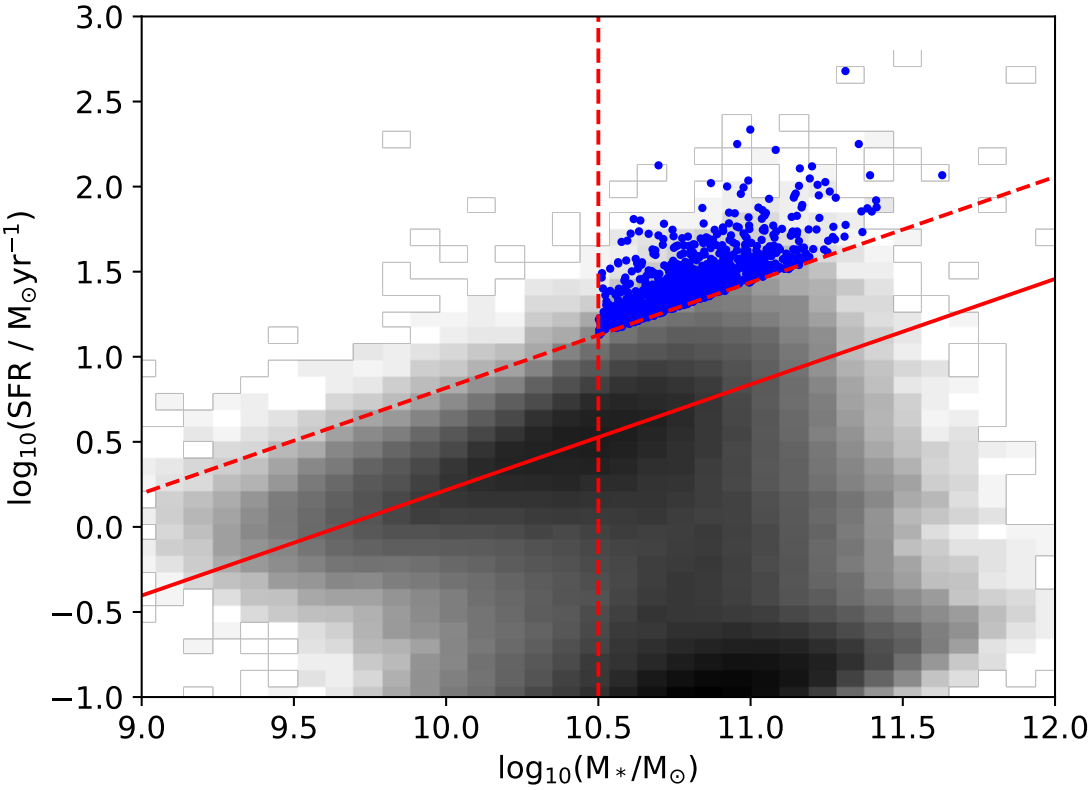

Figure 4.1: Star formation main sequence diagram of star forming SDSS DR7 galaxies. Quiescent galaxies are removed by implementing a cut in sSFR at $10^{-10.5}$ yr^{-1}. The solid red line denotes the linear fit to the star formation main sequence and we select starburst 0.6 dex above this line, represented by the dashed diagonal line and have masses above $10^{10.5}$ $M_{\odot}yr^{-1}$. Using this method we select 887 starburst galaxies (blue dots).

Next, we calculate SFR using equations 1 and 2 from Hopkins et al. (2003) (based on a Salpeter IMF) shown below in Eq. 4.2 and 4.3. To convert the Salpeter IMF to a Kroupa IMF, we divide our radio derived SFRs by a factor of 1.5 (Brinchmann et al. 2004).

$$SFR = \frac{f L_{1.4\ GHz}}{1.81 \times 10^{21}\ WHz^{-1}} \tag{4.2}$$

$$f = \begin{cases} 1 & \text{for } L_{1.4\ GHz} > L_c \\ (0.1 + 0.9(L_{1.4\ GHz}/L_c)^{0.3})^{-1} & \text{for } L_{1.4\ GHz} < L_c, \end{cases} \tag{4.3}$$

where L_c = 6.4×10^{21} W Hz^{-1}. The two forms of f in Eq. 4.2 and 4.3 originate from the differing characteristics of highly luminous and relatively faint radio galaxies, such that faint radio galaxies have a steeper radio-IR correlation, whilst highly radio luminous galaxies have a gradients close to unity (Bell 2003).

4.3 AGN in Starburst Galaxies

Many studies such as those by Trouille et al. (2011), Melnick et al. (2015) and Baron et al. (2017) show links between starburst galaxies and AGN feedback. Both phases are thought to have been triggered by the same process; gas-rich major mergers (Zabludoff et al. 1996; Bekki et al. 2005; Hopkins et al. 2006). In this part of our study, we aim to test this connection using optical and radio data to determine whether there is a higher fraction of AGN in starburst galaxies when compared to normal star forming galaxies.

4.3.1 Optically Selected AGN

We begin by inspecting the presence of optical AGN within our SDSS starburst sample and control star former sample. Using the BPT (Baldwin et al. 1981) diagram shown in Fig. 4.2, we calculate the fractions of AGN. By ensuring the [NII], [OIII], Hα and Hβ lines are in emission, we achieve 887 starbursts and 24597 star formers.

Using the Kewley and Schawinski lines (Kewley et al. 2001; Schawinski et al. 2014 respectively) in the BPT diagram, we find the number of starburst galaxies in the seyfert region to be 15 (1.7±0.4% of the whole starburst sample) and star forming galaxies in the

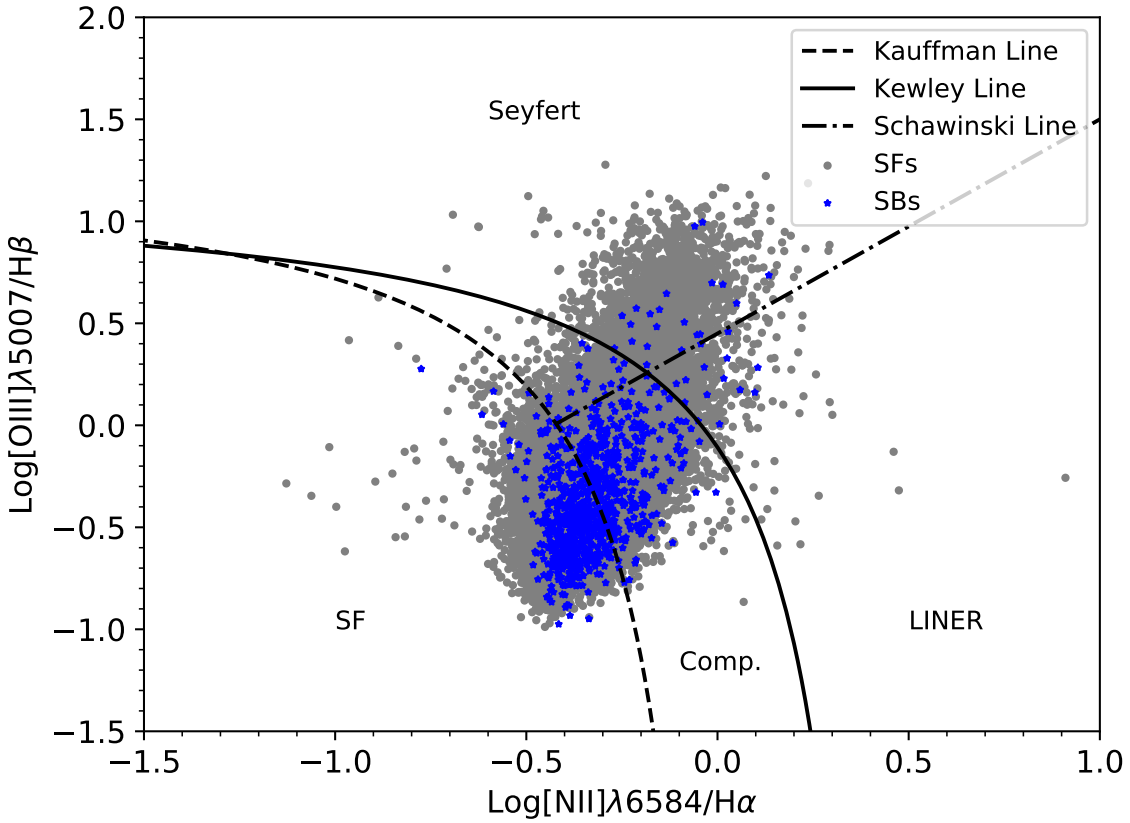

Figure 4.2: This BPT diagram shows the locations of the starburst (blue) and star former galaxies (grey). The majority of the starburst sample lies within the star formation and composite regions whilst a small fraction reside within the seyfert region. There is a larger fraction however, of 'normal' star formers within the seyfert region. This suggests starburst galaxies contain fewer AGN than 'normal' star formers.

seyfert region to be 1509 (6.1±0.2% of the whole star forming sample). This result could suggest that either another process, other than AGN feedback, is quenching star formation in starburst galaxies or that the overlap time between these phases is very short and the starburst phase ends very quickly after the AGN phase begins.

4.3.2 Radio Selected AGN

Selecting AGN optically using the BPT diagram is standard practice amongst many studies. However, optical wavelengths are prone to suffer from dust obscuration, meaning the fraction of AGN in starbursts could be higher but are hidden in a dusty shroud. Radio wavelengths however, are less obscured and could reveal how many radio AGN are hidden if any. Best et al. (2005) find that the radio AGN fraction ranges from nearly zero for galaxies $M_* < 10^{10}$ $M_\odot$

to 30 per cent for galaxies with stellar mass, $M_* \approx 5{\times}10^{11}$ $M_\odot$.

To select radio AGN, we apply a single radio power cut at $L_{1.4\ GHz} > 10^{24}$ WHz^{-1} (Meurs & Wilson 1984; Condon 1989; Sadler et al. 2002) as objects typically considered radio quiet have radio luminosity functions that sharply drop off after $L_{1.4\ GHz}$=10^{23} WHz^{-1} and are very rare above 10^{24} WHz^{-1}.

We find that 1 (0.17±0.17%) of radio detected starbursts can be considered radio AGN. We find that 18 (0.50±0.12%) of radio detected star forming galaxies can be considered radio AGN. Of the 18 star forming galaxies with radio AGN, 8 contain optical AGN. These results support the findings of Melnick et al. (2015) who state that starburst galaxies are radio quiet.

4.4 Radio Properties of Starburst Galaxies

Radio luminosity correlates strongly with star formation because of the synchrotron radiation emitted by supernova remnants. We begin by testing the distribution of radio luminosities of our starburst and star forming galaxy samples. Fig. 4.3 show the distributions of our starburst and star former sub-samples with and without optical AGN selection using the method described in section 4.3.1. We quantify the results shown in Fig. 4.3 by calculating the median luminosities for each distribution.

Table 4.1 shows the median luminosities for galaxies with detectable FIRST radio emission in each sample with an error equal to the standard deviation of the distribution. We find that there is no significant difference between the starburst (SB) sub-sample and the star formers (SF) with or without optically selected AGN. When using a 2-sample KS-test we find that all p-values are $\gtrsim 0.4$ confirming the results shown in table 4.1.

Next, we compare star formation rates derived from radio luminosity (calculated using Eq. 4.1, 4.2, 4.3 and adjusted by a factor of 1.5 to convert to a Kroupa IMF) and optically derived star formation rates (Brinchmann et al. 2004 uses the Hα emission line to calculate SFR) from the SDSS DR7 value-added catalogue to test the IMF of the starburst population. Fig. 4.4 shows the correlation between radio and optical star formation rates for the starbursts and star formers. In this plot we exclude optically selected AGN derived in section 4.3.1. There is a significant amount of scatter in radio SFR for both populations towards higher

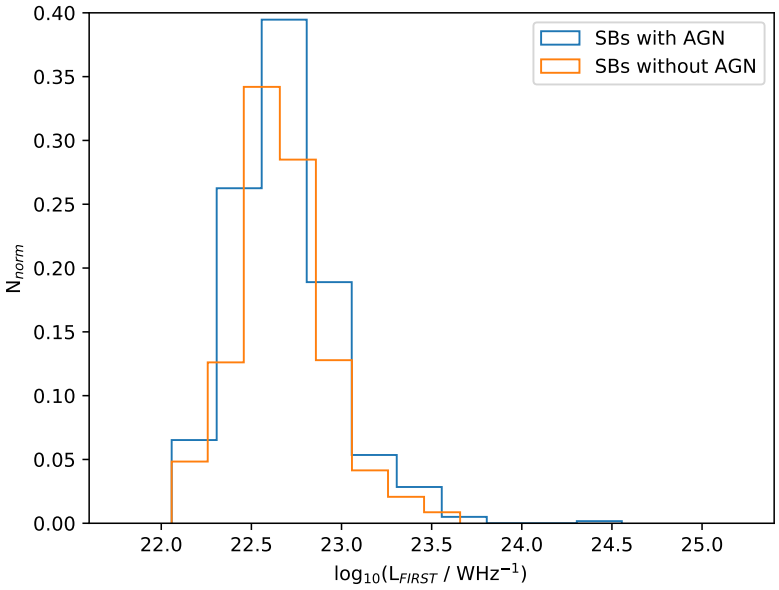

(a)

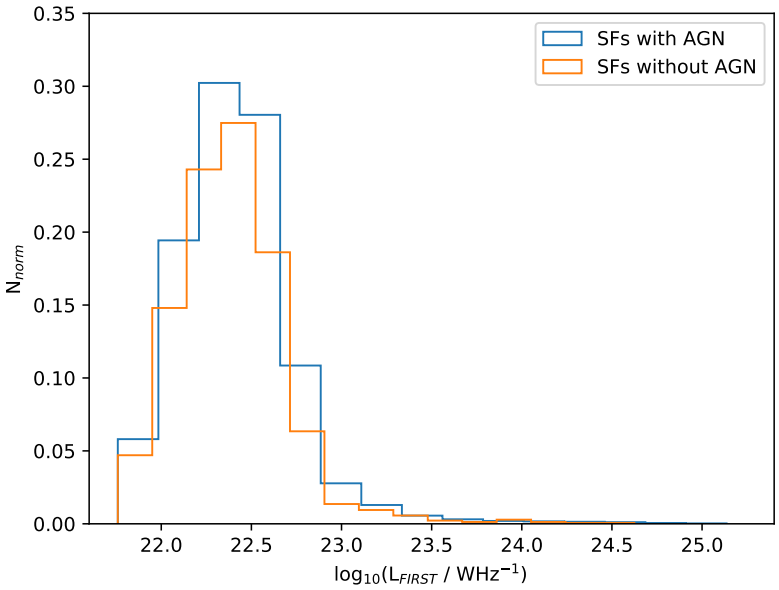

(b)

Figure 4.3: These plots show the radio luminosity distributions for starburst galaxies (SBs; top) and 'normal' star forming galaxies (SFs; bottom). We have also included the distributions of our samples with (blue) and without (orange) optically selected AGN. We consider optically selected AGN to be any galaxy above the Kewley line in Fig. 4.2. The radio distributions of the starburst sample are slightly higher than the 'normal' star forming sub-sample, however, not statistically significant.

Sub-sample	Median $\log_{10}(L_{1.4\ GHz}$ / $WHz^{-1})$
SB (without AGN)	22.6 ± 0.26
SF (without AGN)	22.4 ± 0.31
SB (with AGN)	22.7 ± 0.28
SF (with AGN)	22.4 ± 0.33

Table 4.1: This table shows the median logged radio luminosities of starbursts (SB) with FIRST radio detection and regular star formers (SF) with FIRST radio detection. We include sub-samples of each with and without optically selected AGN. AGN are selected as any galaxy above the Kewley line in 4.2. The error bars included in the table are calculated as the standard deviation of the luminosity distribution. These results show there is no significant difference between the luminosity distributions of the starburst and regular star forming galaxies nor is there any significant difference between samples with and without optically selected AGN.

radio SFR values, we add the caveat that the outliers in this plot could contain hidden AGN components that have not been identified on the BPT diagram shown in Fig. 4.2. In order to produce a fit that represents the data well we omit outliers from the regression model that are beyond 1.5 σ from the median. To ensure we represent the trend of the data well, we use a robust bi-weighted linear regression model. We find that the gradient derived for the starburst population is 0.36±0.07 whilst the star former gradient is 0.52±0.02 (errors listed here are the standard errors outputted from the robust linear model). On Fig. 4.4, we include 95% confidence intervals on each of the linear fits. This means that there is an excess of Hα in the starburst population compared with the star formers. This mismatch implies the IMF in starbursts is top-heavy as Hα traces stars with $M_* > 20\ M_\odot$ and radio traces stars with $M_* > 8\ M_\odot$. However, due to the relatively small sample size compared with the star forming population there is a large error in the fit associated with the starburst sample. The fitting analysis used here, provides the best fit to the data and is therefore an appropriate method when comparing radio-optical slopes.

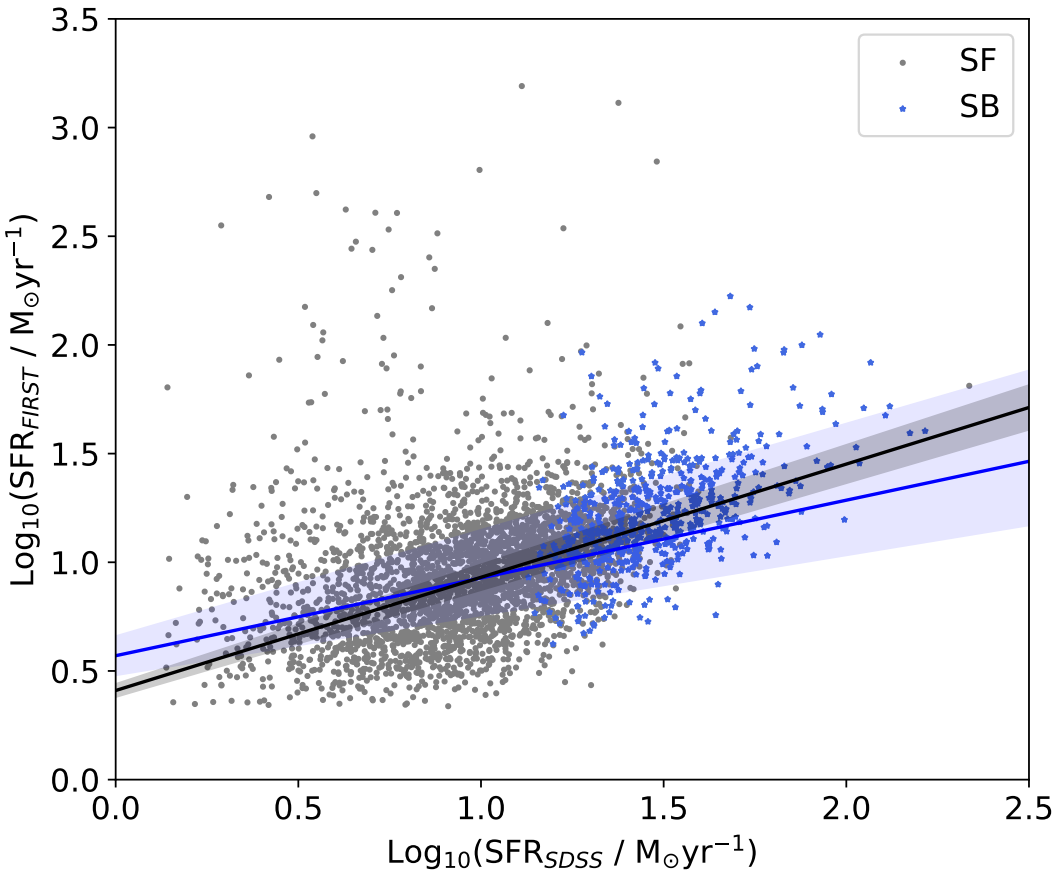

Figure 4.4: This plot shows SFR derived from radio versus optical for the starbursts (blue) and 'normal' star formers (grey) with the corresponding linear fits. We fit robust bi-weighted linear models to each sample with optical AGN and outliers removed to improve the reliability of the fit. The outliers on this plot could have an AGN component that has not been detected through BPT analysis. We consider outliers to be beyond 1.5 σ from the median. The shaded regions of the plot represent the 95% confidence intervals of the linear fit for both populations. We can see that the gradient of the star formers is steeper than that of the starburst (0.52±0.02 compared to 0.36±0.07 respectively), this suggests an excess in Hα emission which infers a top-heavy IMF in the starburst sample.

4.5 Discussion

4.5.1 AGN in Starbursts

Whilst there are many studies which investigate the role AGN play in quenching starbursts, there is not a decisive answer as to whether they play an integral role in suppressing star formation in bursts. In this study, we aimed to test whether AGN play an active role in quenching star formation in starburst galaxies by comparing the AGN fraction in starbursts to the fraction in quiescently ('normal') star forming galaxies.

Using a BPT diagram shown in Fig. 4.2, we find that 1.7±0.4% of starburst galaxies in our sample contain an AGN compared to 6.1±0.2% of normal star formers. This result could suggest that AGN do not play a primary role in quenching the star formation in a burst, as found by Yesuf et al. (2014), or that the overlap time between the starburst phase and AGN phase is very short. Finally it could also mean that the AGN duty cycle is lower in star bursts which allows them to have enhanced star formation.

Previous works have probed the connection between PSBs and AGN. For example, De Propris & Melnick (2014) find that in the post-starburst phase at $0.015 \lesssim z \lesssim 0.058$, there are no AGN present but there is evidence of feedback, this is in contrast to the work by Yesuf et al. (2014) who find that starbursts at $0.03 \lesssim z \lesssim 0.1$, contain 36% more AGN than normal star forming galaxies. In our previous paper, Wilkinson et al. (2017), we find that 8.2% of Hδ strong galaxies (post-starbursts) were considered to be seyferts on the BPT diagram and 4.8% of E+A galaxies were seyferts. This suggests that the AGN phase could follow on from the starburst phase and AGN activity then declines as a galaxy enters and passes through the post-starburst phase. Therefore we consider the hypothesis by Yesuf et al. (2014) unlikely to be true, as they suggest that AGN quench low-level star formation. Our findings suggest that the overlap time between the starburst and AGN phase is very short and therefore detecting starbursts with AGN is very rare. However, we cannot be confident as to whether AGN are the primary quenching mechanism or enhance other mechanisms as suggested by Cicone et al. (2014).

4.5.2 The Starburst IMF

For nearby galaxies and starburst regions, the IMF can be determined directly as done so by Rieke et al. (1993), Stolte et al. (2005) and Schneider et al. (2018) who find evidence of a top-heavy IMF. However, these studies do not provide a large statistical sample which is needed in order to make a confident statement about the form of the IMF in starbursts. Whilst the review by Scalo (1990) suggests that not all starburst galaxies require a top-heavy IMF, the study by Parra et al. (2007) find that large uncertainties affect the confidence at which the IMF can be called top-heavy.

Here, we investigate the radio properties of starburst galaxies with the aim of determining the form of the IMF. We initially inspect the radio luminosity distributions of starburst galaxies and compare to a sample of quiescently star forming galaxies and find that there is a small but not significant enhancement in radio luminosity of the starburst sample. This is to be expected, as in a starburst more supernova are produced which emit synchrotron radiation at radio wavelengths. We next compare optically derived star formation rates by Brinchmann et al. (2004) (who use Hα emission) to star formation rates derived from radio luminosity. Hα emission is a tracer for more massive stars (> 20 M$_\odot$) than radio emission is and therefore an excess is Hα indicates a top-heavy IMF. Fig. 4.4 shows this relation and we find an excess in Hα emission in the starburst sample which suggests the presence of a top-heavy IMF. As we have a relatively small sample of starbursts in comparison to our control sample, the 95% confidence interval is much larger in the starburst fit. Like with Parra et al. (2007), who also have large uncertainties, if we had a larger number of starburst galaxies in our sample, our starburst confidence interval would be narrower and give a more confident result showing a top-heavy IMF which supports the findings of single galaxy studies such as McCrady et al. (2003), Harayama et al. (2008) and Schneider et al. (2018).

4.6 Conclusion

Starburst galaxies are an important phase in galaxy evolution and as the literature has shown, can give further insights into the nature of the IMF. In this study, we discuss the presence of both optical and radio AGN in starburst galaxies. We use their radio properties to determine

any variation in the IMF towards the high end of the stellar mass distribution. Our principle findings are listed here:

1. We find that 63±2.6% of starburst galaxies have radio data within the FIRST catalogue compared with 7.3±0.1% of star formers. This indicates that starburst are more likely to be radio emitters than non-starburst galaxies. This radio emission could be due to either AGN or supernova sources.

2. Starbursts contain a negligible amount of radio-loud AGN ($L_{1.4\ GHz}>10^{24}$ WHz^{-1}). For those that do emit a radio continuum, they can be considered as radio-quiet, this agrees with the findings of Melnick et al. (2015).

3. There is an excess in Hα emission in the starburst sample which suggest a top-heavy IMF. However, due to the relatively small sample size the error on this is significant and our confidence is limited.

4. Galaxies that are quiescently star forming have a greater fraction of AGN than starburst galaxies. This suggests either AGN may not play a significant role in quenching star formation in bursts as previously thought.

These findings suggest that it is likely that starburst galaxies may have a top-heavy IMF as discussed by Baugh et al. (2005), Parra et al. (2007), Lacey et al. (2008) and Schneider et al. (2018). This means that starburst galaxies are likely to produce an excess of O-class stars in comparison to main sequence galaxies. Further study of the gas dynamics in starbursts is needed to understand what causes them to produce higher mass stars. However, like Parra et al. (2007) we find large uncertainties when we fit a linear regression model to our sample, this is due to relatively low numbers compared to our star forming galaxy sample. For a greater accuracy a larger sample is needed, however, due to the rarity of starburst galaxies this will be difficult.

As we find that non-starburst galaxies have a greater fraction of AGN, this could suggest that either AGN do not play a primary role in quenching a burst or that the overlap time the starburst phase and the AGN phase is very quick so galaxies with this overlap are extremely

rare. To investigate the starburst-AGN connection we recommend a spatially resolved study (simulated or observational) is needed to determine whether the AGN in the starburst is triggered around the peak of the burst and whether is has any effect in quenching the burst.

Acknowledgements

This research makes use of the NRAO VLA FIRST Survey and SDSS. The National Radio Astronomy Observatory is a facility of the National Science Foundation operated under cooperative agreement by Associated Universities, Inc.

Funding for the SDSS and SDSS-II has been provided by the Alfred P. Sloan Foundation, the Participating Institutions, the National Science Foundation, the U.S. Department of Energy, the National Aeronautics and Space Administration, the Japanese Monbukagakusho, the Max Planck Society, and the Higher Education Funding Council for England. The SDSS Web Site is http://www.sdss.org/.

The SDSS is managed by the Astrophysical Research Consortium for the Participating Institutions. The Participating Institutions are the American Museum of Natural History, Astrophysical Institute Potsdam, University of Basel, University of Cambridge, Case Western Reserve University, University of Chicago, Drexel University, Fermilab, the Institute for Advanced Study, the Japan Participation Group, Johns Hopkins University, the Joint Institute for Nuclear Astrophysics, the Kavli Institute for Particle Astrophysics and Cosmology, the Korean Scientist Group, the Chinese Academy of Sciences (LAMOST), Los Alamos National Laboratory, the Max-Planck-Institute for Astronomy (MPIA), the Max-Planck-Institute for Astrophysics (MPA), New Mexico State University, Ohio State University, University of Pittsburgh, University of Portsmouth, Princeton University, the United States Naval Observatory, and the University of Washington

5. Summary, Conclusions and Future Work

5.1 Summary & Conclusions

How galaxies transform from star forming spirals to quiescent ellipticals is one of the biggest questions in extragalactic astronomy. By investigating the processes that are thought to cause this transition, we gain a better insight into how galaxies evolve. In this thesis, we have examined the star formation duty cycle of starburst and post-starburst galaxies, particularly how they are classified, their triggers and what processes quench the burst in this important phase of galaxy evolution. The work in this thesis focuses on the following science questions:

- How do different selection methods of post-starburst galaxies have an impact on the properties observed?
- What are the main triggers of starburst, and hence post-starburst galaxies in the Illustris simulation?
- Do starburst galaxies have a top-heavy IMF and produce heavier stars than quiescently star forming galaxies?
- To what extent do AGN play a role in quenching star formation in starburst galaxies which lead to the post-starburst phase?

Below, we summarise the approaches taken to try and answer these questions and describe the main conclusions made from each chapter.

In Chapter 2, we investigated the different techniques used to select post-starburst galaxies. We identify three main approaches within the literature which are (1) strong Hδ absorption, (2) strong Hδ absorption and no [OII] emission and (3) strong Hδ absorption or no [OII] and Hα emission. Using these techniques we adopted three sub-samples and compared their observational properties to reveal an evolutionary sequence.

Properties we examined were colour, morphology, size, environment and the presence of any AGN. When first discovered by Dressler & Gunn (1983), post-starburst galaxies were considered to be blue, further work by Poggianti et al. (1999, 2009) reveal that the colour of post-starburst galaxies are bimodal like the general population of galaxies. In our study, we also witness this bimodality. We find that the median colour of Hδ strong galaxies is positioned within the blue cloud, the median colour of E+As is in the green valley and pure E+As are predominantly in the red sequence. This is the first evidence of an evolutionary sequence emerging from these multiple selection criteria, suggesting that as star formation is suppressed the colour evolves upwards towards the red sequence on a colour magnitude diagram as Hα is no longer produced.

As post-starburst galaxies are considered to be in a transitionary phase between star forming spiral and quiescent ellipticals it is reasonable to assume that the morphology of post-starburst galaxies will resemble a S0 morphology, as found by Yang et al. (2004). Using the galaxy zoo catalogue to determine galaxy morphology we find that the majority of Hδ strong galaxies have a spiral morphology, E+As have a roughly equal mix of spiral and elliptical morphologies whereas pure E+As are primarily ellipticals. This difference in morphology is replicated in the size of our samples, as pure E+As are mainly elliptical galaxies we find they are more compact, having a smaller radii than the other two samples which contain significant fractions of spiral morphologies.

Post-starburst galaxies are found in different environments and this could have an impact on the properties we observe. Tran et al. (2003) find that cluster E+As are disk dominated whilst Yang et al. (2004) who focus on field E+As are bulge dominated. This could be due to different processes within these environments having a different effect on the disk. In dense environments where the ICM is hot and the velocity dispersions are high harassment and minor merger events dominate which can leave the disk intact. Meanwhile in the colder and lower velocity field environments, major mergers can dominate which can destroy the galactic disk. Our findings suggest that whilst post-starburst galaxies prefer field environments, there is a higher fraction of pure E+As in denser environments. If quenching and triggering mechanisms in cluster environments protect the disk, then the elliptical pure E+As in those

cluster environments could have been triggered in weaker environments before being quenched in denser environment, supporting the finding of Mahajan (2013) who suggest post-starburst galaxies can undergo pre-processing.

We finally examine the starburst-AGN connection (Melnick et al. 2015) by calculating the fractions of seyferts (from the BPT diagram) and strong AGN (from the WHAN diagram) in our samples. We find that Hδ strong galaxies contain more AGN than E+As and E+As have more AGN than pure E+As. If the evolutionary sequence we have identified is to be believed then as time passes AGN activity decreases from the point of the starburst. However, this is purely speculative and further evidence is needed to determine whether AGN play an active and primary role in quenching star formation in starburst galaxies.

In Chapter 3, we used the Illustris simulation to determine the true triggers of the starburst phase. Using merger trees, we find that 55% of starburst galaxies have not had a merger of any degree in the previous 2 Gyr. This challenges the findings made by Zabludoff et al. (1996) who suggest mergers are the main if not only trigger of the starburst phase. Further investigations into the proximity of our starburst galaxies to their neighbouring galaxies suggest that harassment events (which may or may not result in a future merger) are capable of triggering a nuclear starburst with comparable strength to a merger-driven starburst.

We also investigated the environments of the simulated merger and harassment driven starbursts and find that they are preferentially located in lower density environments compared to the remaining galaxy population. We find that those starburst galaxies without a past merger are in denser environments than those that have suggesting the triggering mechanisms are dependent on the density of the environment. We briefly investigated the presence of AGN in starburst galaxies and find that AGN feedback could be more apparent in merger driven starbursts which produce burstier star formation.

In Chapter 4, we used radio data to investigate the form of the IMF in starburst galaxies. In this chapter, we also investigated the extent AGN could play in quenching star formation in bursts. When comparing Hα nebular emission (attributed to stellar masses >20 $M_{\odot}$) to supernova remnant radio emission (attributed to stellar masses ~8 $M_{\odot}$), we find that starbursts show some evidence for an excess of Hα emission compared to normal star formers. This

means that higher mass stars are produced in bursts compared with quiescent star formation, which suggests the IMF of starbursts is top-heavy. Our results support the findings of McCrady et al. (2003), Harayama et al. (2008) and Schneider et al. (2018) who suggest the IMF in starburst galaxies and starburst regions is top-heavy. We also find that, like Parra et al. (2007), uncertainties limit our confidence in this claim and it could be that not all starbursts have a top-heavy IMF as found by Scalo (1990).

We used a BPT diagram to determine the fractions of AGN within starburst galaxies. We find there are ~4 times fewer AGN in starburst galaxies than there are in normal star forming galaxies. Our results disagree with the finding by Yesuf et al. (2014), who find there are significantly more AGN in starburst galaxies than other galaxy populations. Our previous results found in Ch. 2 suggest that AGN feedback declines with time from the starburst, which could suggest AGN are active at some point in the duty cycle of starburst galaxies, however to what extent AGN suppress bursty star formation is still unknown. Our findings suggest that either AGN feedback is not the primary quenching process that suppresses star formation or that there is a time-lag between the peak of the starburst phase and the AGN phase such that the overlap time between these two phases is very short and therefore detecting galaxies with both starburst and AGN signatures is very rare.

5.1.1 Overall Summary

In this thesis we have explored the star formation duty cycle of the starburst and post-starburst phase. We have focused on the triggering mechanisms that initiate the starburst phase and how they produce more massive stars than ordinary galaxies, how the observed properties of post-starburst galaxies are dependant on how they are selected and whether AGN play an active role in quenching star formation.

We have found that mergers and harassment events are capable of triggering starbursts with comparable strengths. Whilst mergers are more dominant in field environments, harassment events are responsible for triggering starbursts in denser environments. Through observing the evolutionary sequence of the post-starburst phase we have seen that galaxies are various in colour, morphology and environment and with time post-starbursts become redder, more

elliptical and found in denser environments either through pre-processing or having heterogeneous parent populations (Tran et al. 2003). Whilst we find AGN play a role in the duty cycle of starburst galaxies, further work is needed to determine to what extent they are the primary quenching process. We have also found that starburst galaxies produce more massive stars such that their IMF can be considered top-heavy.

5.2 Future Work

This thesis has shed light on the duty cycle of starburst and post-starburst galaxies. However, there are still some unanswered questions we feel that need to be answered. Below we state some of those questions and how we believe they can be answered.

What is the primary quenching mechanism that suppresses star formation in bursts?

In chapters 3 and 4, we investigated the possibility of AGN feedback as the quenching process that suppresses star formation in bursts, however, due to the limits and uncertainties faced in the Illustris simulation and the lack of AGN numbers in our SDSS DR7 starburst sample we cannot be confident in claiming that AGN are the primary quenching mechanism. Further work is needed to investigate the link between AGN feedback and starburst galaxies. We feel that to truly understand what quenching mechanisms occur in starbursts we need to examine the gas dynamics. Stars cannot form without a reservoir of cold gas which is fuel for star formation. By understanding what is happening to the gas when star formation is suppressed will allow us to determined what processes are responsible for quenching star formation.

To resolve the cold molecular clouds, higher resolution simulations are needed like Illustris TNG or the Horizon Runs. The new Illustris-TNG simulation (Nelson et al. 2018b; Naiman et al. 2017; Springel et al. 2017; Pillepich et al. 2017; Marinacci et al. 2017) is split into three spatial volumes: TNG50, TNG100 and TNG300 which are named in accordance to the comoving box size. Whilst TNG100 matches the original Illustris simulation in resolution and volume, the TNG50 run achieves a dark matter resolution of 4.5×10^5 $M_\odot$ and baryonic matter mass resolution of 8.5×10^4 $M_\odot$. At $z = 0$, TNG50 achieves a collisionless softening of 280 pc and a minimum gas softening of 74 pc (Nelson et al. 2018a). Another benefit of the

Illustris TNG simulation is that more physics and improved feedback models have been added which will increase the fraction of starbursts. In Illustris-1, starbursts were under produced and did not represent the observed fractions well. Whilst the fraction of starburst found in TNG100 may only be slightly improved due to the improved physics, the higher resolution in TNG50 should significantly improve the fraction of starburst galaxies found. However, how comparable this new fraction will be to observations is still unknown as the simulation is still ongoing and has not yet reached $z = 0$.

With the improvements Illustris TNG50 offers, molecular clouds will be better resolved such that it may be possible to determine the gas kinematics and potentially examine the gas temperature. As mentioned above, star formation is fuelled by cold gas, yet studies such as French et al. (2015) and Yesuf et al. (2017) find cold molecular gas reservoirs in 27% of post-starburst galaxies. Recent work by French et al. (2018) find that the cold gas remaining after a starburst is not dense enough to gravitationally collapse and therefore form stars. Whilst Osman & Bekki (2017) suggest that E+As with cold gas arise from counter-rotating gas in the disk. In order to understand why the gas in starburst galaxies becomes sparse and under dense, Illustris TNG may help us to find out what proportion of the gas is pushed out from the core by winds driven by supernova or AGN, how much is heated such that star cannot form and how much is consumed when forming stars. By knowing what is happening to the gas will tell us what process is primarily responsible for quenching star formation.

To what extent do minor mergers play a role in triggering starbursts compared to major mergers?

Throughout the literature, the triggering of starburst galaxies has been attributed to major mergers (Mihos & Hernquist 1996; Zabludoff et al. 1996). Yet there is a growing amount of evidence that pulls away from this original hypothesis (Robaina et al. 2009). In chapter 3, we found that only 45% of starbursts in the Illustris simulation have undergone a recent merger of which 39% of those were major mergers. To understand the role which minor mergers play as opposed to major mergers, deeper images are required and the locations of starburst regions to be accurately determined.

Observational evidence for minor mergers triggering starbursts can be found in the tadpole galaxy which is thought to be triggered by a minor merger. Jarrett et al. (2006) finds the starburst region in the tadpole galaxy is off-nuclear and located in the tail, which contains several supermassive star clusters ($\sim 10^6$ $M_\odot$). Further work by Robaina et al. (2009) finds that at intermediate redshifts ($0.4 < z < 0.8$) less than 10% of star formation is triggered by major mergers. This supports our belief that more investigation is needed into other mechanisms other than major mergers to understand starburst triggering.

Kaviraj (2010) find hidden (low luminosity) tidal features when using using deeper imaging. These hidden features give us a better understanding of a galaxy's past interactions, such a mergers. This leaves the question as to how many other galaxies exhibit similar hidden features, especially starbursts. The Large Synoptic Survey Telescope (LSST; Collaboration et al. 2017) that is currently under construction will provide deeper optical images than previously seen in surveys. Stacking images from LSST will allow us to detect faint extended light sources around galaxies which will reveal the presence of any hidden tidal features allowing astronomers to determine the nature of past mergers. For starburst galaxies, LSST results will allow us to understand what role minor mergers play in triggering bursts. LSST will also allow for morphological studies at higher redshifts, which will tell us if post-starburst galaxies contain more disk features as opposed to massive early-types suggested by Tran et al. (2003).

Does environment determine the processes that drive evolution in starburst galaxies or are differences in post-starburst properties caused by a heterogeneous parent population?

In chapter 2 we found that pure E+As were more likely to be found in higher density environments compared to Hδ strong and regular E+A galaxies. Pure E+As are redder in colour and elliptical in morphology. In chapter 3 we found that denser environments produced more harassment events triggering starbursts. Environment correlated with many aspects of starburst and post-starburst properties, so does environment drive the evolution of starbursts. Tran et al. (2003) find that cluster E+As are more disk dominated, this disagrees with our finding from chapter 2, where we find pure E+As in denser environments are bulge domin-

ated. However, the results from Tran et al. (2003) support our findings of harassment events triggering starbursts in denser environments (in chapter 3) as harassments do less damage to the disk than major mergers which are more prominent in field environments. Yet, Tran et al. (2003) find that the diverse nature of post-starburst galaxies indicates a heterogeneous parent population. This leaves the question as to whether the environment or a difference in parent galaxies gives rise to the variety of properties we see in post-starburst galaxies.

To study this effect we feel a comparative observational study is needed that investigates the differences between parent cluster spirals, cluster ellipticals, field spirals and field ellipticals. Comparing these four sub-populations will enable astronomers to determine which has the greatest effect, environment or parent population. Do spirals produce more disk dominated E+As regardless of environment or does a higher density environment protect the disk more than in the field?

A. Appendix

A.1 Data Table of Hδ Strong Galaxies

RA	DEC	z	modelMag_r	Hδ EQW	[OII] EQW	Hα EQW
158.18666	-0.99612224	0.06424	17.35	3.111	-10.40	-5.381
157.80263	-0.19006772	0.09485	17.40	3.095	3.528	-2.315
158.33212	0.41619706	0.09748	17.13	3.169	-0.7523	-9.179
170.21848	0.40813988	0.02499	17.39	4.727	0.0	-17.43
202.35512	-0.3990438	0.01082	16.23	3.324	0.0	-27.45
208.68558	0.11839871	0.02990	16.72	5.181	0.0	-14.46
209.39925	-0.14322935	0.02936	17.23	3.591	-15.90	-4.087
224.34	-0.9479952	0.09937	17.19	3.516	-5.961	-5.199
228.77312	-1.2261021	0.05138	17.21	3.329	-27.89	-13.37
232.0963	-1.2327907	0.07691	17.31	3.273	-7.098	-12.02
188.60008	-1.8239527	0.09180	16.98	3.527	-9.154	-7.504
198.48306	-3.5272985	0.06527	16.68	3.664	-0.4564	-9.876
237.85156	-0.65194124	0.07763	17.40	5.137	-14.47	-13.38
243.82037	0.17022394	0.06510	17.77	3.147	0.08608	0.5316
260.1155	56.767834	0.02888	16.88	4.747	48.79	-38.96
1.1329895	-1.2365906	0.08870	17.21	3.026	-29.27	-8.162
2.3507519	0.5378388	0.07976	17.62	3.909	-6.930	-10.10
3.8989153	-0.162447	0.06807	17.31	3.094	-7.374	-9.918
13.288886	1.1444149	0.03366	17.04	3.580	-14.06	-7.813
20.674257	-1.094729	0.06285	17.46	3.897	4.181	-10.54
35.789154	-0.3464188	0.07268	17.72	3.089	-8.137	-19.59
38.085907	0.86684686	0.05422	17.53	4.337	-5.787	-2.292

RA	DEC	z	modelMag_r	Hδ EQW	[OII] EQW	Hα EQW
52.884266	-1.0106257	0.02188	17.01	3.094	0.0	-23.89
52.828674	1.1496015	0.08397	17.71	3.424	-3.845	-10.21
23.162766	14.080566	0.02290	16.50	3.598	-2.064	-10.66
23.82481	15.312834	0.07081	17.73	3.087	0.2309	-0.9496
23.863693	15.308285	0.07049	17.12	6.546	-5.307	-4.179
27.386972	13.145138	0.01680	17.33	3.566	0.0	-0.1478
124.72001	47.448757	0.04394	17.29	3.006	-23.97	-9.450
54.325775	-5.921	0.03452	16.61	4.538	-6.834	-11.56
165.63283	65.91201	0.06514	17.11	3.407	-5.62	-6.916
194.3117	67.18985	0.05065	16.75	3.168	-9.822	-5.648
160.14043	3.266654	0.06415	16.82	5.030	-19.06	-15.50
164.65678	1.733783	0.03998	17.73	3.992	-15.23	-22.61
164.23073	2.9684107	0.07653	17.43	3.071	-5.36	-4.108
195.12473	2.5232432	0.06663	16.45	4.909	0.7905	-15.09
211.10828	2.028758	0.0455	17.49	4.542	-21.73	-29.28
133.0422	2.8402317	0.02900	15.89	3.253	-14.87	-23.34
159.02155	4.467947	0.07133	16.51	4.326	-8.458	-8.203
158.52637	3.337569	0.08046	17.41	3.789	-6.738	-16.87
217.26277	4.6783834	0.02691	14.81	3.902	-10.62	-10.83
220.70956	3.460915	0.02904	17.22	3.246	1.246	-4.034
222.85446	3.5074332	0.06617	17.35	3.627	-26.63	-8.041
229.72464	3.152665	0.08142	17.20	3.221	-10.40	-8.102
236.75813	2.4691188	0.04616	17.67	3.972	-3.516	-1.310
239.46712	2.2602186	0.08816	17.46	5.470	-23.70	-23.74
168.30252	63.92036	0.03448	16.41	3.0720	-9.676	-18.72
231.4073	58.7866	0.04813	16.96	3.756	-16.67	-11.68
243.29514	47.115532	0.09163	17.63	9.130	0.0	-21.07
317.72897	-7.70676	0.0797	16.58	3.555	-8.032	-1.384

RA	DEC	z	modelMag_r	Hδ EQW	[OII] EQW	Hα EQW
328.25525	-7.838636	0.07327	17.15	3.269	-5.030	-1.225
327.71625	-8.140127	0.07827	17.63	4.005	-286.7	-37.31
327.6664	-8.204268	0.07662	16.48	3.791	3.877	-19.72
351.5922	-8.601274	0.09745	17.61	3.391	-3.443	-3.614
351.60574	-9.615762	0.09801	17.74	3.142	1.615	-0.7319
10.177038	-9.425453	0.03721	17.47	3.284	-21.20	-9.198
12.442707	-10.622458	0.07888	17.66	3.598	-2.954	-1.011
23.726746	-10.511684	0.09920	17.63	3.476	-4.311	-3.938
33.535473	-7.8704658	0.06880	17.67	3.716	-14.09	-9.592
324.04913	10.414776	0.07965	17.73	3.022	-22.20	-16.19
322.23737	10.803194	0.09615	17.73	3.444	-17.83	-17.62
334.80777	12.97223	0.02643	16.60	4.165	0.0	-17.36
338.72073	13.285104	0.06701	17.43	3.128	2.443	-0.4627
340.08838	14.517162	0.08725	16.69	4.111	-3.598	-7.900
350.8342	14.343788	0.09165	17.26	3.5629	-47.19	-21.56
350.75522	14.351918	0.09048	17.29	8.303	47.73	-18.46
126.38462	41.959312	0.05778	17.42	3.668	-3.770	-2.711
139.74976	49.985573	0.03399	17.44	3.053	0.2823	0.8373
137.2846	49.55731	0.03441	16.80	3.113	-2.726	-10.74
139.7416	51.177715	0.06757	17.67	3.445	-20.57	-13.61
203.5109	61.645462	0.04435	17.60	3.092	-3.517	-0.6774
210.76	59.827965	0.09802	17.51	3.369	-3.504	-3.849
219.23099	57.47933	0.06407	17.58	4.066	-5.062	-0.4831
240.07214	46.859882	0.04318	16.81	3.024	0.0	-1.526
169.61629	4.620956	0.07463	17.00	4.362	-1.555	-0.8194
168.30164	4.3327975	0.07676	17.74	12.49	12.04	-13.45
183.68001	4.9318094	0.07357	17.01	4.373	-0.2897	-12.97
196.1836	3.690694	0.04023	16.86	3.347	2.780	-6.466

RA	DEC	z	modelMag_r	Hδ EQW	[OII] EQW	Hα EQW
196.60014	5.3786116	0.04363	17.47	3.471	-11.97	-15.48
210.42436	3.6572232	0.03485	17.24	3.602	-12.71	-17.79
116.67849	26.355337	0.02374	16.96	4.990	0.0	-9.780
131.0497	37.605705	0.02627	15.78	3.788	0.0	-5.928
134.53395	44.82465	0.08547	17.69	5.106	-15.81	-11.29
133.29578	44.036514	0.09927	17.41	15.04	-16.92	-8.378
132.95091	44.24777	0.08294	17.53	3.402	-8.205	-6.209
132.035	44.567417	0.08233	17.55	5.223	-18.84	-15.73
207.52985	-2.420493	0.02410	15.83	3.250	0.0	-7.038
224.1282	-1.2172909	0.04186	16.83	3.287	-24.51	-23.70
149.42918	44.88816	0.02613	17.07	3.981	2.497	1.206
156.2755	45.062523	0.07439	16.63	3.780	-3.185	-5.413
178.5285	48.7707	0.07530	17.63	4.857	-13.67	-13.07
183.36089	51.019066	0.08311	17.45	3.003	-2.671	-3.255
255.3766	34.832214	0.06322	17.73	3.955	-11.11	-15.91
254.75208	32.62161	0.09473	17.10	4.152	-2.590	-19.73
149.01282	50.220226	0.06611	17.39	3.061	-20.68	-27.45
151.83534	50.33845	0.06700	16.65	3.242	0.0	-12.81
176.16666	53.557064	0.06864	17.19	3.103	-0.9826	-3.382
187.28934	53.667706	0.03670	17.20	5.8309	-18.46	-4.847
200.03069	52.96751	0.09763	17.43	3.163	-11.85	-1.794
235.23978	41.488438	0.07753	16.62	3.523	-6.344	-20.97
244.53522	41.765953	0.03831	17.57	3.310	-10.92	-8.867
324.646	-6.5286183	0.04811	17.66	3.098	-19.44	-11.36
126.72788	35.562584	0.06266	17.47	3.259	-13.42	-10.10
119.53341	23.563095	0.04712	17.76	3.192	-11.56	-11.94
135.17526	36.20052	0.08397	17.68	3.755	-2.955	-1.355
137.67018	37.29843	0.02987	16.08	3.612	0.0	-11.17

RA	DEC	z	modelMag_r	Hδ EQW	[OII] EQW	Hα EQW
188.03102	11.109093	0.07628	17.72	3.05	-1.905	-5.132
147.33418	8.884623	0.09774	16.32	3.608	-3.726	-1.314
58.252457	-0.96195817	0.07521	17.34	3.397	-2.383	-14.65
123.14582	25.343908	0.0825	17.43	11.05	-15.25	-2.942
134.8158	32.89418	0.06362	17.49	10.54	-55.16	-15.88
134.87724	33.290073	0.08666	17.58	5.428	-9.253	-6.920
147.65714	38.279705	0.0446	17.68	3.1	-27.18	-24.70
140.78027	8.715511	0.07842	17.60	3.305	-13.75	-18.62
171.43004	56.847607	0.05607	17.30	3.654	13.81	-5.500
239.02866	43.578045	0.06	16.61	3.14	-19.33	-8.427
242.45622	40.283382	0.05673	17.23	3.37	-13.11	-10.50
226.42166	35.911896	0.09707	17.12	4.529	-2.320	-4.334
236.02072	29.387854	0.0345	17.25	3.828	-8.972	-8.496
234.52489	35.39985	0.0665	17.17	3.724	-3.216	-0.3390
242.2905	30.152184	0.05966	17.28	3.671	-27.32	-9.424
248.43617	26.186827	0.05088	16.43	3.238	-4.851	-6.053
254.03658	21.826956	0.07861	17.03	3.17	2.634	-3.282
253.27173	22.557247	0.0359	17.3	3.169	-10.43	-4.616
156.66467	39.74187	0.06211	15.65	4.251	10.80	-3.950
166.85443	40.405018	0.07586	17.75	5.051	-7.76	-14.59
168.67557	41.37361	0.07325	16.37	3.053	2.145	-2.275
187.82706	41.81043	0.09836	16.71	3.265	-3.592	0.1862
246.38982	23.282112	0.06141	16.99	3.029	-12.92	-3.5
244.07072	26.118795	0.04824	15.99	3.644	9.151	-7.657
152.95036	10.54477	0.07139	16.9	9.341	-1.43	-7.799
156.80943	11.061117	0.03293	15.52	6.461	-5.254	-1.895
171.01694	7.108122	0.09225	17.75	3.005	-4.14	-2.823
187.41635	7.2631917	0.08339	17.46	3.5	-14.24	-2.77

RA	DEC	z	modelMag_r	Hδ EQW	[OII] EQW	Hα EQW
215.44687	36.454975	0.09017	16.95	3.362	-10.43	-13.07
237.23695	28.224857	0.07484	16.84	3.117	-4.293	-7.034
242.30553	23.465311	0.03284	16.71	3.515	-8.749	-6.381
234.00829	39.978664	0.03291	17.73	3.288	-55.14	-10.64
206.94398	12.667744	0.08115	17.75	3.487	-2.588	-4.835
112.01133	39.627888	0.07605	17.75	3.011	-10.1	-10.49
111.76712	39.916508	0.09837	17.61	4.139	-5.982	-11.96
135.18028	61.260414	0.04281	17.64	3.12	-35.85	-45.84
193.52888	10.596575	0.09721	17.54	3.124	-5.749	-13.77
196.5501	7.277027	0.06239	16.39	5.294	-2.598	-3.677
196.4347	10.763716	0.07967	17.15	3.155	0.8652	-1.811
226.76643	6.5594263	0.07796	17.68	3.016	-5.063	-3.79
232.889	6.142524	0.05058	17.039	3.734	-6.746	-8.641
234.03603	5.793154	0.03973	16.87	4.426	-10.17	-10.9
224.26173	29.998806	0.062	17.37	3.175	-1.662	-12.18
234.30115	25.908466	0.03166	15.93	3.281	-9.937	-12.47
237.12952	25.646343	0.07002	17.24	3.615	-7.23	-3.507
116.90634	51.070045	0.05841	16.66	5.056	-7.783	-14.4
180.73112	40.211002	0.08847	17.56	3.592	-0.8686	-9.799
193.09158	39.998695	0.02614	16.86	3.4	-9.755	-9.683
192.99188	41.069267	0.08032	17.58	4.904	-12.26	-8.182
199.18513	39.612217	0.08318	17.67	3.18	-0.03835	8.685
205.30061	30.17	0.03417	17.44	3.209	-9.936	-9.245
201.19797	36.455555	0.0174	17.44	4.538	0.0	-11.85
201.33095	30.966238	0.06496	17.65	3.522	-12.46	-25.41
201.8043	32.08852	0.02453	17.65	3.204	0.0	-5.834
226.04832	23.299273	0.04563	17.13	3.118	-2.48	-0.03157
227.34096	26.609896	0.07187	16.87	3.504	0.3016	-0.5167

RA	DEC	z	modelMag_r	Hδ EQW	[OII] EQW	Hα EQW
229.79701	20.950146	0.04215	17.43	3.186	3.501	0.2603
234.20845	20.941196	0.09621	17.72	3.14	1.448	-0.9353
240.5638	16.03893	0.03711	17.66	6.522	9.597	-0.6274
245.12573	14.370863	0.05385	17.69	9.221	-1.978	-0.3927
245.67767	14.516945	0.02872	17.11	4.215	-27.14	-17.91
245.19727	14.813197	0.08981	17.61	3.267	-11.52	-8.67
172.82442	26.790241	0.07127	17.66	3.933	-1.817	-10.8
184.79172	28.44243	0.07458	17.68	3.575	0.1533	-1.948
188.42639	26.617367	0.023813	16.84	3.111	0.0	-18.52
193.22987	28.948774	0.08464	16.72	3.253	-10.3	-12.56
135.3094	20.625496	0.03162	17.68	3.178	6.713	0.4475
135.50768	19.667898	0.08294	17.5	3.497	-3.897	-2.094
137.1927	18.78061	0.04226	16.9	4.267	-4.055	-8.558
135.93266	18.568682	0.06717	17.46	3.088	-9.808	-11.8
139.30975	20.064835	0.03054	17.06	3.066	-11.17	-14.19
141.36958	21.547058	0.05619	17.22	3.229	-13.25	-23.25
159.77817	26.675001	0.07571	17.55	3.059	-10.06	-13.35
159.75092	20.08469	0.05489	16.97	4.033	-7.185	-7.902
124.25336	12.316989	0.07928	17.38	3.797	-0.08672	-9.073
135.55566	17.059856	0.05664	17.54	3.11	-9.917	-10.8
161.50983	21.81594	0.05284	17.37	5.711	9.095	-0.8565
161.4934	16.16967	0.06823	17.41	3.343	-8.674	-6.892
178.08803	16.437202	0.08041	17.3	3.282	-17.05	-15.3
235.94952	11.495944	0.095	16.89	3.153	-2.215	-7.86
128.41946	9.252407	0.07759	16.52	3.161	-1.936	0.3821
152.53065	15.012845	0.0309	17.5	3.102	3.967	0.1193
155.3558	18.52554	0.09631	17.6	9.835	8.4	-11.13
204.61134	16.803802	0.04136	17.75	3.508	-19.53	-15.77

RA	DEC	z	modelMag_r	Hδ EQW	[OII] EQW	Hα EQW
187.70886	21.207005	0.06975	16.93	3.683	8.2	-33.21
180.65135	23.783106	0.02204	17.48	3.725	0.0	-0.05574

Table A.1: Data table showing the coordinates of the Hδ strong galaxies from the study in Ch. 2. We include the r-band magnitudes and equivalent widths of the Hδ, [OII] and Hα lines. Values are given to four significant places, excluding RA and DEC values.

Bibliography

Abazajian K. N., et al., 2009, ApJS, 182, 543

Abel T., Bryan G. L., Norman M. L., 2000, ApJ, 540, 39

Abel T., Bryan G. L., Norman M. L., 2001, in Umemura M., Susa H., eds, Astronomical Society of the Pacific Conference Series Vol. 222, The Physics of Galaxy Formation. p. 129

Abel T., Bryan G. L., Norman M. L., 2002, Science, 295, 93

Alam S., Ho S., Silvestri A., 2016, MNRAS, 456, 3743

Andreon S., Ettori S., 1999, ApJ, 516, 647

Anglés-Alcázar D., Faucher-Giguère C.-A., Kereš D., Hopkins P. F., Quataert E., Murray N., 2017, MNRAS, 470, 4698

Antonucci R., 1993, ARA&A, 31, 473

Bahcall J. N., Kirhakos S., Saxe D. H., Schneider D. P., 1997, ApJ, 479, 642

Bait O., Barway S., Wadadekar Y., 2017, MNRAS, 471, 2687

Baldry I. K., Glazebrook K., Brinkmann J., Ivezić Ž., Lupton R. H., Nichol R. C., Szalay A. S., 2004, ApJ, 600, 681

Baldry I. K., Balogh M. L., Bower R. G., Glazebrook K., Nichol R. C., Bamford S. P., Budavari T., 2006, MNRAS, 373, 469

Baldwin J. A., Phillips M. M., Terlevich R., 1981, PASP, 93, 5

Balogh M. L., Morris S. L., 2000, MNRAS, 318, 703

Balogh M. L., Morris S. L., Yee H. K. C., Carlberg R. G., Ellingson E., 1999, ApJ, 527, 54

Balogh M. L., Navarro J. F., Morris S. L., 2000, ApJ, 540, 113

Balogh M. L., Baldry I. K., Nichol R., Miller C., Bower R., Glazebrook K., 2004, ApJL, 615, L101

Bamford S. P., et al., 2009, MNRAS, 393, 1324

Barnes J. E., Hernquist L. E., 1991, ApJL, 370, L65

Barnes J. E., Hernquist L., 1992, ARA&A, 30, 705

Barnes J. E., Hernquist L., 1996, ApJ, 471, 115

Baron D., Netzer H., Poznanski D., Prochaska J. X., Förster Schreiber N. M., 2017, MNRAS, 470, 1687

Baskin A., Laor A., 2005, MNRAS, 358, 1043

Bastian N., Covey K. R., Meyer M. R., 2010, ARA&A, 48, 339

Baugh C. M., Lacey C. G., Frenk C. S., Granato G. L., Silva L., Bressan A., Benson A. J., Cole S., 2005, MNRAS, 356, 1191

Becker R. H., White R. L., Helfand D. J., 1995, ApJ, 450, 559

Bekki K., Shioya Y., Couch W. J., 2001, ApJL, 547, L17

Bekki K., Couch W. J., Shioya Y., Vazdekis A., 2005, MNRAS, 359, 949

Bell E. F., 2003, ApJ, 586, 794

Bell E. F., de Jong R. S., 2001, ApJ, 550, 212

Bell E. F., et al., 2004a, ApJL, 600, L11

Bell E. F., et al., 2004b, ApJ, 608, 752

Bell E. F., Phleps S., Somerville R. S., Wolf C., Borch A., Meisenheimer K., 2006, ApJ, 652, 270

Bellhouse C., et al., 2017, ApJ, 844, 49

Bendtz K., et al., 2013, Physical Review Letters, 110, 121803

Best P. N., Kauffmann G., Heckman T. M., Brinchmann J., Charlot S., Ivezić Ž., White S. D. M., 2005, MNRAS, 362, 25

Blake C., et al., 2004, MNRAS, 355, 713

Bland-Hawthorn J., Gerhard O., 2016, ARA&A, 54, 529

Blanton M. R., et al., 2003, ApJ, 594, 186

Bond J. R., Kofman L., Pogosyan D., 1996, Nature, 380, 603

Boroson T. A., Green R. F., 1992, ApJS, 80, 109

Bournaud F., Combes F., 2002, A&A, 392, 83

Bournaud F., Jog C. J., Combes F., 2005, A&A, 437, 69

Bray A. D., et al., 2016, MNRAS, 455, 185

Bremer M. N., et al., 2018, MNRAS, 476, 12

Brinchmann J., Charlot S., White S. D. M., Tremonti C., Kauffmann G., Heckman T., Brinkmann J., 2004, MNRAS, 351, 1151

Bromm V., Larson R. B., 2004, ARA&A, 42, 79

Bromm V., Coppi P. S., Larson R. B., 1999, ApJL, 527, L5

Bromm V., Coppi P. S., Larson R. B., 2002, ApJ, 564, 23

Brown M. J. I., et al., 2009, ApJ, 703, 150

Bruzual G., Charlot S., 2003, MNRAS, 344, 1000

Butcher H., Oemler Jr. A., 1978, ApJ, 219, 18

Butcher H., Oemler Jr. A., 1984, ApJ, 285, 426

Byrd G., Valtonen M., 1990, ApJ, 350, 89

Cacciato M., Dekel A., Genel S., 2012, MNRAS, 421, 818

Caldwell N., Rose J. A., 1997, AJ, 113, 492

Caldwell N., Rose J. A., Sharples R. M., Ellis R. S., Bower R. G., 1993, AJ, 106, 473

Cales S. L., et al., 2013, ApJ, 762, 90

Calzetti D., 2001, PASP, 113, 1449

Calzetti D., 2013, Star Formation Rate Indicators. p. 419

Calzetti D., Harris J., Gallagher III J. S., Smith D. A., Conselice C. J., Homeier N., Kewley L., 2004, AJ, 127, 1405

Cappellari M., et al., 2006, MNRAS, 366, 1126

Cappellari M., et al., 2012, Nature, 484, 485

Carter D., Prieur J. L., Wilkinson A., Sparks W. B., Malin D. F., 1988, MNRAS, 235, 813

Cautun M., van de Weygaert R., Jones B. J. T., Frenk C. S., 2014, MNRAS, 441, 2923

Ceverino D., Dekel A., Bournaud F., 2010, MNRAS, 404, 2151

Chabrier G., 2003, PASP, 115, 763

Chabrier G., 2005, in Corbelli E., Palla F., Zinnecker H., eds, Astrophysics and Space Science Library Vol. 327, The Initial Mass Function 50 Years Later. p. 41

Chang T.-C., van Gorkom J. H., Zabludoff A. I., Zaritsky D., Mihos J. C., 2001, AJ, 121, 1965

Cheung E., et al., 2015, MNRAS, 447, 506

Chevalier R. A., Clegg A. W., 1985, Nature, 317, 44

Chisholm J., Matsushita S., 2016, ApJ, 830, 72

Cicone C., et al., 2014, A&A, 562, A21

Cid Fernandes R., Heckman T., Schmitt H., González Delgado R. M., Storchi-Bergmann T., 2001, ApJ, 558, 81

Cid Fernandes R., Stasińska G., Schlickmann M. S., Mateus A., Vale Asari N., Schoenell W., Sodré L., 2010, MNRAS, 403, 1036

Cid Fernandes R., Stasińska G., Mateus A., Vale Asari N., 2011, MNRAS, 413, 1687

Codis S., Pichon C., Devriendt J., Slyz A., Pogosyan D., Dubois Y., Sousbie T., 2012, MNRAS, 427, 3320

Coil A. L., Weiner B. J., Holz D. E., Cooper M. C., Yan R., Aird J., 2011, ApJ, 743, 46

Cole S., Lacey C. G., Baugh C. M., Frenk C. S., 2000, MNRAS, 319, 168

Colless M., 1999, Philosophical Transactions of the Royal Society of London Series A, 357, 105

Combes F., Sanders R. H., 1981, A&A, 96, 164

Condon J. J., 1989, ApJ, 338, 13

Condon J. J., 1992, ARA&A, 30, 575

Condon J. J., Matthews A. M., 2018, PASP, 130, 073001

Condon J. J., Cotton W. D., Broderick J. J., 2002, AJ, 124, 675

Costa E., et al., 2010, Experimental Astronomy, 28, 137

Couch W. J., Sharples R. M., 1987, MNRAS, 229, 423

Courteau S., de Jong R. S., Broeils A. H., 1996, ApJL, 457, L73

Cox T. J., Dutta S. N., Di Matteo T., Hernquist L., Hopkins P. F., Robertson B., Springel V., 2006, ApJ, 650, 791

Crain R. A., et al., 2015, MNRAS, 450, 1937

Croton D. J., et al., 2006, MNRAS, 365, 11

Daddi E., et al., 2007, ApJ, 670, 156

Dalla Vecchia C., Schaye J., 2008, MNRAS, 387, 1431

Dalla Vecchia C., Schaye J., 2012, MNRAS, 426, 140

Darg D. W., et al., 2010, MNRAS, 401, 1552

Debattista V. P., Mayer L., Carollo C. M., Moore B., Wadsley J., Quinn T., 2006, ApJ, 645, 209

Debuhr J., Quataert E., Ma C.-P., 2012, MNRAS, 420, 2221

Deharveng L., et al., 2010, A&A, 523, A6

Dekel A., Sari R., Ceverino D., 2009, ApJ, 703, 785

de Marchi G., Paresce F., 2001, in Schielicke E. R., ed., Astronomische Gesellschaft Meeting Abstracts Vol. 18, Astronomische Gesellschaft Meeting Abstracts

De Propris R., Melnick J., 2014, MNRAS, 439, 2837

de Swart J. G., Bertone G., van Dongen J., 2017, Nature, 1, 0059

de Vaucouleurs G., 1948, Annales d'Astrophysique, 11, 247

Di Matteo T., Springel V., Hernquist L., 2005, Nature, 433, 604

Di Matteo P., Bournaud F., Martig M., Combes F., Melchior A.-L., Semelin B., 2008, A&A, 492, 31

Dressler A., 1980, ApJ, 236, 351

Dressler A., Gunn J. E., 1982, ApJ, 263, 533

Dressler A., Gunn J. E., 1983, ApJ, 270, 7

Dressler A., Gunn J. E., 1992, ApJS, 78, 1

Driver S. P., et al., 2006, /mnras, 368, 414

Ebeling H., Stephenson L. N., Edge A. C., 2014, ApJL, 781, L40

Elbaz D., et al., 2007, A&A, 468, 33

Elbaz D., et al., 2011, A&A, 533, A119

Ellis S. C., Driver S. P., Allen P. D., Liske J., Bland-Hawthorn J., De Propris R., 2005, MNRAS, 363, 1257

Faber S. M., et al., 2007, ApJ, 665, 265

Fabricant D. G., McClintock J. E., Bautz M. W., 1991, ApJ, 381, 33

Faucher-Giguère C.-A., 2018, MNRAS, 473, 3717

Fellhauer M., et al., 2006, ApJ, 651, 167

Ferland G. J., Persson S. E., 1989, ApJ, 347, 656

Ferland G. J., Peterson B. M., Horne K., Welsh W. F., Nahar S. N., 1992, ApJ, 387, 95

Feruglio C., Maiolino R., Piconcelli E., Menci N., Aussel H., Lamastra A., Fiore F., 2010, A&A, 518, L155

Fierlinger K. M., Burkert A., Ntormousi E., Fierlinger P., Schartmann M., Ballone A., Krause M. G. H., Diehl R., 2016, MNRAS, 456, 710

Figer D. F., Kim S. S., Morris M., Serabyn E., Rich R. M., McLean I. S., 1999, ApJ, 525, 750

Fraser-McKelvie A., Brown M. J. I., Pimbblet K. A., Dolley T., Crossett J. P., Bonne N. J., 2016, MNRAS, 462, L11

Fraser-McKelvie A., Brown M. J. I., Pimbblet K., Dolley T., Bonne N. J., 2018, MNRAS, 474, 1909

French K. D., Yang Y., Zabludoff A., Narayanan D., Shirley Y., Walter F., Smith J.-D., Tremonti C. A., 2015, ApJ, 801, 1

French K. D., Zabludoff A. I., Yoon I., Shirley Y., Yang Y., Smercina A., Smith J. D., Narayanan D., 2018, ApJ, 861, 123

Frenk C. S., White S. D. M., Efstathiou G., Davis M., 1990, ApJ, 351, 10

Galloway M. A., et al., 2015, MNRAS, 448, 3442

Gavazzi G., Contursi A., Carrasco L., Boselli A., Kennicutt R., Scodeggio M., Jaffe W., 1995, A&A, 304, 325

Gebhardt K., et al., 2000, ApJL, 539, L13

Genel S., et al., 2014, MNRAS, 445, 175

Gómez P. L., et al., 2003, ApJ, 584, 210

González Delgado R. M., Heckman T., Leitherer C., 2001, ApJ, 546, 845

Goto T., 2005, MNRAS, 357, 937

Goto T., 2006, MNRAS, 369, 1765

Goto T., 2007a, MNRAS, 377, 1222

Goto T., 2007b, MNRAS, 381, 187

Goto T., et al., 2003a, PASJ, 55, 739

Goto T., et al., 2003b, PASJ, 55, 757

Goto T., et al., 2003c, PASJ, 55, 771

Gregg M., West M., 2017, in Early stages of Galaxy Cluster Formation. p. 13

Gregory S. A., Thompson L. A., 1978, ApJ, 222, 784

Gunawardhana M. L. P., et al., 2011, MNRAS, 415, 1647

Gunn J. E., Gott III J. R., 1972, ApJ, 176, 1

Guth A. H., 1981, Physical Review D, 23, 347

Harayama Y., Eisenhauer F., Martins F., 2008, ApJ, 675, 1319

Hashimoto Y., Oemler Jr. A., Lin H., Tucker D. L., 1998, ApJ, 499, 589

Hatch N. A., Kurk J. D., Pentericci L., Venemans B. P., Kuiper E., Miley G. K., Röttgering H. J. A., 2011, MNRAS, 415, 2993

Hayward C. C., Kereš D., Jonsson P., Narayanan D., Cox T. J., Hernquist L., 2011, ApJ, 743, 159

Heckman T. M., Armus L., Miley G. K., 1990, ApJS, 74, 833

Heckman T. M., Lehnert M. D., Strickland D. K., Armus L., 2000, ApJS, 129, 493

Hogg D. W., et al., 2003, ApJ, 585, L5

Hogg D. W., Masjedi M., Berlind A. A., Blanton M. R., Quintero A. D., Brinkmann J., 2006, ApJ, 650, 763

Hong S., et al., 2011, The Astrophysical Journal, 731, 45

Hopkins A. M., et al., 2003, ApJ, 599, 971

Hopkins P. F., Hernquist L., Cox T. J., Di Matteo T., Robertson B., Springel V., 2006, ApJS, 163, 1

Hopkins P. F., Hernquist L., Cox T. J., Kereš D., 2008a, ApJS, 175, 356

Hopkins P. F., Cox T. J., Kereš D., Hernquist L., 2008b, ApJS, 175, 390

Hopkins P. F., Quataert E., Murray N., 2012, MNRAS, 421, 3522

Hou S. Q., He J. J., Parikh A., Kahl D., Bertulani C. A., Kajino T., Mathews G. J., Zhao G., 2017, ApJ, 834, 165

Hubble E., 1929, Proceedings of the National Academy of Science, 15, 168

Hubble E. P., 1936, Realm of the Nebulae

Huber P. J., 1981, Robust statistics

Huchra J., Burg R., 1992, ApJ, 393, 90

Huchra J., Davis M., Latham D., Tonry J., 1983, ApJS, 52, 89

Hunter D. A., Elmegreen B. G., Ludka B. C., 2010, AJ, 139, 447

Ishigaki M., Goto T., Matsuhara H., 2007, MNRAS, 382, 270

Jarrett T. H., et al., 2006, AJ, 131, 261

Jogee S., et al., 2004, ApJL, 615, L105

Kaiser M. E., et al., 1999, Ap&SS, 269, 431

Kauffmann G., et al., 2003, MNRAS, 346, 1055

Kaviraj S., 2010, MNRAS, 406, 382

Kaviraj S., Kirkby L. A., Silk J., Sarzi M., 2007, MNRAS, 382, 960

Kawata D., Mulchaey J. S., 2008, ApJL, 672, L103

Kennicutt Jr. R. C., 1998, ARA&A, 36, 189

Kewley L. J., Heisler C. A., Dopita M. A., Lumsden S., 2001, ApJS, 132, 37

Kewley L. J., Geller M. J., Jansen R. A., Dopita M. A., 2002, AJ, 124, 3135

Khachikian E. Y., Weedman D. W., 1974, ApJ, 192, 581

Kirshner R. P., Oemler Jr. A., Schechter P. L., Shectman S. A., 1981, ApJL, 248, L57

Koenig X. P., Leisawitz D. T., Benford D. J., Rebull L. M., Padgett D. L., Assef R. J., 2011, ApJ, 744, 130

Kormendy J., Bender R., 1996, ApJL, 464, L119

Kormendy J., Kennicutt Jr. R. C., 2004, ARA&A, 42, 603

Kormendy J., Richstone D., 1995, ARA&A, 33, 581

Koski A. T., 1978, ApJ, 223, 56

Kroupa P., 2001, MNRAS, 322, 231

Kroupa P., Weidner C., Pflamm-Altenburg J., Thies I., Dabringhausen J., Marks M., Maschberger T., 2013, The Stellar and Sub-Stellar Initial Mass Function of Simple and Composite Populations. p. 115

Kruk S. J., et al., 2017, MNRAS, 469, 3363

Kruk S. J., et al., 2018, MNRAS, 473, 4731

Lacey C. G., Baugh C. M., Frenk C. S., Silva L., Granato G. L., Bressan A., 2008, MNRAS, 385, 1155

Lahav O., et al., 1995, Science, 267, 859

Lake G., Katz N., Moore B., 1998, ApJ, 495, 152

Lamareille F., 2010, A&A, 509, A53

Lambourne R. J. A., 2010, Relativity, Gravitation and Cosmology

Larson R. B., Tinsley B. M., Caldwell C. N., 1980, ApJ, 237, 692

Leitherer C., Lamers H. J. G. L., 1991, ApJ, 373, 89

Lemaître G., 1927, Annales de la Société Scientifique de Bruxelles, 47, 49

Lemaux B. C., Tomczak A. R., Lubin L. M., Wu P.-F., Gal R. R., Rumbaugh N., Kocevski D. D., Squires a. G. K., 2016, preprint (arXiv:1608.00973)

Lépine-Szily A., Descouvemont P., 2012, International Journal of Astrobiology, 11, 243

Libeskind N. I., et al., 2018, MNRAS, 473, 1195

Lilly S. J., Carollo C. M., Pipino A., Renzini A., Peng Y., 2013, ApJ, 772, 119

Lin L., et al., 2010, ApJ, 718, 1158

Lintott C. J., et al., 2008, MNRAS, 389, 1179

Lintott C., et al., 2011, MNRAS, 410, 166

Liu C. T., Kennicutt Jr. R. C., 1995, ApJ, 450, 547

Loh Y.-S., Ellingson E., Yee H. K. C., Gilbank D. G., Gladders M. D., Barrientos L. F., 2008, ApJ, 680, 214

Lorenzo M. F., Sulentic J., Verdes-Montenegro L., Ruiz J. E., Sabater J., Sánchez S., 2012, Astronomy & Astrophysics, 540, A47

LSST Collaboration , 2017, preprint (arXiv:1708.04058)

Madau P., Dickinson M., 2014, ARA&A, 52, 415

Magorrian J., et al., 1998, AJ, 115, 2285

Mahajan S., 2013, MNRAS, 431, L117

Margoniner V. E., de Carvalho R. R., Gal R. R., Djorgovski S. G., 2001, ApJL, 548, L143

Marinacci F., et al., 2017, preprint (arXiv:1707.03396)

Marks M., Kroupa P., Dabringhausen J., Pawlowski M. S., 2012, MNRAS, 422, 2246

Masters K. L., et al., 2010a, MNRAS, 405, 783

Masters K. L., et al., 2010b, MNRAS, 411, 2026

McCrady N., Gilbert A. M., Graham J. R., 2003, ApJ, 596, 240

McIntosh D. H., et al., 2014, MNRAS, 442, 533

McLure R. J., Kukula M. J., Dunlop J. S., Baum S. A., O'Dea C. P., Hughes D. H., 1999, MNRAS, 308, 377

McPartland C., Ebeling H., Roediger E., Blumenthal K., 2016, MNRAS, 455, 2994

Melnick J., Telles E., De Propris R., Chu Z.-H., 2015, A&A, 582, A37

Mendez A. J., Coil A. L., Lotz J., Salim S., Moustakas J., Simard L., 2011, ApJ, 736, 110

Meurs E. J. A., Wilson A. S., 1984, A&A, 136, 206

Mihos J. C., Hernquist L., 1994, ApJL, 431, L9

Mihos J. C., Hernquist L., 1996, ApJ, 464, 641

Miller G. E., Scalo J. M., 1979, ApJS, 41, 513

Mo H. J., Mao S., White S. D. M., 1998, MNRAS, 295, 319

Mo H., van den Bosch F. C., White S., 2010, Galaxy Formation and Evolution

Moore B., Katz N., Lake G., Dressler A., Oemler A., 1996, Nature, 379, 613

Moore B., Lake G., Katz N., 1998, ApJ, 495, 139

Mulchaey J. S., Zabludoff A. I., 1998, ApJ, 496, 73

Naab T., Burkert A., 2003, ApJ, 597, 893

Naiman J. P., et al., 2017, preprint (arXiv:1707.03401)

Nakamura F., Umemura M., 2001, ApJ, 548, 19

Nelson D., et al., 2015, A&C, 13, 12

Nelson D., et al., 2018a, MNRAS, 475, 624

Nelson D., et al., 2018b, MNRAS, 477, 450

Newton R. D. A., Kay S. T., 2013, MNRAS, 434, 3606

Noeske K. G., et al., 2007, ApJL, 660, L43

Nomoto K., Kobayashi C., Tominaga N., 2013, ARA&A, 51, 457

Norton S. A., Gebhardt K., Zabludoff A. I., Zaritsky D., 2001, ApJ, 557, 150

Oegerle W. R., Hill J. M., Hoessel J. G., 1991, ApJL, 381, L9

Offner S. S. R., Clark P. C., Hennebelle P., Bastian N., Bate M. R., Hopkins P. F., Moraux E., Whitworth A. P., 2014, Protostars and Planets VI, pp 53–75

Osman O., Bekki K., 2017, MNRAS, 471, L87

Pan D. C., Vogeley M. S., Hoyle F., Choi Y.-Y., Park C., 2012, MNRAS, 421, 926

Papovich C., et al., 2012, ApJ, 750, 93

Parra R., Conway J. E., Diamond P. J., Thrall H., Lonsdale C. J., Lonsdale C. J., Smith H. E., 2007, ApJ, 659, 314

Peng Y.-j., et al., 2010, ApJ, 721, 193

Peng Y., Maiolino R., Cochrane R., 2015, Nature, 521, 192

Pillepich A., et al., 2017, MNRAS, 475, 648

Pimbblet K. A., Smail I., Edge A. C., O'Hely E., Couch W. J., Zabludoff A. I., 2006, MNRAS, 366, 645

Planck Collaboration, 2014, A&A, 571, A1

Poggianti B. M., Smail I., Dressler A., Couch W. J., Barger A. J., Butcher H., Ellis R. S., Oemler Jr. A., 1999, ApJ, 518, 576

Poggianti B. M., et al., 2006, ApJ, 642, 188

Poggianti B. M., et al., 2009, ApJ, 693, 112

Poggianti B. M., et al., 2016, AJ, 151, 78

Porter L. A., Somerville R. S., Primack J. R., Johansson P. H., 2014, MNRAS, 444, 942

Pracy M. B., Couch W. J., Blake C., Bekki K., Harrison C., Colless M., Kuntschner H., de Propris R., 2005, MNRAS, 359, 1421

Prescott M., et al., 2011, MNRAS, 417, 1374

Prialnik D., 2009, An Introduction to the Theory of Stellar Structure and Evolution

Quilis V., Moore B., Bower R., 2000, Science, 288, 1617

Quinn P. J., Salmon J. K., Zurek W. H., 1986, Nature, 322, 329

Quintero A. D., et al., 2004, ApJ, 602, 190

Rakos K. D., Schombert J. M., 1995, ApJ, 439, 47

Rieke G. H., Loken K., Rieke M. J., Tamblyn P., 1993, ApJ, 412, 99

Riess A. G., et al., 2018, ApJ, 861, 126

Robaina A. R., et al., 2009, ApJ, 704, 324

Rodighiero G., et al., 2011, ApJL, 739, L40

Rodighiero G., et al., 2014, MNRAS, 443, 19

Rodríguez Del Pino B., Bamford S. P., Aragón-Salamanca A., Milvang-Jensen B., Merrifield M. R., Balcells M., 2014, MNRAS, 438, 1038

Rodriguez-Gomez V., et al., 2015, MNRAS, 449, 49

Rodriguez-Gomez V., et al., 2016, MNRAS, 458, 2371

Rosa M., Joubert M., Benvenuti P., 1984, A&AS, 57, 361

Sadler E. M., et al., 2002, MNRAS, 329, 227

Salim S., et al., 2007, ApJS, 173, 267

Salomé Q., Salomé P., Miville-Deschênes M.-A., Combes F., Hamer S., 2017, A&A, 608, A98

Salpeter E. E., 1955, ApJ, 121, 161

Sánchez-Blázquez P., Gibson B. K., Kawata D., Cardiel N., Balcells M., 2009, MNRAS, 400, 1264

Santini P., et al., 2017, ApJ, 847, 76

Scalo J., 1990, in Fabbiano G., Gallagher J. S., Renzini A., eds, Astrophysics and Space Science Library Vol. 160, Windows on Galaxies. p. 125

Schawinski K., et al., 2007, ApJS, 173, 512

Schawinski K., et al., 2009, MNRAS, 396, 818

Schawinski K., et al., 2014, MNRAS, 440, 889

Scheuer P. A. G., Readhead A. C. S., 1979, Nature, 277, 182

Schlegel D. J., et al., 2015, in American Astronomical Society Meeting Abstracts #225. p. 336.07

Schmitt H. R., Storchi-Bergmann T., Cid Fernandes R., 1999, MNRAS, 303, 173

Schneider F. R. N., et al., 2018, Science, 359, 69

Schweizer F., 1982, ApJ, 252, 455

Sekiguchi K., Anderson K. S., 1987, AJ, 94, 644

Sellwood J. A., Carlberg R. G., 1984, ApJ, 282, 61

Sellwood J. A., Wilkinson A., 1993, Reports on Progress in Physics, 56, 173

Sersic J. L., 1968, Atlas de galaxias australes

Seyfert C. K., 1943, ApJ, 97, 28

Shapiro P. R., Field G. B., 1976, ApJ, 205, 762

Shen S., Mo H. J., White S. D. M., Blanton M. R., Kauffmann G., Voges W., Brinkmann J., Csabai I., 2003, MNRAS, 343, 978

Skibba R. A., et al., 2009, MNRAS, 399, 966

Smethurst R. J., et al., 2015, MNRAS, 450, 435

Smith H. E., Lonsdale C. J., Lonsdale C. J., 1998, ApJ, 492, 137

Smith R. J., et al., 2010, MNRAS, 408, 1417

Snyder G. F., Cox T. J., Hayward C. C., Hernquist L., Jonsson P., 2011, ApJ, 741, 77

Sparre M., Springel V., 2016, MNRAS, 462, 2418

Sparre M., Springel V., 2017, MNRAS, 470, 3946

Sparre M., et al., 2015, MNRAS, 447, 3548

Sparre M., Hayward C. C., Feldmann R., Faucher-Giguère C.-A., Muratov A. L., Kereš D., Hopkins P. F., 2017, MNRAS, 466, 88

Speagle J. S., Steinhardt C. L., Capak P. L., Silverman J. D., 2014, ApJS, 214, 15

Spergel D. N., et al., 2007, ApJS, 170, 377

Springel V., 2010, ARA&A, 48, 391

Springel V., Hernquist L., 2003, MNRAS, 339, 289

Springel V., Di Matteo T., Hernquist L., 2005, MNRAS, 361, 776

Springel V., Frenk C. S., White S. D. M., 2006, Nature, 440, 1137

Springel V., et al., 2017, MNRAS, 475, 676

Stolte A., Brandner W., Grebel E. K., Lenzen R., Lagrange A.-M., 2005, ApJL, 628, L113

Strateva I., et al., 2001, AJ, 122, 1861

Strauss M. A., et al., 2002, AJ, 124, 1810

Tanaka M., 2012, PASJ, 64, 37

Taranu D. S., Hudson M. J., Balogh M. L., Smith R. J., Power C., Oman K. A., Krane B., 2014, MNRAS, 440, 1934

Taylor E. N., et al., 2014, MNRAS, 446, 2144

Thies I., Kroupa P., 2007, ApJ, 671, 767

Thies I., Kroupa P., 2008, MNRAS, 390, 1200

Tojeiro R., et al., 2013, MNRAS, 432, 359

Tonnesen S., Bryan G. L., van Gorkom J. H., 2007, ApJ, 671, 1434

Toomre A., 1964, ApJ, 139, 1217

Tran K.-V. H., Franx M., Illingworth G., Kelson D. D., van Dokkum P., 2003, ApJ, 599, 865

Tran K.-V. H., Franx M., Illingworth G. D., van Dokkum P., Kelson D. D., Magee D., 2004, ApJ, 609, 683

Tremonti C. A., Moustakas J., Diamond-Stanic A. M., 2007, ApJL, 663, L77

Treyer M., et al., 2007, ApJS, 173, 256

Trouille L., Tremonti C., Hickox R., 2011, in American Astronomical Society Meeting Abstracts #218. p. 123.03

Urry C. M., Padovani P., 1995, PASP, 107, 803

van den Bergh S., 1976, ApJ, 206, 883

van den Bosch F. C., Aquino D., Yang X., Mo H. J., Pasquali A., McIntosh D. H., Weinmann S. M., Kang X., 2008, MNRAS, 387, 79

van Dokkum P. G., Conroy C., 2010, Nature, 468, 940

van Gorkom J. H., 2004, Clusters of Galaxies: Probes of Cosmological Structure and Galaxy Evolution, p. 305

Veilleux S., Osterbrock D. E., 1987, ApJS, 63, 295

Veilleux S., Cecil G., Bland-Hawthorn J., 2005, ARA&A, 43, 769

Vergani D., et al., 2010, A&A, 509, A42

Vogelsberger M., Genel S., Sijacki D., Torrey P., Springel V., Hernquist L., 2013, MNRAS, 436, 3031

Vogelsberger M., et al., 2014a, MNRAS, 444, 1518

Vogelsberger M., et al., 2014b, Nature, 509, 177

Vollmer B., 2013, The Influence of Environment on Galaxy Evolution. p. 207

White S. D. M., Rees M. J., 1978, MNRAS, 183, 341

Whitmore B. C., Gilmore D. M., Jones C., 1993, ApJ, 407, 489

Wild V., Walcher C. J., Johansson P. H., Tresse L., Charlot S., Pollo A., Le Fèvre O., de Ravel L., 2009, MNRAS, 395, 144

Wilkinson C. L., Pimbblet K. A., Stott J. P., 2017, MNRAS, 472, 1447

Wilkinson C. L., Pimbblet K. A., Stott J. P., Few C. G., Gibson B. K., 2018, MNRAS, 479, 758

Willett K. W., et al., 2013, MNRAS, 435, 2835

Wyder T. K., et al., 2007, ApJS, 173, 293

Xu G., 1995, ApJS, 98, 355

Yang Y., Zabludoff A. I., Zaritsky D., Lauer T. R., Mihos J. C., 2004, ApJ, 607, 258

Yang X., Mo H. J., van den Bosch F. C., Pasquali A., Li C., Barden M., 2007, ApJ, 671, 153

Yasui C., Kobayashi N., Saito M., Izumi N., 2016, AJ, 151, 115

Yesuf H. M., Faber S. M., Trump J. R., Koo D. C., Fang J. J., Liu F. S., Wild V., Hayward C. C., 2014, ApJ, 792, 84

Yesuf H. M., French K. D., Faber S. M., Koo D. C., 2017, MNRAS, 469, 3015

Zabludoff A. I., Zaritsky D., Lin H., Tucker D., Hashimoto Y., Shectman S. A., Oemler A., Kirshner R. P., 1996, ApJ, 466, 104

Zhang Z., Shi Y., Rieke G. H., Xia X., Wang Y., Sun B., Wan L., 2016, ApJL, 819, L27

Zwaan M. A., Kuntschner H., Pracy M. B., Couch W. J., 2013, MNRAS, 432, 492

Zwicky F., 1933, Helvetica Physica Acta, 6, 110